

PRRIP DRAFT

***Peer Reviewed, Revised, and Supported by Technical Advisory Committee in 2012
Pending Governance Committee Approval of Peer Review and Revisions in 2014
Manuscript Development for Possible Publication in 2014***

**PLATTE RIVER RECOVERY IMPLEMENTATION PROGRAM
DIRECTED VEGETATION RESEARCH STUDY**

**CAN SHORT DURATION HIGH FLOWS BE USED TO
REMOVE VEGETATION FROM BARS IN THE
CENTRAL PLATTE RIVER?**



Natasha Pollen-Bankhead¹, Robert Thomas², and Andrew Simon¹

¹ Formerly at USDA-ARS National Sedimentation Laboratory, Oxford, MS. Now at Cardno ENTRIX, Oxford, MS.

² Formerly at Department of Civil and Environmental Engineering, University of Tennessee, Knoxville, TN. Now at Department of Earth Sciences, University of Leeds, UK.

Point of Contact: Natasha Pollen-Bankhead; Email: natasha.bankhead@cardno.com; Tel. (662) 236 6983.

EXECUTIVE SUMMARY

The diversion and storage of water for agricultural, municipal and industrial uses has caused significant alteration of the hydrologic regime of the central Platte River, allowing the colonization and proliferation of vegetation which has effectively created semi-permanent islands, narrowed anabranches and reduced available habitat for endangered species by increasing the resistance of bar deposits to erosion. Increasing and/or improving available riverine habitat in the central Platte River is therefore fundamentally related to recreating a dynamic, braided stream channel through the removal of vegetation. Traditional methods of vegetation removal, such as spraying and disking, are both costly and time-consuming and therefore it has been suggested that it may be possible to use in-stream flows to uproot plants. Plans to remove vegetation in this manner must be based on a fundamental understanding and quantification of the effects of vegetation on in-stream flows, sediment transport and substrate reinforcement and the effects of in-stream flows on vegetation.

The overall project aim was to determine the potential for short duration, high flows (SDHFs) of varying magnitude and duration to uproot early succession species growing on bars within the Platte River, as part of the Program's Flow-Sediment-Mechanical (FSM) strategy. To meet this aim, we must be able to quantify the resisting forces provided by the sediment and plant roots against the driving force provided the flow. Flowing water causes the stems and leaves of plants to either oscillate, but essentially remain upright, or to bend and/or streamline. The force and/or moment exerted on stems and leaves is transmitted through the plant stem to the plant roots, albeit with some energy loss. Simultaneously, the energy of the flow is focussed at the base of the plant stem, and sediment is scoured from around the stem and/or the roots. Recognition of these processes provides the framework for this research. First, laboratory experiments were undertaken to quantify the magnitude of the drag forces that are applied to plant stems by flowing water. Second, fieldwork was undertaken to quantify the behavior of plant stems and leaves in response to drag forces. Third, well-established relationships were used to estimate the maximum scour depths produced by flows of different magnitudes and durations. Fourth, the resistance of plant stems, roots and rhizomes against rupture (tensile failure) and pullout were quantified through direct measurement at field sites. These data were input into the RipRoot fiber bundle model to determine species-specific resistance for different burial/scour depths.

Uprooting tests showed that the one-year-old cottonwood seedlings had the lowest uprooting forces, ranging from 8.2 to 64.3 Newtons (N) (mean value of 32.0 N, sample size, $n = 50$). Resistance to removal for Reed canarygrass stems ranged from 2.5 to 192 N (mean value of 58.3 N, sample size, $n = 100$). Finally, *Phragmites* provided the largest uprooting forces out of the four species tested. Forces required for failure of the *Phragmites* stems ranged from 8.9 to 740 N (mean value of 254.5 N, sample size, $n = 115$).

A comparison of drag forces (i.e. the driving force acting on the vegetation) measured in the flume study, with uprooting forces (i.e. the resisting force) measured in the field, was carried out for each species to determine the likelihood of plant removal by SDHFs. For cottonwood seedlings, drag forces measured during flume experiments (up to 0.25 ms^{-1}) suggested that some seedlings may experience bending, and only the very youngest and/or, most shallowly rooted seedlings could be removed through drag forces. Flow velocities that could be experienced during SDHFs in the central Platte River may, however, be as

high as 1.5 ms^{-1} . Drag forces at this range of velocities would be higher, and would be sufficient to bend almost all young cottonwood seedlings to the point of being streamlined with the flow; similar to the lower flow velocities, applied force from drag at the upper end of the velocity range could remove younger/ more shallowly rooted seedlings. For Reed canarygrass, the drag force acting on lower stem density grass (400 stems per m^2) was lower than both the forces required for uprooting and bending. In the case of the higher stem density of 800 stems per square meter, higher drag forces were recorded, almost always exceeding the force required for grass stem bending. Some weaker, more exposed grass stems may experience breaking or uprooting at higher flow velocities, but this is likely to be limited, and bending will tend to be the dominant process observed. In the case of *Phragmites*, the drag forces from the flume study were lower than both the forces required for bending and for uprooting. At the upper limit of flow velocities, drag forces exceeded the full range of bending forces, but according to estimates from RipRoot model runs, were still insufficient to initiate uprooting of even the weakest and sparsest patches of *Phragmites*. As with Reed canarygrass, at high flows bending will be the dominant result rather than uprooting or stem breaking.

Predicted values of local scour around stems of bar vegetation were shown to be relatively small compared to the rooting depths of the plants measured in the field, in particular *Phragmites*. The results from the analysis presented here suggest that even at very high discharges, equilibrium (maximum) scour depths, would be insufficient to scour out all but the shallowest rooted vegetation. Newly germinated cottonwood seedlings and other annual species could be scoured at high flows where rooting depths have not yet greatly exceeded the potential scour depths of up to 5.50 cm at 8,000 cfs and up to 6.70 cm at the 100-year recurrence interval of approximately 27,600 cfs at the gage at Odessa. The scour results confirm the idea that once bar vegetation has established, and rooting depths have exceeded potential local scour depths, even at the 100-year recurrence interval discharge, the combination of drag and scour are unlikely to remove the three species tested in this study.

Overall the implications of the results of this study for management of vegetation on bars in the central Platte River are:

1. Stands of vegetation, including *Phragmites* (> 1 year-old), Reed canarygrass (> 1 year-old), and cottonwood trees whose taproots have rooted below the shallow zone of local scour (> 1-year-old), likely cannot be removed through drag and local scour alone, even at the 100-year recurrence interval discharge;
2. At most, a few *young* cottonwood and willow seedlings (less than 1-year-old) could potentially be removed from bars through drag/local scour, where rooting depths are still small;
3. The best opportunity for removal of cottonwood and willow seedlings by SDHFs is in the same year as seedling germination;
4. Likelihood of cottonwood and willow seedlings being removed by SDHFs reduces dramatically with each additional growing season between high flow events. For cottonwood seedlings, mean uprooting force increased quadrupled from 32 to 139 N for one and two-year-old plants respectively;
5. Lateral scour of bank and bar edges, and scour by ice could be important mechanisms for undercutting, scour and removal of vegetation, and should be studied further.

TABLE OF CONTENTS

EXECUTIVE SUMMARY	ii
TABLE OF CONTENTS.....	iv
TABLE OF FIGURES	vi
LIST OF TABLES.....	ix
1 BACKGROUND AND PROBLEM STATEMENT	1
1.1 Aim and objectives	3
2 QUANTIFYING DRIVING AND RESISTING FORCES ACTING ON VEGETATION: THEORY	6
2.1 Driving forces	6
2.2 Resisting forces.....	8
2.2.1 Scour around the stems of plants	10
3 QUANTIFYING DRIVING AND RESISTING FORCES ACTING ON VEGETATION:	
METHODOLOGY	18
3.1 Study Sites	18
3.2 Driving forces	20
3.2.1 Field protocol.....	20
3.2.2 Image processing methodology	21
3.2.3 Laboratory flume experiments: measuring driving force.....	24
3.3 Resisting forces.....	28
3.3.1 Field protocol: Root tensile strengths	28
3.3.2 Field protocol: Plant removal tests.....	28
3.3.3 Laboratory experiments: root network resistance to removal.....	29
3.3.4 Numerical modeling: root network resistance to removal	31
4 RESULTS	33
4.1 Driving forces	33
4.1.1 Basic geometric properties.....	33
4.1.2 Plant bending forces.....	33
4.1.3 Plant flexural stiffness.....	36
4.1.4 Plant projected area.....	36
4.1.5 Drag coefficients and drag forces	39
4.2 Resisting forces.....	41
4.2.1 Root architecture	41
4.2.2 Root and rhizome strengths.....	44
4.2.3 Plant resistance to pullout	45
4.3 Comparing root strength, uprooting resistance and plant bending forces.....	48
4.3.1 Measurement uncertainty and modeling implications	49
4.3.2 Results of laboratory experiments to test pullout forces under controlled soil moisture conditions.....	51
4.3.3 Modeling plant pullout forces using RipRoot.....	52
4.3.4 Modeling resistance of plant patches to removal using validated RipRoot model.	57
5 IMPLICATIONS FOR THE MANAGEMENT OF VEGETATION.....	59
5.1 Comparing drag forces (driving) with uprooting forces (resisting) of vegetation.....	59

5.2	Magnitude and duration of flow events required for scour of bar vegetation on the Platte River, NE	65
5.2.1	Maximum (equilibrium) scour depths at the base of plant stems	66
5.2.2	Time taken to reach Equilibrium scour depths	70
5.2.3	Recurrence Interval analysis of local scour around plant stems	72
5.2.4	Local scour summary	73
6	LINKING EXPERIMENTAL RESULTS TO REAL WORLD MANAGEMENT OF THE CENTRAL PLATTE RIVER	74
6.1	Flow velocities capable of uprooting plants through drag forces	74
6.2	Discussion of directed vegetation study findings, in light of 2012 Elm Creek FSM Annual Monitoring Report (Tetra Tech, 2012).	79
7	CONCLUSIONS	80
8	REFERENCES	86
		112

TABLE OF FIGURES

Figure 1. A) Low-level aerial view of the Platte River. Note significant cottonwood establishment. B) Dry south channel of the Platte River. Note establishment of grasses on mid-channel bars. Images courtesy of Will Graf. 2

Figure 2. Driving and resisting forces acting on submerged vegetation. 3

Figure 3. Continuum of processes for plant removal showing possible scenarios for balance of driving forces (flow) and resisting forces (roots). At the left end of the figure (1), driving force exceeds root strength and the plant can be removed without scour of the substrate. At the right end of the figure (3), scour has reduced the resisting force of the roots to zero, and the plant is removed by the force of the flow. In reality plant removal is likely to occur at some point between (1) and (3) at a point (2) along the continuum where scour has reduced the resisting force of the roots to a point where the flow can remove the plant from its substrate. 4

Figure 4. Schematic representation of scour around a plant stem (after Richardson and Davis, 2001 and Schnauder and Moggridge, 2009). 11

Figure 5. Shields diagram for incipient motion (modified from Buffington, 1999). The y-axis is defined by Equation 11 and the x-axis is defined by Equation 12. 11

Figure 6. Conceptualization of vegetation scour problem as analogous to the bridge pier scour problem (modified after Jones and Sheppard, 2000). The variables are defined as follows: 17

Figure 7. A) Stand of *Phragmites* growing on an in-channel sandbar, B) a 3 to 5-year old cottonwood tree, C) 1 to 2-year old sandbar willow tree excavated from a sandbar, D) Reed canarygrass growing at the channel edge. 18

Figure 8. Map showing the location of the three vegetation study sites in this project. 19

Figure 9. Frontal photographs of red alder at wind speeds of 0 and 20 m s⁻¹. Note that although the images are from experiments conducted in wind, the drag force mechanism is exactly the same as that in water because, at least in a fluid dynamical sense, air behaves like a fluid but with a much lower density than water. From Vollsinger et al. (2005). 20

Figure 10. A) Plant bending apparatus showing reel, telescopic arm, specially-designed mount and camera tripod. B) Close up of load cell during bending test. C) View of the bending test apparatus in action. 22

Figure 11. Image processing methodology. First, a single optimum bounding area was obtained for all the images in a test (Figure 11A). Second, each image was cropped and split into Cyan, Magenta, Yellow and Key black (CMYK) color channels (Figure 11B). Third, the Yellow channel was thresholded, and any areas of falsely identified vegetation were manually masked (Figure 11C). Fourth, the number of pixels classified as ‘vegetation’ and the total number of pixels within the bounding area and their quotient were computed. 23

Figure 12. Sample of the constructed cottonwood plants used in the flume study. 24

Figure 13. Sample of the rods used to mimic Reed canarygrass and *Phragmites* in the flume study. 25

Figure 14. Example of the flume set up for a *Phragmites* run. 26

Figure 15. Photos of the Root-Puller constructed at the USDA-ARS-NSL. (1) original large puller built by USDA-ARS-NSL being used to measure the strength of riparian tree roots. (2) close-up of the way that the load cell and roots are connected to the winching cable. 29

Figure 16. Root-puller device being used to measure the strength of excavated *Phragmites* roots and rhizomes, in a sandbar along the Elm Creek reach of the Platte River, NE. 30

Figure 17. Plant-pulling device being used to measure the force required to extract young phragmites stems from a sandbar in the Elm Creek reach along the Platte River, NE..... 30

Figure 18. Distributions of measured stem diameters..... 34

Figure 19. Distributions of measured stem lengths..... 34

Figure 20. Maximum force to bend stem against stem diameter. 35

Figure 21. Loading curves for bending tests on: A) Cottonwoods, B) *Phragmites*, and C) Reed canarygrass. Flexural rigidity is defined as the slope of these curves. Following equation 30, the y-axis is the applied force normalized by $2(3L - a)/a$ and the x-axis is the deflection of the stem normalized by the distance from the base of the stem to the point at which the force is applied. Flexural rigidity is defined as the slope of these curves. 37

Figure 22. Plant projected area against horizontal displacement for bending tests on: A) Cottonwoods, B) *Phragmites*, and C) Reed canarygrass. 38

Figure 23. Drag forces computed using Equation 4 for the species and experimental parameters tested herein. 40

Figure 24. A) Rootball of Reed canarygrass B) 1-year-old cottonwood seedling 42

Figure 25. A) Young willow seedling, B) Young *Phragmites* stems with vertical rhizome attached to deeper horizontal rhizome, C) Mature *Phragmites* rhizome..... 43

Figure 26. Breaking forces for roots and rhizomes of the three species tested for root strength..... 44

Figure 27. Full range of breaking or pullout forces for each of the four species studied in uprooting tests on sandbars of the Platte River, NE. Diamonds represent mean values. 46

Figure 28. Vertical rooting extent measured after uprooting tests. Diamonds represent mean values with full ranges measured. 47

Figure 29. Horizontal rooting extent measured after uprooting tests. Diamonds represent mean values with full ranges measured. 47

Figure 30. Plots comparing plant pullout forces with root breaking and stem bending forces..... 50

Figure 31. Minimum, maximum and mean pullout forces for one-year-old cottonwood seedlings under controlled soil moisture conditions. 51

Figure 32. Measured versus modeled values for each species. The vertical lines represent minimum and maximum values, the diamonds represent mean values. 53

Figure 33. Minimum force required to initiate uprooting of plants, at varying rooting depths. 54

Figure 34. A) Modeled minimum, maximum and mean uprooting forces, and measured uprooting forces for one-year-old cottonwood seedlings B) Modeled minimum, maximum and mean uprooting forces, and measured uprooting forces for two-year-old cottonwood seedlings. 56

Figure 35. Resistance of plant patches to removal by uprooting. Vertical lines indicate minimum and maximum uprooting force per patch of plants. Diamonds indicate mean values. 58

Figure 36. Drag forces calculated for flow velocities beyond those used in the flume experiments..... 60

Figure 37. Maximum drag (driving) forces calculated from flume study, and estimated for maximum in-field velocities, compared with patch uprooting resistance, and bending resistance. A) shows results for 1-year-old cottonwood seedlings with stem density of 26 stems per m^2 and B) shows results for 2-year-old cottonwood seedlings with stem density of 13 stems per m^2 61

Figure 38. Maximum drag (driving) forces calculated from flume study, and estimated for maximum in-field velocities, compared with patch uprooting resistance, and bending resistance A) shows results Reed canarygrass with a stem density of 400 stems per m^2 and B) shows results for Reed canarygrass with a stem density of 800 stems per m^2 63

Figure 39. Maximum drag (driving) forces calculated from flume study, and estimated for maximum in-field velocities, compared with patch uprooting resistance, and bending resistance. Data shown are for *Phragmites* stems with a density of 200 stems per m²..... 64

Figure 40. Cross sections at river miles 230.8, 228.7 and 210.6 as given by Holburn et al. (2006), and used in this study to estimate discharge at different flow stages. 65

Figure 41. Equilibrium scour depths at RM 230.8 for A) *Phragmites* stems and B) Cottonwood or Reed canarygrass stems..... 67

Figure 42. Equilibrium scour depths at RM 228.7 for A) *Phragmites* stems and B) Cottonwood or Reed canarygrass stems..... 68

Figure 43. Equilibrium scour depths at RM 210.6 for A) *Phragmites* stems and B) Cottonwood or Reed canarygrass stems..... 69

Figure 44. Time to reach equilibrium scour depth for A) *Phragmites* stems and B) Cottonwood or Reed canarygrass stems at RM 230.8..... 70

Figure 45. Time to reach equilibrium scour depth for A) *Phragmites* stems and B) Cottonwood or Reed canarygrass stems at RM 228.7..... 71

Figure 46. Time to reach equilibrium scour depth for A) *Phragmites* stems and B) Cottonwood or Reed canarygrass stems at RM 210.6..... 72

Figure 44. Flow record from gage 06700000 Platte River near Odessa. 73

Figure 45. Velocities relating to the ability of drag forces to uproot patches of one-year old cottonwoods. 75

Figure 46. Velocities relating to the ability of drag forces to uproot patches of two-year old cottonwoods. 76

Figure 47. Velocities relating to the ability of drag forces to uproot patches of Reed canarygrass..... 77

Figure 48. Velocities relating to the ability of drag forces to uproot patches of *Phragmites*. 78

Figure 47. Time to reach equilibrium scour depth for *Phragmites* stems at RM 228.7..... 114

LIST OF TABLES

Table 1. Experimental matrix for flume study.....	27
Table 2. Summary of the input parameters that are required for the Monte Carlo version of the RipRoot model (modified from Thomas and Pollen-Bankhead, 2010), reasons each parameter is required and method of measurement.....	32
Table 3. Basic geometric properties of stems tested for flexibility.....	33
Table 4. Minimum, maximum and mean forces for stem bending measured in the field.*Greater than 20 samples were tested but some were removed from the analysis where orientation of bending and direction of flow did not match.....	35
Table 5. Input parameters for RipRoot modeling.....	53
Table 6. Recurrence intervals of flows at USGS gages 06770000, 06770200, and 06768000 calculated by the authors using Log-Pearson III analysis.....	73

1 BACKGROUND AND PROBLEM STATEMENT

In planform, rivers exhibit a continuum of form with three end-members: braided, meandering and straight (Leopold and Wolman, 1957). A number of definitions of the term ‘braided river’ have appeared in the literature. Friedkin (1945: 16) noted that rivers are described as braided when “the channel is extremely wide and shallow and the flow passes through a number of small interlaced channels separated by bars”. The most commonly cited definitions are those of Lane (1957) and Leopold and Wolman (1957). Combining these definitions, a braided river can be defined as one that “flows in two or more anastomosing channels around alluvial islands” (Leopold and Wolman, 1957: 53) “presenting from the air the intertwining effect of a braid” (Lane, 1957: 88).

Classically, braiding has been associated with a combination of factors such as high slope, abundant bedload, coarse grain size, and flashy discharge (e.g. Leopold and Wolman, 1957; Schumm and Khan, 1972; Fredsøe, 1978; Schumm et al., 1987). Conversely, Friedkin (1945) noted that in his laboratory tests conducted at constant discharge, braiding resulted even when no sand was fed at the entrance of the flume, provided that the banks were readily eroded. Paola (2001: 22) stated that braiding “is the fundamental instability of streams flowing in noncohesive material.” Channels formed in material with little or no cohesion or vegetative stability to restrict channel widening tend to braid (e.g. Simpson and Smith, 2001). Those with cohesive banks (Thorne and Abt, 1993) and/or vegetation (Mosley, 2001) become progressively more sinuous (i.e. meandering) or anastomosed (Smith and Smith, 1980; Nanson and Knighton, 1996), especially if there is some base-level control.

These latter points are of significant importance for the present study. The diversion and storage of water for agricultural, municipal and industrial uses has caused significant alteration of the hydrologic regime of the central Platte River. High flows occur less frequently, mean low flows have been elevated, and there has been a decrease in sediment supply (Williams, 1978; Hadley et al., 1987). Data from USGS gauge 06768000 (Platte River near Overton, NE) show that between 1920 and 2009, decadal-average annual peak flows declined from $527 \text{ m}^3\text{s}^{-1}$ to $106 \text{ m}^3\text{s}^{-1}$. Exposed sand bars have, therefore, been progressively colonized by vegetation, leading to the formation of semi-permanent islands, and narrowing of the braided, wide and shallow channels of the Platte by 30-90% (Williams, 1978; Figure 1).

The Platte River Recovery Implementation Program (Program) was initiated early in 2007 to address the issue of declining habitat availability for endangered bird species. Specifically, the Program seeks to maintain and create habitat for whooping crane, least tern, and piping plover. To fulfill this objective, it is necessary to reduce the occurrence of mature vegetation on sandbars within the Platte River. Creative ways are therefore being sought to remove vegetation from in-channel sand bars and then manage future re-colonization. At present, these tasks are undertaken through disking and spraying of vegetation. As a more cost and time efficient alternative, it has been suggested that Short Duration High Flows (SDHFs) might be able to remove vegetation from these in channel bars. The purpose of this study is to investigate whether flows of up to 8,000 cfs would indeed be capable of playing a role in removing vegetation, and/or managing future re-colonization following vegetation removal.

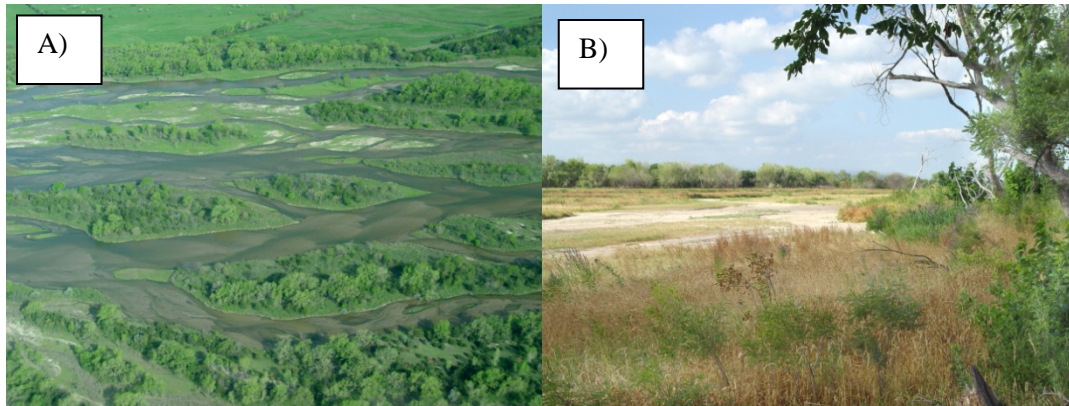


Figure 1. A) Low-level aerial view of the Platte River. Note significant cottonwood establishment. B) Dry south channel of the Platte River. Note establishment of grasses on mid-channel bars. Images courtesy of Will Graf.

Determining the effectiveness of in-stream flows for removing vegetation is a matter of quantifying the driving forces provided by the flow acting on the channel boundary (predominantly sand and gravel) and modified by the drag provided by the above-ground biomass, and the resistance of the boundary as modified by the additional resistance provided by roots and/or rhizomes (Figure 2). The driving force acting on a plant is controlled by the flow depth and velocity, the drag coefficient of the plant species being studied, and the flexibility of the plant. Measurement of these above-ground vegetation properties allows for calculation of the force being applied to the below-ground structure of the plants. The roots of a plant act to anchor the plant into the substrate. To measure resisting forces of individual plants of different ages and species it is therefore necessary to measure the tensile strength of the plant roots (resistance to rupture or pullout), stems (and rhizomes where applicable), the geometric properties of the roots (e.g. root diameter and maximum rooting depth), and number of roots. This data, along with substrate properties, can then be used to model the range of plant resistances that might occur within a given reach of the river. Where the driving force acting on a given plant, or patch of plants, exceeds the resisting force provided by the roots or stems of the same plant, or patch of plants, vegetation removal will be initiated.

It therefore follows that for a plant to be removed from its substrate either: 1. the roots, rhizomes and/or stems of the plant must be snapped or pulled from the substrate by the force acting on the above-ground part of the plant by the flow of water or ice; or 2. the sediment surrounding the roots of the plant must be scoured sufficiently by water or ice for the plant to simply be washed away. As the force required to remove a plant from its substrate changes over time according to rooting, and/or burial, depth (Ennos, 1990; Pollen-Bankhead et al., in press), the driving force required to remove a particular plant from its substrate may actually occur at some point along the continuum between these two alternatives (Figure 3), with the depth of scour required for plant removal being dependent on the local properties of the substrate and the properties of the roots of the plant in question.

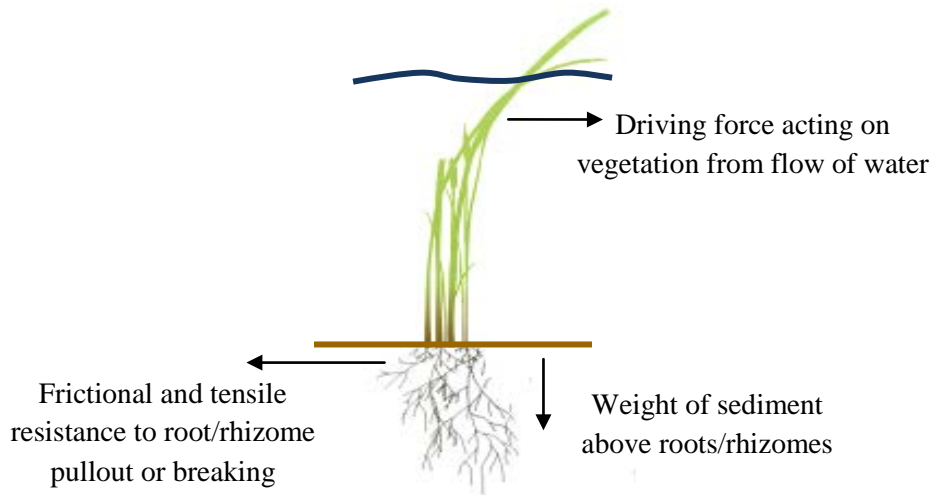


Figure 2. Driving and resisting forces acting on submerged vegetation.

1.1 Aim and objectives

The overall project aim is to determine the potential for short duration, high flows of varying magnitude and duration to uproot early succession species growing on bars within the Platte River, as part of the Program's Flow-Sediment-Mechanical (FSM) strategy. To accomplish this aim, a series of objectives have been identified:

- 1) Quantify the driving forces acting on different vegetation types at different flow depths/ discharges;
- 2) Quantify changing plant resistance to removal by flow with increasing scour of sediment;
- 3) Quantify the depth of substrate scour that would occur during flows of different magnitude and duration;
- 4) Quantify root and rhizome parameters required to calculate the resistance of different plant species (*Phragmites australis*; *Populus deltoides*; *Phalaris arundinacea*) of varying ages and plant densities, to removal by the flow of water in the Platte River; and
- 5) Determine what magnitude-duration of flow is required to remove plants of various species and ages from bars of the central Platte River.

The species to be tested were agreed upon between the authors and PRRIP, and were selected based on both their prevalence, and the desire to learn more about management options for these species, in particular, *Phragmites* and Reed canarygrass. These species establish easily on bars in the Central Platte river system, and can develop thick stands that can be detrimental to the availability of habitat for whooping crane, least tern, and piping plover.

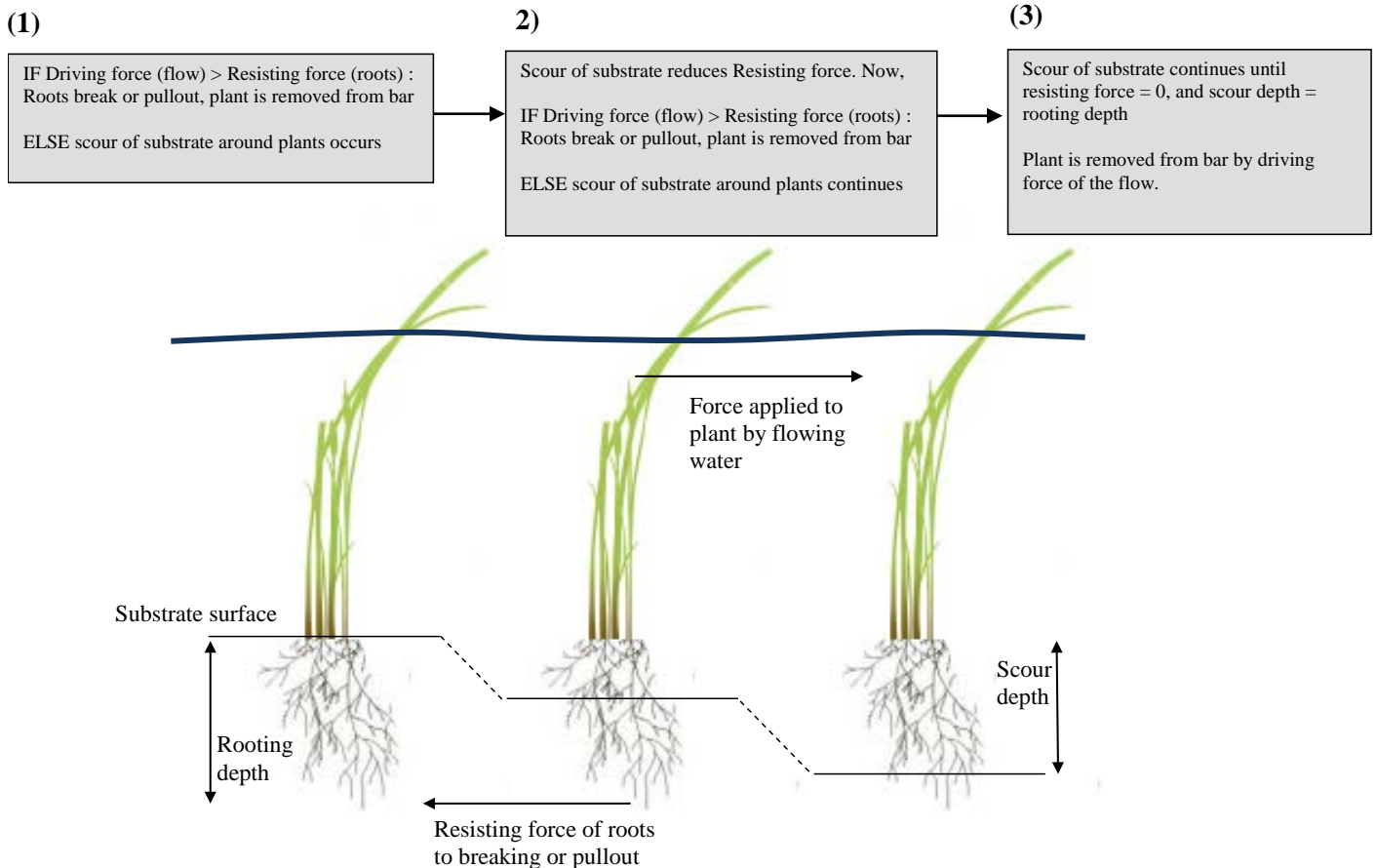
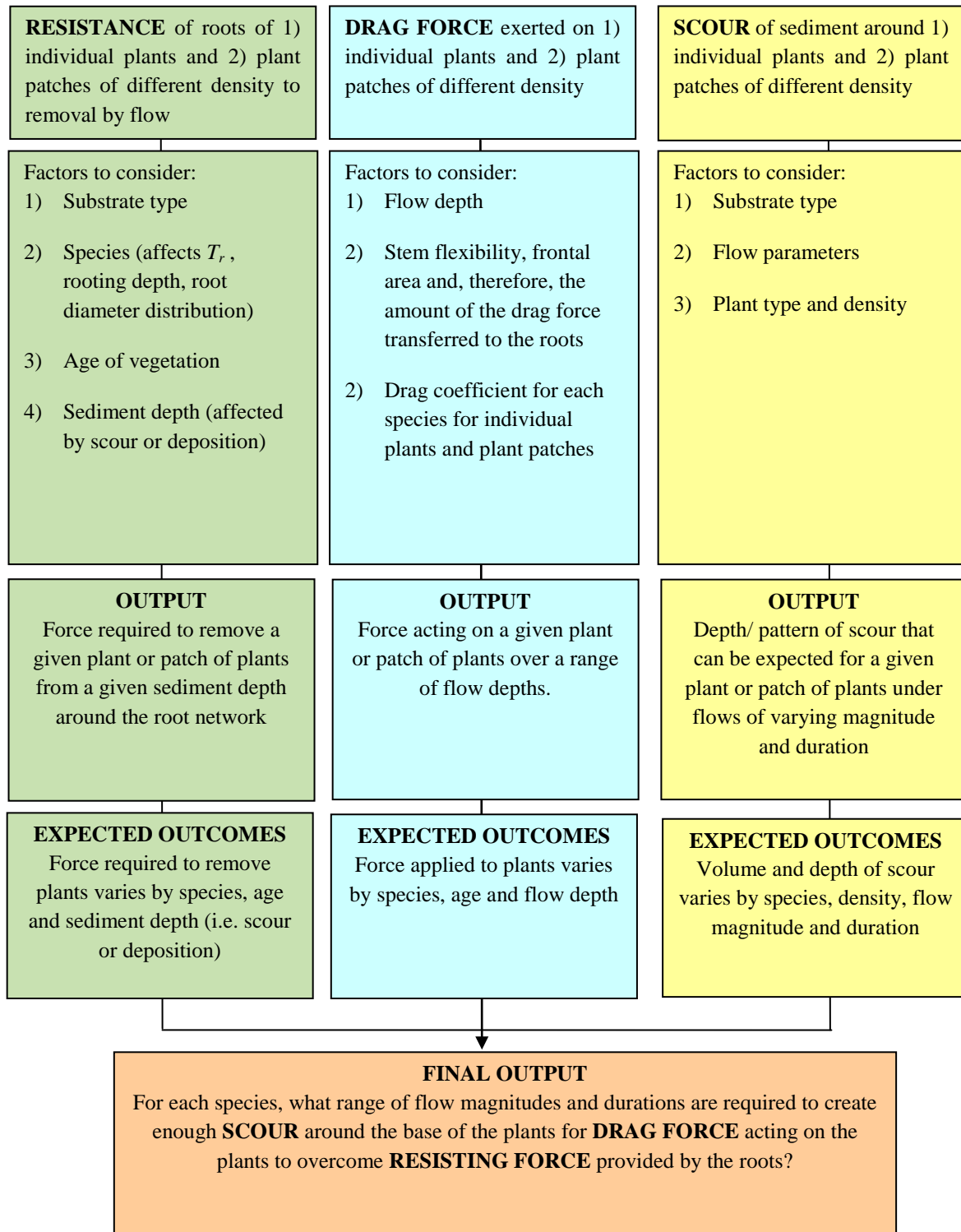


Figure 3. Continuum of processes for plant removal showing possible scenarios for balance of driving forces (flow) and resisting forces (roots). At the left end of the figure (1), driving force exceeds root strength and the plant can be removed without scour of the substrate. At the right end of the figure (3), scour has reduced the resisting force of the roots to zero, and the plant is removed by the force of the flow. In reality plant removal is likely to occur at some point between (1) and (3) at a point (2) along the continuum where scour has reduced the resisting force of the roots to a point where the flow can remove the plant from its substrate.

The following flow chart provides a visual aid for understanding the structure of this study. The three parts of the study include fieldwork to 1) measure the resistance of plants to uprooting(resisting force), 2) flume experiments to measure the drag force acting on the different plants (driving force), and 3) calculations of local scour around vegetation stems and the effect of this on the balance between the driving and resisting forces. Finally, all three parts of the study will be brought together to determine whether sdhfs of up to 8,000 cfs as planned by prrip will lead to vegetation removal through scour and drag forces alone, or whether mechanical removal of vegetation will be necessary to clear bars and improve habitat.



2 QUANTIFYING DRIVING AND RESISTING FORCES ACTING ON VEGETATION: THEORY

2.1 Driving forces

In recent years, a significant amount of work has been undertaken to study the interaction between immersed vegetation and the water around it (e.g. Li and Shen, 1973; Petryk and Bosmajian 1975; Bertram 1984; Pasche and Rouvé, 1985; Fathi-Moghadam and Kouwen, 1997; Nepf, 1999; Freeman et al. 2000; López and García, 2001; Bennett et al., 2002; Stone and Shen 2002; Järvelä 2002; 2004; Wilson et al., 2003; 2006; McBride et al. 2007; White and Nepf 2008). Most researchers have commenced with consideration of the fundamental equations describing the time-averaged turbulent flow of an incompressible fluid (Equation 1; López and García, 2001). For a unit volume of water, the change in fluid momentum in all three directions is balanced by the gravitational force acting on that unit volume of water:

$$\frac{\partial}{\partial x} \left(\mu \frac{\partial \bar{u}}{\partial x} - \overline{\rho u' u'} \right) + \frac{\partial}{\partial y} \left(\mu \frac{\partial \bar{u}}{\partial y} - \overline{\rho u' v'} \right) + \frac{\partial}{\partial z} \left(\mu \frac{\partial \bar{u}}{\partial z} - \overline{\rho u' w'} \right) + \rho g h S_0 = 0 \quad (1)$$

where ∂ = partial differential operator, μ = dynamic viscosity of water ($\sim 1.4 \times 10^{-3}$ N s m⁻²), ρ = mass density of water (~ 1000 kg m⁻³), g = acceleration due to gravity (~ 9.81 m s⁻²), h = flow depth (m), S_0 = bed slope (m m⁻¹), and u , v and w = instantaneous velocities (m s⁻¹) in the along-stream (x), across-stream (y) and vertical (z) directions, respectively. Overbars represent time-averaged values and primes refer to fluctuations about these values.

López and García (2001) argue that the first and second terms of Equation 1 are dominated by the third and fourth terms so that only those terms need to be retained (López and García, 2001):

$$\frac{\partial}{\partial z} \left(\mu \frac{\partial \bar{u}}{\partial z} - \overline{\rho u' w'} \right) + g h S_0 = 0 \quad (2)$$

Further, Equation 2 also needs to be averaged in a horizontal plane to properly represent the flow through vegetation in a one-dimensional frame (López and García, 2001):

$$\frac{\partial}{\partial z} \left(\mu \frac{\partial U}{\partial z} - \overline{\rho U' W'} \right) - \frac{1}{2} C_D \rho a U^2 + g h S_0 = 0 \quad (3)$$

where the uppercase U and W denote time- and space- (in a horizontal plane) averaged velocities, C_D = dimensionless drag coefficient, and a = frontal area of vegetation per unit volume of fluid (m⁻¹).

This averaging process has, therefore, introduced an additional term into Equation 3 that accounts for the effects of vegetation:

$$\frac{F_D}{V} = \frac{1}{2} C_D \rho \alpha U^2 \quad (4)$$

where F_D = drag force (N), V = volume of fluid in which vegetation is immersed (m^3). Equation 4 may also be applied to patches of vegetation by using the appropriate area and a reduced C_D value (e.g. Nepf, 1999).

García et al. (2004) rearranged Equation 3 to obtain an equation for the drag coefficient, C_D , in a horizontal plane:

$$C_D = 2 \frac{ghS_0 + \frac{\partial}{\partial z} \left(\mu \frac{\partial U}{\partial z} - \rho \overline{U'W'} \right)}{\rho \alpha U^2} \quad (5)$$

They note that Equation 5 provides a means of estimating vertical profiles of the drag coefficient by measuring the channel slope, the obstruction density and profiles of the mainstream velocity and dominant Reynolds stress in steady, uniform flows.

Dunn et al. (1996), showed that in a one-dimensional frame of reference, Equation 3 could be further reduced, yielding a backwater curve for open-channel flow through emergent vegetation. They found that the mean drag coefficient, $\overline{C_D}$, for patches of vegetation could be estimated using:

$$\overline{C_D} = 2gh \frac{S_0 - S_f - \frac{dh}{dx} \left(1 - \beta \frac{[Q/A]^2}{gh} \right)}{ah\beta [Q/A]^2} \quad (6)$$

where S_f = friction slope estimated using Manning's equation, Q = flow discharge (m^3s^{-1}), A = flow area (m^2) and β = a coefficient accounting for the vertical distribution of the streamwise velocity ($\approx 1 + gn^2/R^{2/3}\kappa^2$ if the von Kàrmàn-Prandtl law of the wall holds throughout the flow depth; Falconer, 1993; Lin and Falconer, 1997; Falconer *et al.*, 2005), n = Manning's roughness coefficient ($\text{s m}^{-1/3}$), R = hydraulic radius (m), and κ = von Kàrmàn constant (≈ 0.33 in suspended sediment-laden flows; Bennett *et al.*, 1998).

Therefore, the primary mechanism by which flowing water exerts a force upon vegetation is through drag. Submerged or emergent vegetation reacts to the drag exerted by water by either remaining erect, oscillating in response to turbulent fluctuations, or bending. The magnitude of the drag force is a function of plant flexibility, frontal projected area, relative depth of submergence, and density (Li and Shen, 1973; Petryk and Bosmajian 1975; Pasche and Rouvé, 1985; Fathi-Moghadam and Kouwen, 1997; Nepf, 1999; Freeman et al. 2000; Bennett et al., 2002; Stone and Shen 2002; Järvelä 2002; 2004; Wilson et al., 2003; 2006; White and Nepf 2008), which may all vary by plant type and age. According to Newton's Second

Law, vegetation must also affect the flow patterns. It does so by adding roughness and hence reducing the velocity in vegetated areas, introducing turbulence and inducing scour along the vegetation-channel interface, and forcing flow back towards the open channel (Bertram 1984; McBride et al. 2007; White and Nepf 2008).

2.2 Resisting forces

The force required to remove a plant from its substrate before the entire root ball has been scoured out by water or ice is a function of a number of variables, including the number of roots, the strength and diameter distributions of those roots, and the orientation of those roots (Wu et al., 1979; Waldron and Dakessian, 1981; Greenway, 1987; Gray and Sotir, 1996; Simon and Collison, 2002; Pollen and Simon, 2005; Pollen-Bankhead and Simon, 2009). The elastic (Young's) moduli of the roots, antecedent soil and root moistures, and frictional forces between the soil and roots have also been shown to be important (Pollen, 2007; Fan and Su, 2008).

In simplest terms, the force required to break an individual root is given by:

$$F_b = A_r T_r \quad (7)$$

where F_b = root breaking force (N), A_r = the cross-sectional area of the root at the point of rupture (mm^2), and T_r = tensile strength of the root (MPa).

The force required to pull an individual root out of the soil without breaking is a function of the surface area of the root embedded within the soil and the cohesive and frictional resistance developed between the root and soil and can be represented by:

$$F_p = \pi D_r L_r \tau_f f \quad (8)$$

where F_p = root pullout force (N), D_r = diameter of the root (m), L_r = rooting depth (~length) of the root (m), f is the dimensionless coefficient of friction between soil and wood, which ranges from 0.7 to 0.9 (Potyondy, 1961; Gray and Sotir, 1996: 82) and τ_f = shear strength of the soil (Pa), given by (Fredlund et al., 1978):

$$\tau_f = c' + (\sigma - \mu_a) \tan \phi' + (\mu_a - \mu_w) \tan \phi^b \quad (9)$$

where c' = effective cohesion (Pa), σ = normal force acting on the outside skin of the root (Pa), μ_w = pore-water pressure (Pa), ϕ' = effective angle of internal friction ($^\circ$), μ_a = pore-air pressure (Pa) and ϕ^b = angle representing the increase in shear strength for an increase in matric suction ($^\circ$).

Equations 7 and 8 quantify the forces required to either break or pullout an individual root, but to correctly model the reinforcement provided by an entire root ball or root bundle, we must also consider the mechanism by which a force is applied to, and distributed amongst, multiple rather than individual roots. Until recently, the most common method for predicting root-reinforcement based on root tensile strength values were simple perpendicular root models, such as that of Wu et al. (1979):

$$\Delta S = 1.2 RAR \sum_{j=1}^{j=J} T_{r_j} \quad (10)$$

where ΔS = root-reinforcement (Pa), 1.2 is a factor that accounts for the orientation of roots, RAR = the ratio of the cross sectional area of the roots divided by the area of the shearing surface (dimensionless), T_r = root tensile strength (Pa), and the subscript j identifies the j^{th} root out of J roots.

In the Wu et al. (1979) approach, the tensile strengths of all the roots are summed. This assumes that the full tensile strength of each root is mobilized during soil shearing, and that the roots all break simultaneously (Waldron and Dakessian, 1981; Greenway, 1987; Pollen et al., 2004; de Baets et al., 2008). In reality, roots break progressively as a load is applied to a root ball, thereby reducing the overall load that can be supported by the root ball. Pollen et al. (2004) and Pollen and Simon (2005) showed that the use of simple perpendicular models such as that of Wu et al. (1979) can overestimate the actual load that can be supported by a given number of roots by an order of magnitude. In response to this finding, a new model, RipRoot, was developed (Pollen and Simon, 2005; Pollen, 2007) that incorporated a progressive breaking algorithm developed from the fiber bundle models of the materials sciences (Daniels, 1945; Hidalgo et al., 2001). Fiber bundle models work by apportioning the total load applied to a bundle of fibers and then monitoring whether the load applied to a fiber exceeds its strength. In RipRoot, when a load was applied to the root ball, it was apportioned equally between all the intact roots. The maximum load that could be supported by the root ball corresponded not to the weakest or strongest root, but to one of the roots in the middle (Thomas and Pollen-Bankhead, 2010). RipRoot was validated using direct-shear tests of soils permeated with various densities of switchgrass roots (Pollen and Simon, 2005), and was shown to provide much more accurate comparisons to measured data.

To account for some of the remaining inaccuracies, Pollen (2007) included root pullout as an alternative failure mechanism. In this approach, it was assumed that the normal force acting upon the outside skin of roots was zero and that all soil strength was due to effective cohesion and matric suction. Pullout was shown to be particularly important for shorter roots and in soils with lower cohesion (Pollen, 2007), such as those with a high sand content like the Platte River. Thomas and Pollen-Bankhead (2010) included the effects of friction between the root and the soil by computing the normal force using Rankine's active earth-pressure theory (Terzaghi and Peck, 1967: 193-200). In addition, Thomas and Pollen-Bankhead (2010) used RipRoot in a Monte Carlo simulation framework in order to model potential variability in plant areal densities, root diameter distributions and root lengths. Monte Carlo simulations hence provide a mechanism by which to test and validate the sensitivity of the various input parameters and to reduce uncertainty in predicted erosion thresholds.

Since the publication of RipRoot by Pollen and Simon (2005), the use of progressive breaking algorithms such as the one used in the RipRoot model has become the method of choice for many studies of root-reinforcement (e.g. Docker and Hubble, 2008; Loades et al., 2009; Mickovski et al., 2009; Schwarz et al., 2010). Although the model was originally developed for use with slope and streambank stability models, the model output provides the maximum load that can be supported by a given number of roots. In the case of a streambank, for example, the maximum load that can be supported by the roots is then applied to

the area of the bank the roots are growing in, to give an additional cohesion due to roots per unit area of streambank. In the case of plant removal from a substrate, the maximum load the roots of a given plant are predicted to be able to support can be directly compared to the force that is applied to that plant by the flowing water. This would provide the threshold driving force required to exceed the resisting force.

2.2.1 Scour around the stems of plants

As flowing water approaches a plant stem, water piles up on the upstream side of the stem and flow is accelerated around it, causing the formation of horseshoe vortices (Figure 4; Richardson and Davis, 2001). As bed material is progressively scoured, the strength of horseshoe vortices reduce and eventually equilibrium is reached and scouring ceases (Richardson and Davis, 2001). In addition to horseshoe vortices that form around the base of the stem, vertical vortices, called wake vortices, form downstream of the stem (Figure 4). Both horseshoe and wake vortices may remove material from around the base of the stem. The ability of a fluid to erode non-cohesive sediment (e.g. sand and gravel) is dependent upon both the properties of the fluid (i.e. its density, viscosity and velocity) and the properties of the sediment, such as its size, shape, density and arrangement (Knighton, 1998). Shields (1936) conducted laboratory flume studies examining incipient motion and bed-load transport of non-cohesive, nearly uniform grains. The dimensionless critical shear stress, which appears on the y-axis of the Shields diagram (Figure 5), is defined as:

$$\tau_c^* = \frac{\tau_c}{g(\rho_s - \rho)D_{50}} \quad (11)$$

where τ_c = critical shear stress (Pa), g = acceleration due to gravity (9.807 m s^{-2}), ρ_s = density of sediment (kg m^{-3}), and ρ = density of water (kg m^{-3}). The critical shear stress, τ_c , can be determined from $\tau_c = c_f \rho U^2$, where c_f = a non-dimensional bed roughness coefficient (~ 0.00416 for sand beds; Hanson and Cook, 1997) and U = flow velocity. τ_c^* can be interpreted as the ratio of the average drag force per unit area to the average gravitational force resisting motion per unit area. The critical roughness Reynolds number, which appears on the x-axis of the Shields diagram, is defined as:

$$\text{Re}_c^* = \sqrt{\frac{\tau_c^* (\rho_s - \rho) g D_{50}}{\rho}} \frac{D_{50}}{\nu} \quad (12)$$

where ν = kinematic viscosity of water ($\text{m}^2 \text{s}^{-1}$).

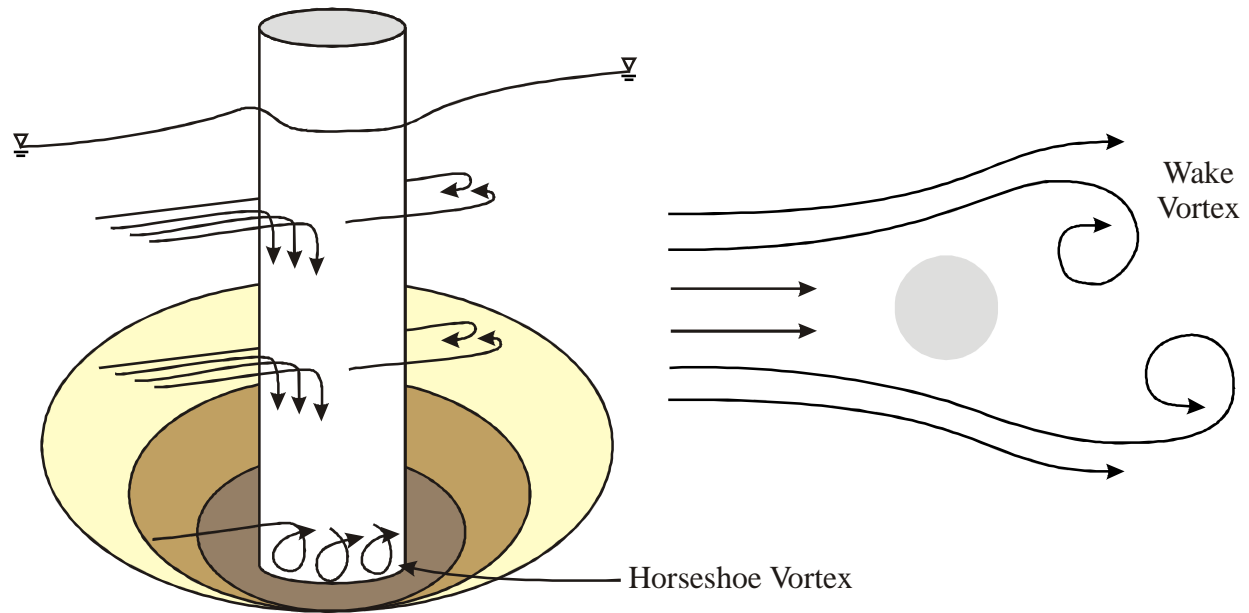


Figure 4. Schematic representation of scour around a plant stem (after Richardson and Davis, 2001 and Schnauder and Moggridge, 2009).

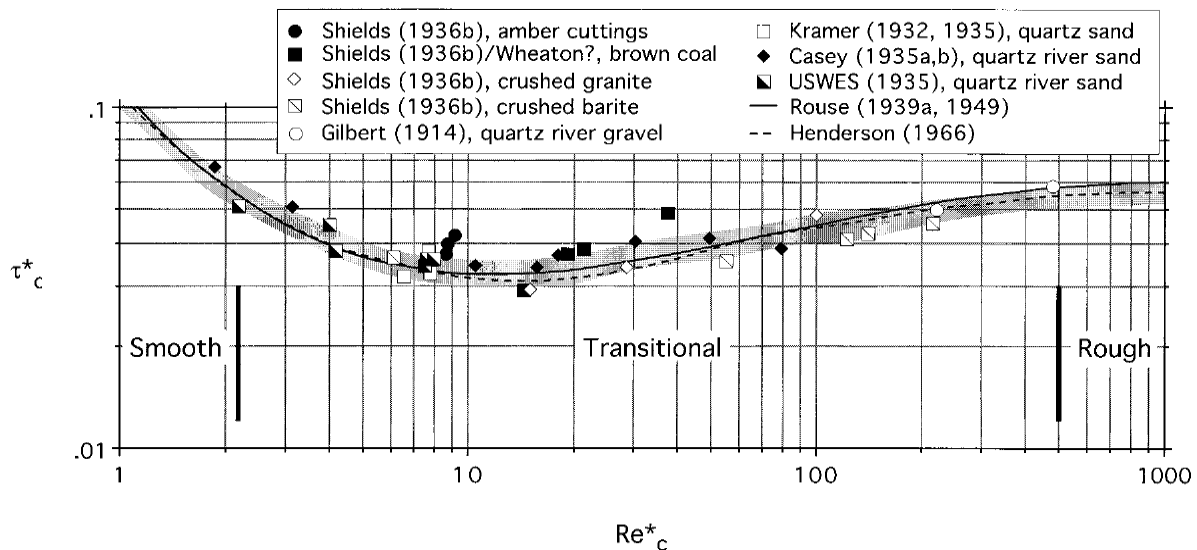


Figure 5. Shields diagram for incipient motion (modified from Buffington, 1999). The y-axis is defined by Equation 11 and the x-axis is defined by Equation 12.

The roughness Reynolds number is defined using the shear velocity, $u_* = \sqrt{\tau_o/\rho}$, as the velocity scale and the particle diameter as the length scale. At the onset of motion, $\tau_o \approx \tau_c$ and Equation 12 is obtained. Re_c^* can be interpreted as being proportional to the ratio between the particle size and the thickness of the viscous sublayer, and therefore its value indicates the extent to which particles protrude into the turbulent boundary layer.

Following the discussion above, the factors which affect the magnitude of local scour depth around bridge piers are (Richardson and Davis, 2001):

1. the velocity of the approach flow;
2. the depth of flow;
3. the stem diameter;
4. the size and gradation of bed material;
5. the bed configuration (in the sense of ripples, dunes, plane bed, antidunes or bars); and
6. ice formation or jams and debris.

The formation of horseshoe and wake vortices around the stem of a plant and their role in scouring sediment from the base of stems is similar to that around bridge piers (e.g. Richardson and Davis, 2001); although bridge piers are solid, inflexible and impermeable, the use of equations commonly used to estimate scour around piers can also be used to conceptualize scour at the base of a plant stem. The results calculated from such bridge pier scour equations will provide upper limits for potential scour depths as it could be expected that rigid, impermeable objects would create larger horseshoe and wake vortices than flexible porous stems that can in some cases bend to protect the substrate beneath. In addition, plant stem density affects the flow velocities, drag coefficients and sediment transport characteristics measured within and around the stems (Tanino and Nepf, 2008; Zong and Nepf, 2010).

It is commonly assumed that a functional relationship, \mathfrak{F} , can be established between the equilibrium scour depth, y_s , and the fluid density, ρ , the fluid kinematic viscosity, ν , the mean flow velocity, U , the flow depth, h , the sediment density, ρ_s , the median grain size of the bed sediment, d_{50} , the geometric standard deviation of the sediment, σ_g , the acceleration due to gravity, g ($\approx 9.807 \text{ m s}^{-2}$), and the pier diameter, b :

$$y_s = \mathfrak{F}\{\rho, \nu, U, h, \rho_s, d_{50}, \sigma_g, g, b\} \quad (13)$$

In applying this functional relationship to the stems of vegetation, the mean stem diameter is assumed to be equivalent to the bridge pier diameter.

If it is assumed that: 1. flows are highly turbulent, which is the case in most rivers, 2. the ratio between the densities of sediment and water are approximately constant, and 3. sediment gradation effects can be ignored in the mixed sand and fine gravel substrate of the Platte, this relationship can be rewritten in terms of three non-dimensional parameters:

$$\frac{y_s}{b} = \mathfrak{F}\left\{\frac{U^2}{gd_{50}}, \frac{h}{b}, \frac{d_{50}}{b}\right\} \quad (14)$$

These three parameters describe the ability of the flow to entrain particles from the bed, the relative flow depth and the relative sediment size. In the sections that follow, we outline four methods by which the functional relationships $\mathfrak{F}\left(\frac{U^2}{gd_{50}}\right)$, $\mathfrak{F}\left(\frac{h}{b}\right)$, and $\mathfrak{F}\left(\frac{d_{50}}{b}\right)$ have been described.

2.2.1.1 *Froehlich (1988).*

Froehlich (1988) wrote Equation 14 as:

$$\frac{y_s}{b} = 0.32 \left(\frac{U^2}{gd_{50}} \right)^{0.1} \left(\frac{h}{b} \right)^{0.36} \left(\frac{d_{50}}{b} \right)^{0.02} \quad (15)$$

2.2.1.2 *Melville and Sutherland (1988).*

Melville and Sutherland (1988) defined $\mathfrak{F} \left(\frac{U^2}{gd_{50}} \right)$ as:

$$\mathfrak{F} \left\{ \frac{U^2}{gd_{50}} \right\} = \frac{[U - \max(U_a - U_c, 0)]}{U_c} \quad (16)$$

where U_c = threshold mean flow velocity to entrain sediment of size d_{50} , U_a = threshold mean flow velocity to entrain sediment of size $d_{max}/1.8$, and d_{max} is the maximum size of sediment particles sampled from the bed. Both U_c and U_a are obtained by extracting the appropriate critical shear velocity, u_{*c} , from Shields' diagram (Figure 5) and then assuming that the vertical profile of the mean flow velocity, U can be approximated by the logarithmic law of the wall (see Melville and Sutherland, 1988 for details). U_a is reduced by a factor of 0.8 to account for the effects of sediment being transported either in suspension or as bedload (Melville and Sutherland, 1988).

Melville and Sutherland (1988) defined $\mathfrak{F} \left(\frac{h}{b} \right)$ as:

$$\begin{aligned} \mathfrak{F} \left(\frac{h}{b} \right) &= 1.0, & \text{if } h/b \geq 2.6 \\ \mathfrak{F} \left(\frac{h}{b} \right) &= 0.78 \left(\frac{h}{b} \right)^{0.255}, & \text{if } h/b < 2.6 \end{aligned} \quad (17)$$

Melville and Sutherland (1988) defined $\mathfrak{F} \left(\frac{d_{50}}{b} \right)$ as:

$$\begin{aligned} \mathfrak{F} \left(\frac{d_{50}}{b} \right) &= 1.0, & \text{if } b/d_{50} \geq 25 \\ \mathfrak{F} \left(\frac{d_{50}}{b} \right) &= 0.57 \log \left(2.24 \frac{b}{d_{50}} \right), & \text{if } b/d_{50} < 25 \end{aligned} \quad (18)$$

2.2.1.3 HEC 18 (Richardson and Davis, 2001).

Richardson and Davis (2001) proposed a similar relationship to that of Melville and Sutherland (1988) during the development of HEC 18 for the Federal Highway Administration. The HEC 18 equation can be written as:

$$\frac{y_s}{h} = 2.0K_1K_2K_3\mathfrak{S}\left(\frac{d_{50}}{b}\right)\left(\frac{b}{h}\right)^{0.65}\left(\frac{U}{\sqrt{gh}}\right)^{0.43} \quad (19)$$

where K_1 and $K_2 = 1.0$ for the cases of both a single cylinder and a group of cylinders, and K_3 = a correction factor accounting for the scale of bedforms. Richardson and Davis (2001) defined K_3 as being equal to 1.1 if the largest bedform is less than 3.0 m in height, between 1.1 and 1.2 if the largest bedform height is between 3 and 9 m and as being equal to 1.3 if the largest bedform height is greater than 9 m.

Richardson and Davis (2001) defined $\mathfrak{S}\left(\frac{d_{50}}{b}\right)$ as:

$$\mathfrak{S}\left(\frac{d_{50}}{b}\right) = 1.0, \quad \text{if } d_{50} < 2 \text{ mm or } d_{95} < 20 \text{ mm}$$

$$\mathfrak{S}\left(\frac{d_{50}}{b}\right) = 0.4 \min \left[\max \left(\frac{U - U_{icd_{50}}}{U_{cd_{50}} - U_{icd_{95}}}, 0 \right)^{0.15}, 1 \right], \quad \text{otherwise} \quad (20)$$

where U_{cd_x} = threshold mean flow velocity for “incipient motion” of the grain size d_x , computed using $U_{cd_x} = 6.19h^{1/6}d_x^{1/3}$, and U_{icd_x} = threshold mean flow velocity for “incipient scour” in the accelerated flow region at the base of the stem for the grain size d_x , computed using $U_{icd_x} = 0.645\left(\frac{d_x}{b}\right)^{0.053} U_{cd_x}$.

2.2.1.4 Superposition of components method (Richardson and Davis, 2001).

In the fourth approach adopted for estimating the equilibrium scour depth around the base of plant stems, total scour is computed by separating the scour-producing components (Figure 6), determining the scour depth for each component and summing the results (Richardson and Davis, 2001):

$$y_s = y_{s \text{ stem}} + y_{s \text{ rb}} + y_{s \text{ r}} \quad (21)$$

where the subscripts *stem*, *rb* and *r* represent the components of scour due to the stem, root ball and roots, respectively. Here, we briefly outline the methodology detailed by Richardson and Davis (2001). The interested reader is referred to that publication for further information.

The stem scour component, $y_{s \text{ stem}}$, is computed as:

$$\frac{y_{s\ stem}}{h} = 2.0K_1K_2K_3K_b \mathfrak{S} \left(\frac{d_{50}}{b} \right) \left(\frac{b}{h} \right)^{0.65} \left(\frac{U}{\sqrt{gh}} \right)^{0.43} \quad (22)$$

where K_b = coefficient to account for the height of the stem above the bed and the shielding effect by the root ball overhang distance, f , in front of the stem (Figure 4). Richardson and Davis (2001) suggest that K_b can be estimated using:

$$K_b = 0.4075 - 0.0669 \frac{f}{b} - \left(0.4271 - 0.0778 \frac{f}{b} \right) \frac{H_{stem}}{b} + \left(0.1615 - 0.0455 \frac{f}{b} \right) \left(\frac{H_{stem}}{b} \right)^2 - \left(0.0269 - 0.012 \frac{f}{b} \right) \left(\frac{H_{stem}}{b} \right)^3 \quad (23)$$

The root ball component assumes that the root ball is essentially a solid mass of diameter $b+2f$ and thickness, T . Richardson and Davis (2001) envision two possible cases. First, the bottom of the root ball is above the bed and in the flow. Second, the bottom of the root ball is on or below the bed. In the first case, the root ball width, $b_{rb} = b+2f$, is reduced to an equivalent “full depth solid pier width” (Richardson and Davis, 2001), b_{rb}^* , using:

$$\frac{b_{rb}^*}{b_{rb}} = e^{-2.705 + 0.51 \ln \left(\frac{T}{y_{rb}} \right) - 2.783 \left(\frac{H_{rb}}{y_{rb}} \right)^3 + \frac{1.751}{e^{(H_{rb}/y_{rb})}}} \quad (24)$$

An adjusted flow depth, h_{rb} , and flow velocity, U_{rb} , are then used in Equation 25 to estimate the scour component:

$$\frac{y_{s\ rb}}{h_{rb}} = 2.0K_1K_2K_3 \mathfrak{S} \left(\frac{d_{50}}{b} \right) \left(\frac{b_{rb}^*}{h_{rb}} \right)^{0.65} \left(\frac{U_{rb}}{\sqrt{gh_{rb}}} \right)^{0.43} \quad (25)$$

where U_{rb} is computed as $U (h / h_{rb})$.

In the second case, the average velocity of the flow at the exposed root ball, U_{rb}^* , is estimated at a height of $h_{rb}^* = H_{stem} + y_{s\ stem} / 2$ above the bed using:

$$\frac{U_{rb}^*}{U_{rb}} = \frac{\ln(10.93 h_{rb}^* / k_s + 1)}{\ln(10.93 h_{rb} / k_s + 1)} \quad (26)$$

where k_s = grain roughness of the bed, which is normally taken as d_{84} for sand-sized bed material and $3.5d_{84}$ for gravel- and coarser-sized bed material, and d_{84} = grain size that 84 percent of the bed material is finer (Richardson and Davis, 2001). The scour component is then estimated using:

$$\frac{y_{srb}}{h_{rb}^*} = 2.0K_1K_2K_3\mathfrak{S}\left(\frac{d_{50}}{b}\right)\left(\frac{b_{rb}}{h_{rb}^*}\right)^{0.65}\left(\frac{U_{rb}^*}{\sqrt{gh_{rb}^*}}\right)^{0.43} \quad (27)$$

Herein, it is assumed that the component due to roots, $y_{s,r}$, is small relative to the other components and therefore, it is not computed.

2.2.1.5 Temporal development of scour.

Stein et al. (1993), Melville and Chiew (1999), and Briaud et al. (2001) present methods for estimating the fraction of the equilibrium scour depth that would be reached in a given duration of time. Herein, we adopt the method suggested by Melville and Chiew (1999):

$$\frac{y_t}{y_s} = e^{-0.03\left|\frac{U_c}{U}\ln\left(\frac{t}{t_{equilibrium}}\right)\right|^{1.6}} \quad (28)$$

where y_t = depth of scour reached during an event of duration t , and $t_{equilibrium}$ = time required to reach the equilibrium scour depth, in seconds. When $U_c > U$, $t_{equilibrium}$ was defined by Melville and Chiew (1999) as:

$$t_{equilibrium} = 4170000\left(\frac{b}{U}\right)\left(\frac{U}{U_c} - 0.4\right), \quad \text{if } h/b > 6$$

$$t_{equilibrium} = 2668800\left(\frac{b}{U}\right)\left(\frac{U}{U_c} - 0.4\right)\left(\frac{h}{b}\right)^{0.25}, \quad \text{otherwise} \quad (29)$$

The relationship between $t_{equilibrium}$ and U/U_c for $U > U_c$ was established by extracting data from Figure 8 of Melville and Chiew (1999). The data were fitted best by the relation $t_{equilibrium} = 2369080(b/U)(U/U_c)^{-3.6}$.

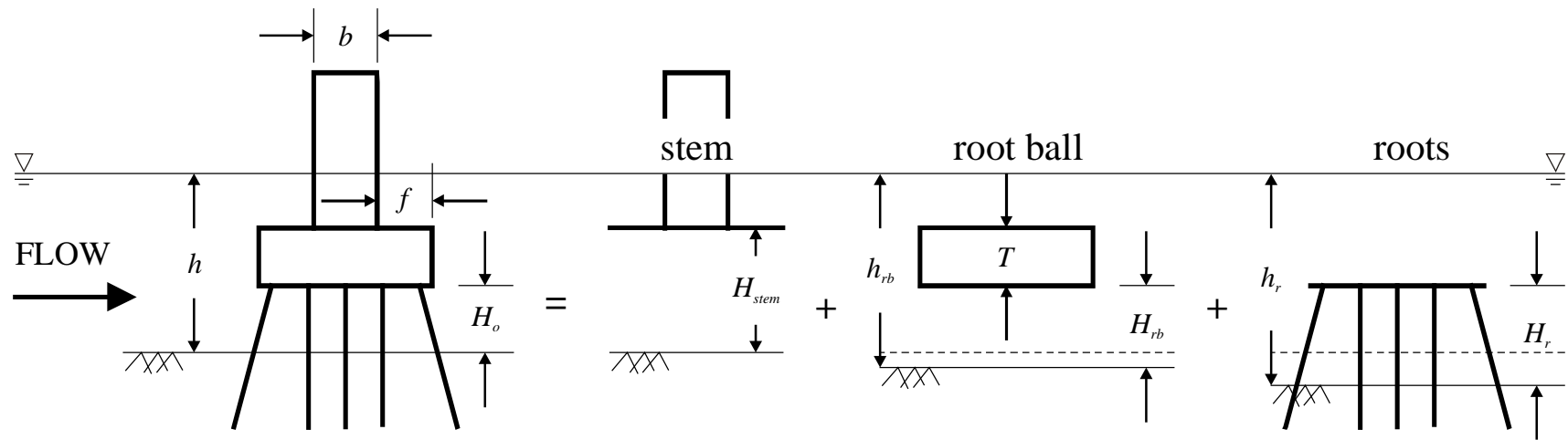


Figure 6. Conceptualization of vegetation scour problem as analogous to the bridge pier scour problem (modified after Jones and Sheppard, 2000).

The variables are defined as follows:

b = Stem diameter, m

f = Distance between the outer edge of the root ball and stem, m

H_o = Height of the root ball above the bed at the beginning of computation, m

$H_{stem} = H_o + T$ = Height of the stem above the bed before scour, m

$H_{rb} = H_o + y_{s\ stem}/2$ = Height of root ball after the stem scour component has been computed, m

$H_r = H_o + y_{s\ stem}/2 + y_{s\ rb}/2$ = Height of the root ball after the stem and root ball scour components have been computed, m

S = Center to center spacing between stems, m

T = Thickness of root ball, m

h = Approach flow depth at the beginning of computations, m

$h_{rb} = h + y_{s\ stem}/2$ = Adjusted flow depth for root ball computations, m

$h_r = h + y_{s\ stem}/2 + y_{s\ rb}/2$ = Adjusted flow depth for root computations, m

3 QUANTIFYING DRIVING AND RESISTING FORCES ACTING ON VEGETATION: METHODOLOGY

3.1 Study Sites

A range of sites were selected to find areas populated with *Phragmites australis*, up to 2 year old cottonwood seedlings (*Populus deltoides*), and Reed canarygrass (*Phalaris arundinacea*) (Figure 7). The locations of selected sites on the Platte River are given in Figure 8.

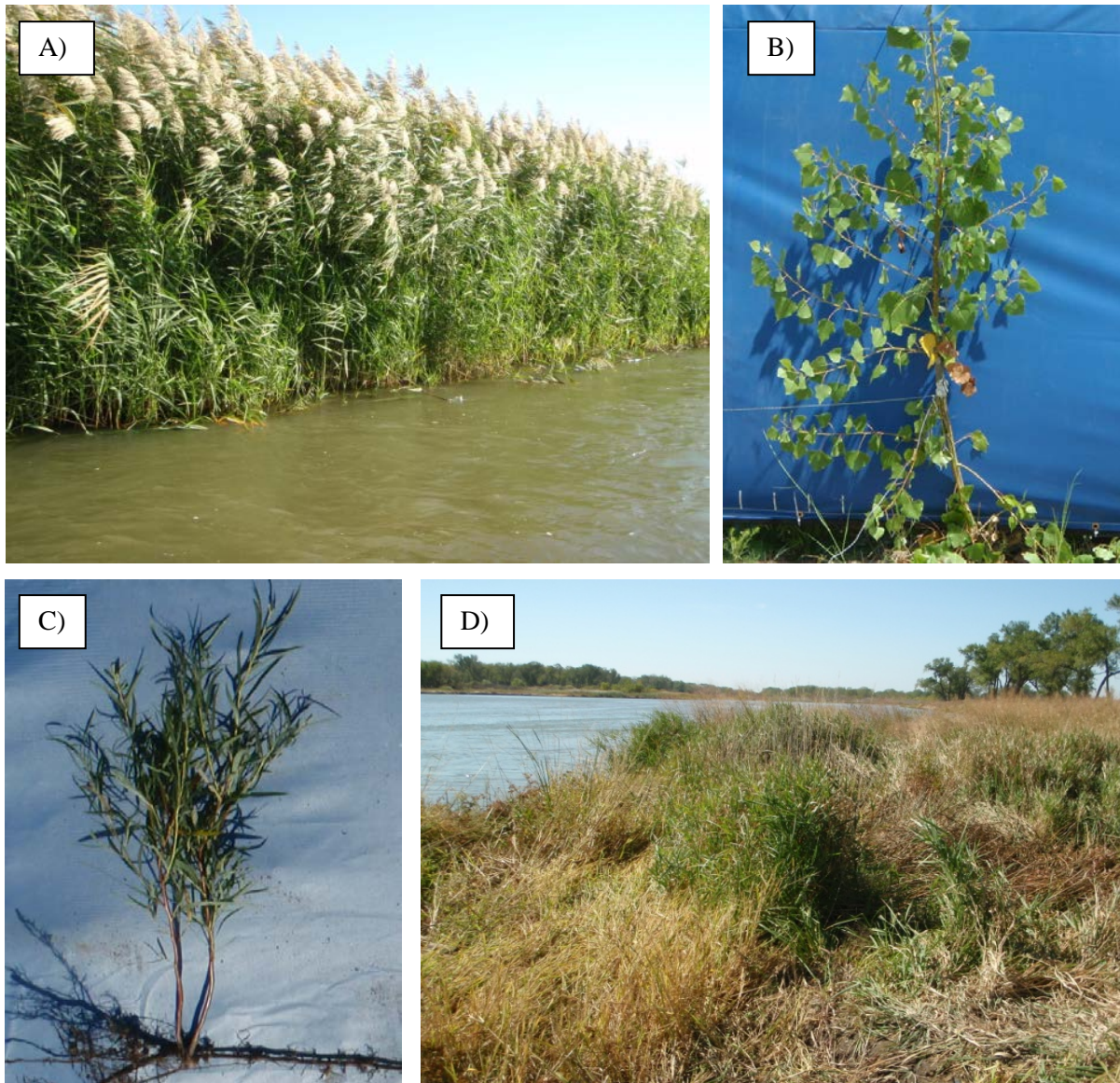


Figure 7. A) Stand of *Phragmites* growing on an in-channel sandbar, B) a 3 to 5-year old cottonwood tree, C) 1 to 2-year old sandbar willow tree excavated from a sandbar, D) Reed canarygrass growing at the channel edge.

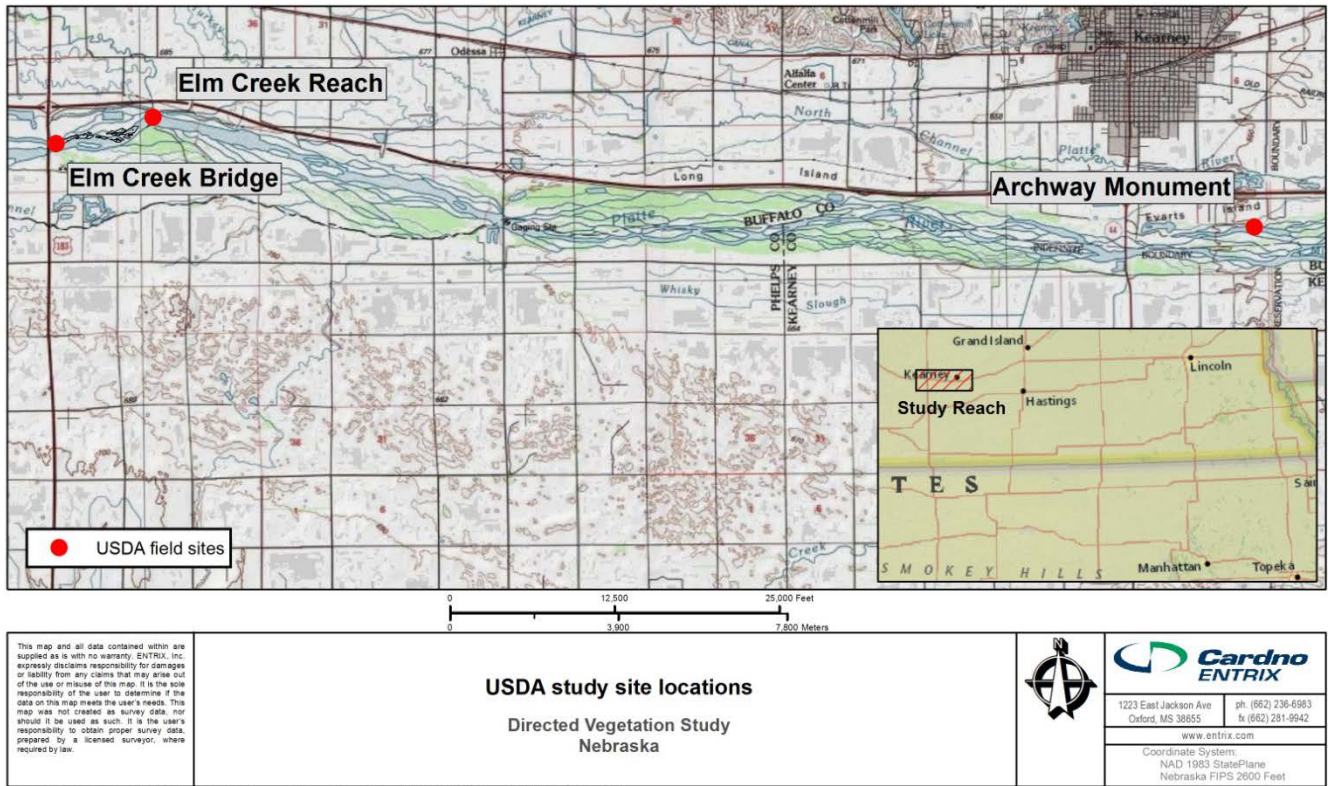


Figure 8. Map showing the location of the three vegetation study sites in this project.

The selection of these three sites was based on a number of factors:

- 1) Their location within the Elm Creek Complex, where PRRIP has extensive monitoring data, and plans to implement field scale adaptive management strategies to test flow hypotheses. Field data and model output could then be validated against the results of these field experiments;
- 2) The vegetation at these three channel bar sites, provided the species and age composition of vegetation agreed upon for testing between the authors and PRRIP;
- 3) The sites were all easily accessible with field equipment.

The areal density of each plant species (number of stems per unit area) were surveyed in five different locations, in order to inform flume experiments used to quantify the driving (drag) force and also for input to the RipRoot model to quantify the resistance of patches of plants of different densities to pullout. Testing and measurement protocols specific to the quantification of either the driving or resisting forces are detailed in the following sections.

3.2 Driving forces

As described in Section 2.1, the magnitude of the driving (drag) force acting upon the stem of a plant is a function of plant flexibility, frontal projected area, relative depth of submergence, and density (Li and Shen, 1973; Petryk and Bosmajian 1975; Pasche and Rouvé, 1985; Fathi-Moghadam and Kouwen, 1997; Nepf, 1999; Freeman et al. 2000; Bennett et al., 2002; Stone and Shen 2002; Järvelä 2002; 2004; Wilson et al., 2003; 2006; White and Nepf 2008), which may all vary by species and age. Quantifying the drag force is complicated by the fact that both the frontal area and the drag coefficient may vary depending upon the flexibility of the plant (which will vary by species and may also vary temporally), extent of submergence and the flow velocity, U (Figure 9). Herein, a coupled field and laboratory methodology has been adopted to quantify the drag force. First, a specially-designed and constructed apparatus was used to simultaneously monitor the angle to which the stem of a plant has been bent, the force required to bend that stem, and the resulting frontal area in the field. Second, a series of laboratory flume experiments were designed to estimate the drag coefficient of plant stems at different flow depths and velocities.

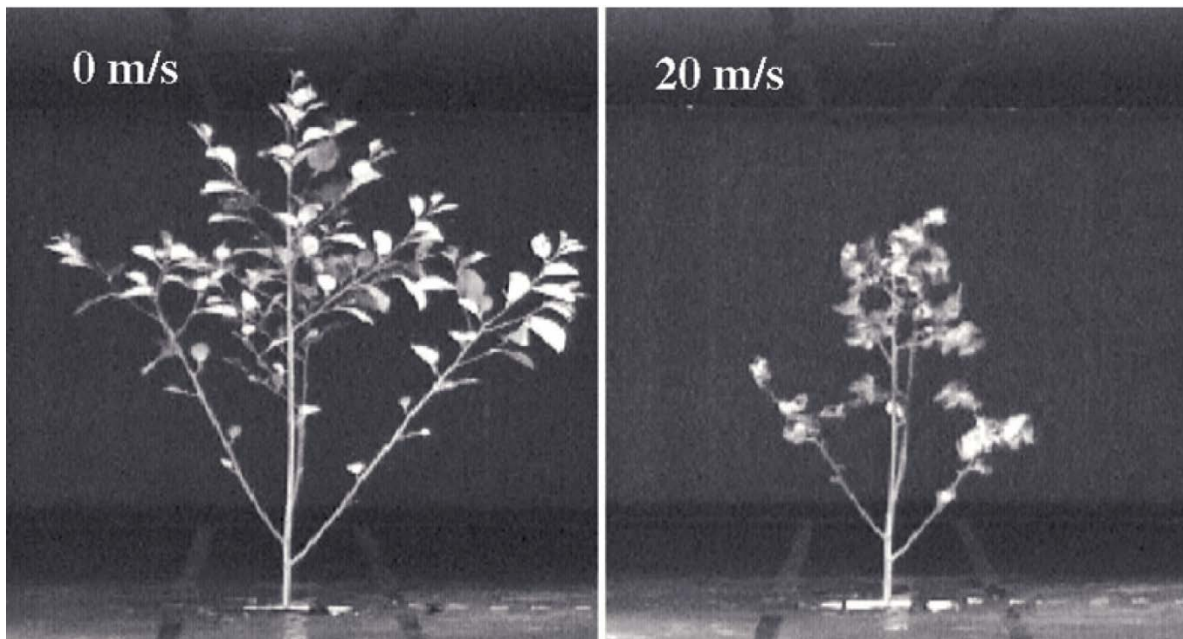


Figure 9. Frontal photographs of red alder at wind speeds of 0 and 20 m s⁻¹. Note that although the images are from experiments conducted in wind, the drag force mechanism is exactly the same as that in water because, at least in a fluid dynamical sense, air behaves like a fluid but with a much lower density than water. From Vollsinger et al. (2005).

3.2.1 Field protocol

To assess the extent to which a given force could bend the stem of a plant and cause it to streamline, we designed an apparatus to apply a known horizontal force to the stem, continuously monitor the distance the stem had been displaced and to quantify the amount of streamlining (reduction in frontal area). The apparatus consisted of (Figure 10):

1. A load cell, calibrated in tension, affixed at a height of approximately $\frac{1}{3}$ the height of the plant;

2. A high-capacity reel spooled with high tension line graduated at 25 mm increments fixed to a telescopic arm that could be adjusted to ensure horizontal loading. The telescopic arm was welded to a specially-designed mount to prevent toppling or sliding of the apparatus;
3. A 12 MP camera fixed on a tripod at the same elevation and horizontal distance from the stem as the reel; and
4. A blue screen placed behind the vegetation to facilitate automated identification of the vegetation on images in order to estimate the frontal area of the plant.

At each stem displacement, the applied load was noted and an image captured. For each species and age range, at least 20 plants were selected for testing and the external and internal (where appropriate) stem diameters and lengths were measured.

The collected data were used to determine the flexibility of vegetation, represented by Young's modulus of elasticity (E), with:

$$E = \frac{J}{I} = \frac{F_D a^2}{2\delta I(3L - a)} \quad (30)$$

where E is Young's modulus of elasticity (N m^{-2}), J = flexural stiffness (N m^2), I is the second moment of inertia ($I = \pi D_s^4/64$, in m^4), D_s is stem diameter (m), a = distance from the base of the stem to the point at which F_D is applied (m), δ = deflection of the stem (m), and L = stem length (m).

3.2.2 Image processing methodology

A method was sought by which to identify and isolate the stems and leaves of vegetation on captured images. Digital images are recorded and stored using an additive three component color model, the Red, Green and Blue model (RGB). Conversely, when documents are printed in color, a subtractive four component model, the Cyan, Magenta, Yellow and Key black (CMYK) color model is used. The stems and leaves of *Phragmites* and Reed canarygrass are commonly shades of yellow-green, which are formed by approximately equal combinations of all three RGB components, but are predominantly formed by the yellow (Y) component of the CMYK model. Tests indicated that the colors of the leaves and stems of cottonwoods are also dominated by the yellow (Y) component. Therefore, if the image background does not contain (much) yellow, the yellow (Y) component can be used to isolate the stems and leaves of all vegetation types. To this end, selected plants were isolated using a blue screen as background and a blue tarp to cover vegetation in the foreground (Figure 10).

Images were processed using a custom script coded within Matlab and illustrated in Figure 11. First, a single optimum bounding area was obtained for all the images in a test (Figure 11A). Second, each image was cropped and split into Cyan, Magenta, Yellow and Key black (CMYK) color channels (Figure 11B). Third, the Yellow channel was thresholded, and any areas of falsely identified vegetation were manually masked (Figure 11C). Fourth, the number of pixels classified as 'vegetation' and the total number of pixels within the bounding area and their quotient were computed.

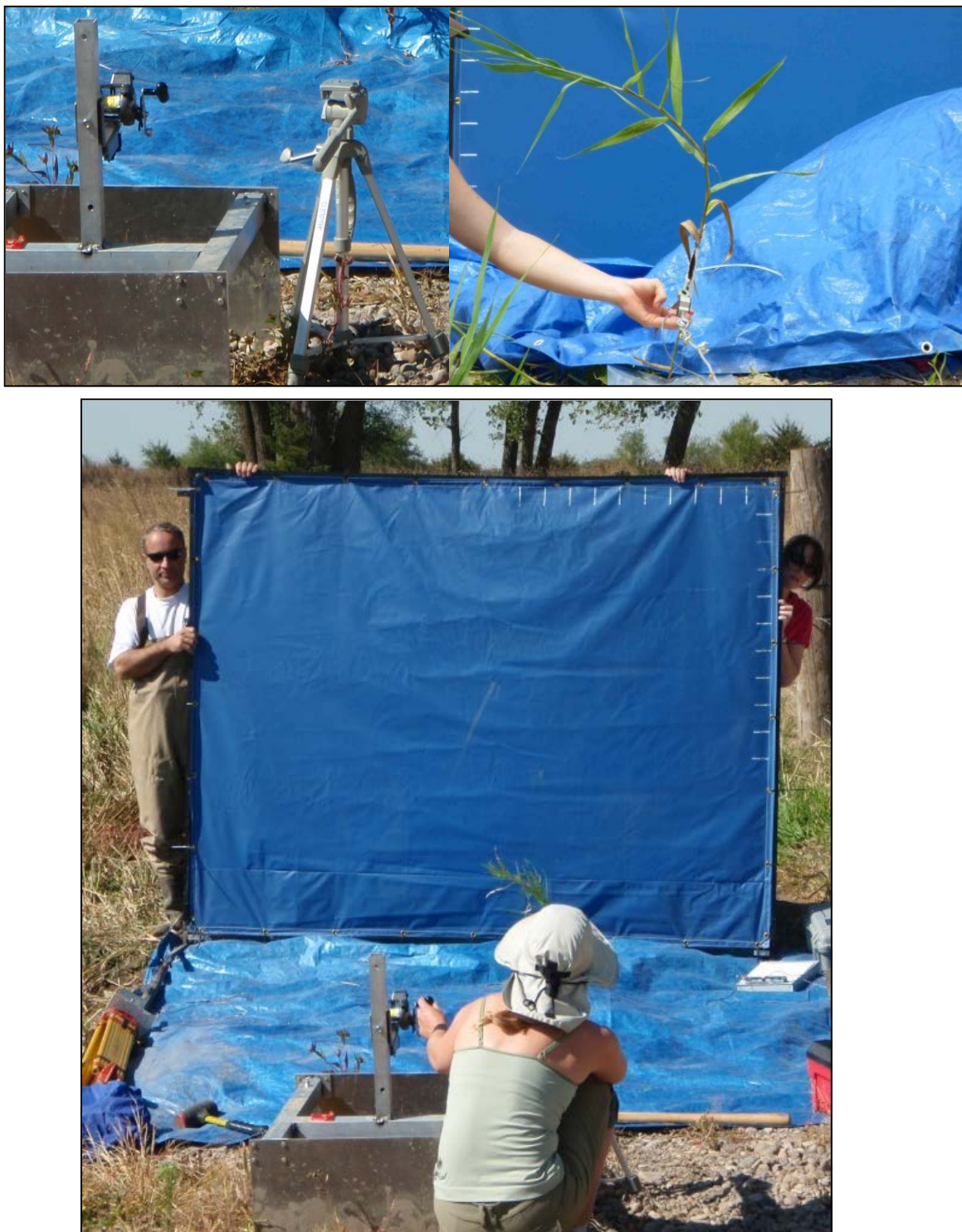


Figure 10. A) Plant bending apparatus showing reel, telescopic arm, specially-designed mount and camera tripod. B) Close up of load cell during bending test. C) View of the bending test apparatus in action.

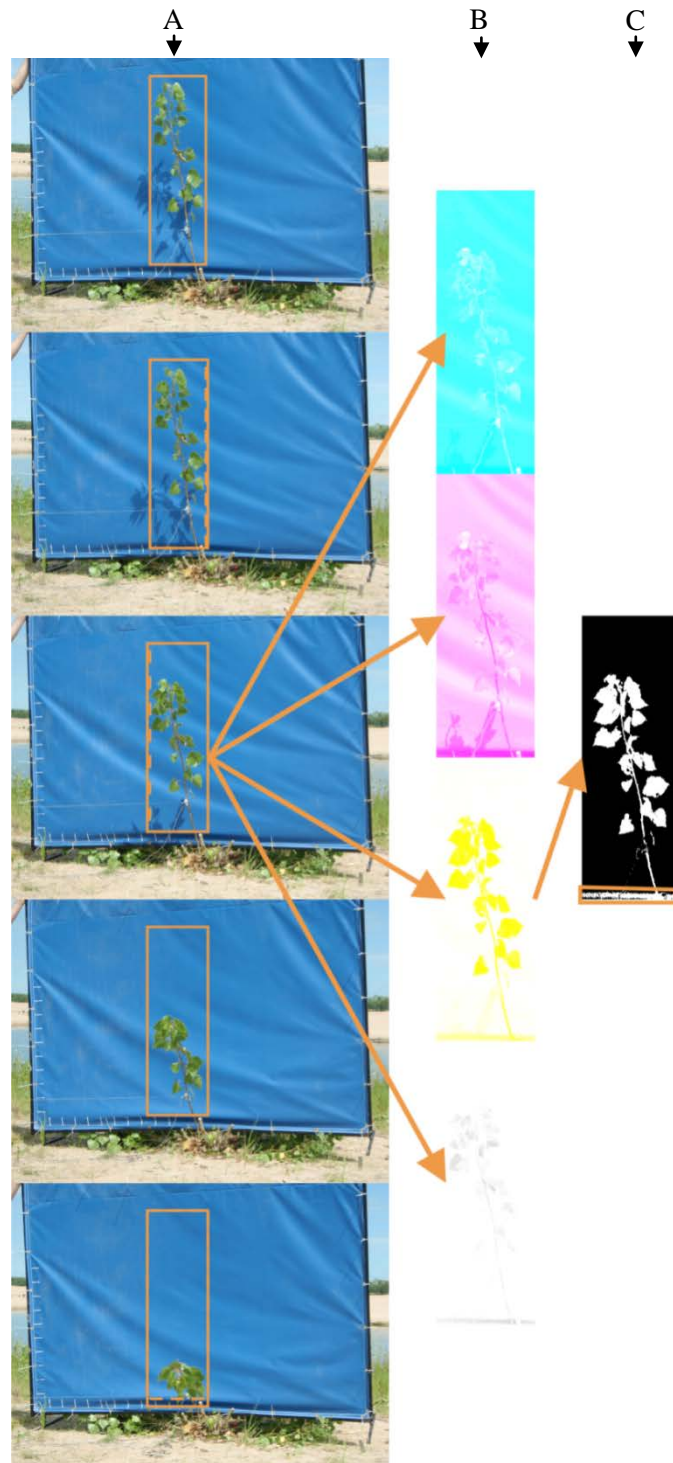


Figure 11. Image processing methodology. First, a single optimum bounding area was obtained for all the images in a test (Figure 11A). Second, each image was cropped and split into Cyan, Magenta, Yellow and Key black (CMYK) color channels (Figure 11B). Third, the Yellow channel was thresholded, and any areas of falsely identified vegetation were manually masked (Figure 11C). Fourth, the number of pixels classified as ‘vegetation’ and the total number of pixels within the bounding area and their quotient were computed.

3.2.3 Laboratory flume experiments: measuring driving force

A series of laboratory flume experiments were designed to permit the estimation of vertical profiles of the drag coefficient (using Equation 5). Although both artificial and natural flexible woody vegetation has been used in some studies to determine the value of resistance coefficients (Fathi-Moghadam and Kouwen, 1997; Freeman et al., 2000; Järvelä , 2002; Wilson et al., 2006), most flume experiments of stream channels use woody vegetation in the simplest form, represented as wooden dowels or similar rigid structures (Pasche and Rouvé, 1985; McBride et al., 2007; White and Nepf, 2008). Herein, artificial materials were selected to mimic field-measured mean stem diameters and flexural stiffnesses.

Artificial cottonwood “plants” were constructed with four “leaves” made of contact paper and attached to the stem with fishing line “branches”. Leaves mimicked the size and shape observed in the field. The leaves of cottonwood seedlings are alternately (spirally) arranged and are generally heart-shaped, which means that they can be approximated reasonably well by a triangle superimposed above a rectangle. In tests on a small number of cottonwood sapling leaves ($n = 10$), the mean breadth of the leaves at their widest point was 40 mm \pm 12 mm, while the mean length of leaves was 45 mm \pm 2.7 mm, with a mean area of 1350 mm² \pm 291 mm². These data were used to inform construction of surrogate "leaves" from plastic sheets that displayed similar flexibility and roughness as real cottonwood leaves. Petioles were constructed using fishing line that again displayed similar flexibility to real cottonwood petioles (Figure 12). To simplify construction, leaves were arranged in an opposite pattern rather than an alternate one but it is not thought that this caused a significant change to the behavior of the mimics. Each cottonwood plant was 30 cm long; leaves 1 and 2 were attached 5 mm from the top, leaves 3 and 4 were attached 55 mm from the top.

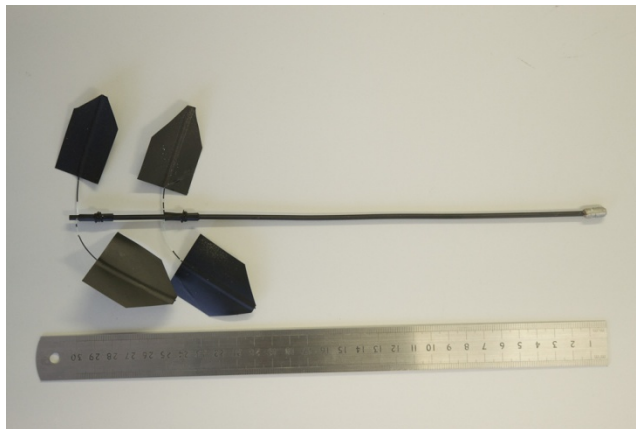


Figure 12. Sample of the constructed cottonwood plants used in the flume study.

For *Phragmites* and Reed canarygrass, only the stems were modeled (Figures 13 and 14) because it was found that leaves were generally high up on stems (and thus significant flow depths/velocities would be required to first bend them and then submerge them), and had a minimal frontal area (see Figure 22). The fiberglass rods used to mimic Reed Canarygrass were 0.45 m long. The Acrylic tubes used to mimic *Phragmites* were \sim 0.40 m long (\pm 0.02 m) and their internal diameters were 3.18 mm with wall thicknesses of 1.59 mm.

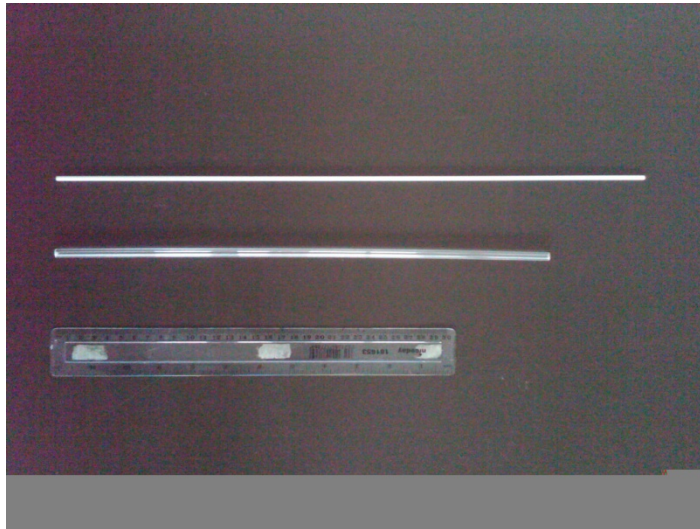


Figure 13. Sample of the rods used to mimic Reed canarygrass and *Phragmites* in the flume study.

Flow depths and plant heights were selected so that cottonwood seedlings were submergent during the experiments, whereas the Reed canarygrass and *Phragmites* were emergent, with the top of the stems just out of the water; this was based on flow depths estimated from the Kearney gage, that suggested that for an 8,000 cfs event, flow depth should be about 0.4 m over the bars studied. Artificial plants were installed in a $6.05 \times 0.61 \times 0.61$ m recirculating flume at areal densities matching those observed in the field (Appendix A, Figure A1). In the case of cottonwoods, because they were distributed relatively sparsely, five different randomly-generated configurations were installed (Appendix A, Figure A2). It was important to replicate stem densities measured in the field because as noted in 2.2.1, a group of obstructions, such as plant stems, influence each other and the flow velocities, drag coefficients and sediment transport characteristics measured within and around them (Tanino and Nepf, 2008; Zong and Nepf, 2010).

Experiments were run using a fixed slope of 0.001 m m^{-1} to approximate that observed on the Lower Platte River (Smith, 1970), two different flow rates ($0.029 \text{ m}^3\text{s}^{-1}$ and $0.048 \text{ m}^3\text{s}^{-1}$, respectively) and three different weir heights (0.30, 0.35 and 0.40 m, respectively; Table 1). An example of the flume set up for a *Phragmites* run is shown in Figure 14. In order to dampen turbulence and provide uniform flow, water passed through a rock damper and an array of 0.30 m long, 0.02 m diameter tubes (baffles) (Figure 14). Water surface elevations were measured over a 0.2 m grid using a point gauge. Ultrasonic Doppler Velocity Profilers (UVPs) were used to record high precision directional velocity data across the entire flow field. The choice of an acoustic measurement technique rather than an optical technique overcomes the limitation imposed by poor optical transmission (Buckee et al., 2001). 10 transducers were multiplexed (where each transducer records a profile in turn), so that while each profile takes up to 18×10^{-3} s to record, they are separated by a 15×10^{-3} s delay between transducers, yielding a total sampling time of up to 33×10^{-3} s (Table 1). The delay ensures that there are no echo effects or cross talk between the transducers, resulting in a data capture rate of approximately 40 Hz. Typical UVP parameters are shown in Table 1. Since the UVP technique is still relatively new, the details of UVP operation are

outlined in Appendix 1 in order to provide background in this methodology. The text, while generic in most areas, specifically relates to the Metflow UVP-XW Revision 3 system (e.g. Best et al., 2001; Brito et al., 2001).



Figure 14. Example of the flume set up for a *Phragmites* run.

For the no vegetation case, streamwise velocity profiles were taken on horizontal planes spaced 0.05 m apart, starting 0.05 m above the bed, i.e., 0.05, 0.10, 0.15, 0.20, and 0.25 m above the bed for the 0.30 m weir and with additional planes added for higher weir heights. By combining data from all the profiles, it is then possible to establish the vertical variations in streamwise velocity at a specific downstream coordinate. For the vegetated cases, streamwise velocity profiles were taken on horizontal planes spaced 0.10 m apart, starting 0.10 m above the bed, i.e., 0.10 and 0.20 m above the bed for the 0.30 m weir, and again adding additional planes for higher weir heights. An example of horizontal UVP profiles for the cottonwood case is shown in Appendix A, Figure A3. In addition, tables of water surface elevations and deviations from those elevations are provided in Appendix A, Tables A2 – A7.

Table 1. Experimental matrix for flume study.

Vegetation scenario	Discharges (m^3s^{-1})		Weir heights (m)		
No vegetation	0.0285	0.0478	0.30	0.35	0.40
Cottonwood, measured areal density (13 stems m^{-2}), random arrangement 1	0.0285	0.0478	0.30	0.35	0.40
Cottonwood, measured areal density (13 stems m^{-2}), random arrangement 2	0.0285	0.0478	0.30	0.35	0.40
Cottonwood, measured areal density (13 stems m^{-2}), random arrangement 3	0.0285	0.0478	0.30	0.35	0.40
Cottonwood, measured areal density (13 stems m^{-2}), random arrangement 4	0.0285	0.0478	0.30	0.35	0.40
Cottonwood, measured areal density (13 stems m^{-2}), random arrangement 5	0.0285	0.0478	0.30	0.35	0.40
Cottonwood, double measured areal density (26 stems m^{-2})	0.0285	0.0478	0.30	0.35	0.40
Phragmites, measured areal density (200 stems m^{-2})	0.0285	0.0478	0.30	0.35	0.40
Reed canarygrass, measured areal density (800 stems m^{-2})	0.0285	0.0478	0.30	0.35	0.40
Reed canarygrass, half measured areal density (400 stems m^{-2})	0.0285	0.0478	0.30	0.35	0.40

3.3 Resisting forces

Much of the work relating to quantifying root strength has been conducted in the field in the analysis of slope and streambank stability to assess potential changes in stability with different types and ages of vegetation (Greenway, 1987; Coppin and Richards, 1990; Gray and Sotir, 1996; Simon and Collison, 2002; Bischetti et al., 2005; Pollen and Simon, 2005, Simon et al., 2006; Pollen, 2007; Tosi, 2007; Danjon et al., 2008; De Baets et al., 2008; Docker and Hubble, 2008; Hales et al., 2009; Pollen-Bankhead and Simon, 2009; Thomas and Pollen-Bankhead, 2010). In the present study, existing protocols that had been established to quantify the geometric properties and strengths of roots were supplemented with new protocols to quantify the relative strengths of stems, roots and rhizomes. The latter were required in order to identify whether it was possible to remove entire plants intact, or whether a particular plant structure would break preferentially before removal.

3.3.1 *Field protocol: Root tensile strengths*

At each study site, plants of each species were excavated by carefully exposing their root architectures and enabling the measurement of typical rooting depths. Root tensile strengths were then measured using a device called the Root-Puller, based on a design by Abernethy and Rutherford (2001) (Figures 15 and 16). This was comprised of a metal frame, with a winch attached to a load cell, connected to an in-field data logger. Different diameter roots were then tested by securing each individual root in a u-bolt that was then connected to the load cell. Cranking the winch applied a tensile stress to the root (measured as a load, in Newtons) that increased until tensile failure of the root occurred. The diameter of each root was recorded along with the logged history of applied force until breaking. The maximum load applied to each root before breaking and the root diameter was then used to calculate the tensile stress of each root. A sample size of >30 roots, was collected to establish a relation between root diameter and root tensile strength, and in the case of *Phragmites*, to establish a rhizome diameter-tensile strength relation. The tensile strength of roots commonly varies with root diameter, with a non-linear decreasing trend of the form $T_r = a D_r^{-b}$ commonly being found (examples include but are not limited to: Waldron and Dakessian, 1981; Riestenberg and Sovonick-Dunford, 1983; Greenway, 1987; Coppin and Richards, 1990; Gray and Sotir, 1996; Abernethy and Rutherford, 2001; Simon and Collison, 2002; Pollen and Simon, 2005; Genet et al., 2006; De Baets et al., 2008; Fan and Su, 2008; Hales et al., 2009).

3.3.2 *Field protocol: Plant removal tests*

The methods outlined in section 3.3.1 permitted the quantification of the geometric properties and strengths of roots, but did not identify whether a particular plant structure (e.g. stem, root or rhizome) would break preferentially before removal nor quantify the load required to break (or pullout) an entire root-ball. To this end, a new apparatus was designed and constructed. This apparatus was comprised of a tripod, winch and load cell, placed above each plant stem (Figure 17). The stems of individual plants were attached to the load cell and the plant winched vertically upwards, thereby measuring the force required to remove the entire root ball from its substrate. The forces required to remove plants of each species were measured during two fieldtrips, along with corresponding stem diameters. After each plant was removed, or the stem snapped, the failure mode was recorded (pullout, stem breaking, roots/rhizomes breaking) and the maximum rooting depth and width of the extracted plant was measured where applicable. Digital

images of each root network were also captured, so that intact root networks could be analyzed using the WinRhizo software to quantify total root length, root volume and root surface area. Lastly, soil samples were taken at each study site to test for variations in bulk unit weight, moisture content, and particle size. These soil parameters were required not only for RipRoot parameterization, but also in calculations of potential scour. In addition to the three species budgeted for in this study, pullout forces for sandbar willow seedlings were also measured in the field, and the results of these tests are also provided in this report.

3.3.3 *Laboratory experiments: root network resistance to removal*

Approximately 30 young cottonwood seedlings were removed from the study sites and placed in 3 containers, with special effort being made to keep the substrate they were growing in largely intact, so that the root networks were as undisturbed as possible. These plants were transported to USDA-ARS-NSL for further testing in an experiment designed to investigate the effect of soil moisture content on resistance to pullout. The boxes were continuously monitored during transport and storage to ensure the plants were kept wet. At the start of the experiments, the soil in each box was allowed to dry out to different soil moisture contents (34.8 %: saturated, 20.7 % and 16.8 %), and then the field apparatus described in section 3.3.2 was used to extract each plant. For each plant, stem diameter and pullout force were recorded so that differences in pullout forces could be compared for different soil moisture contents.

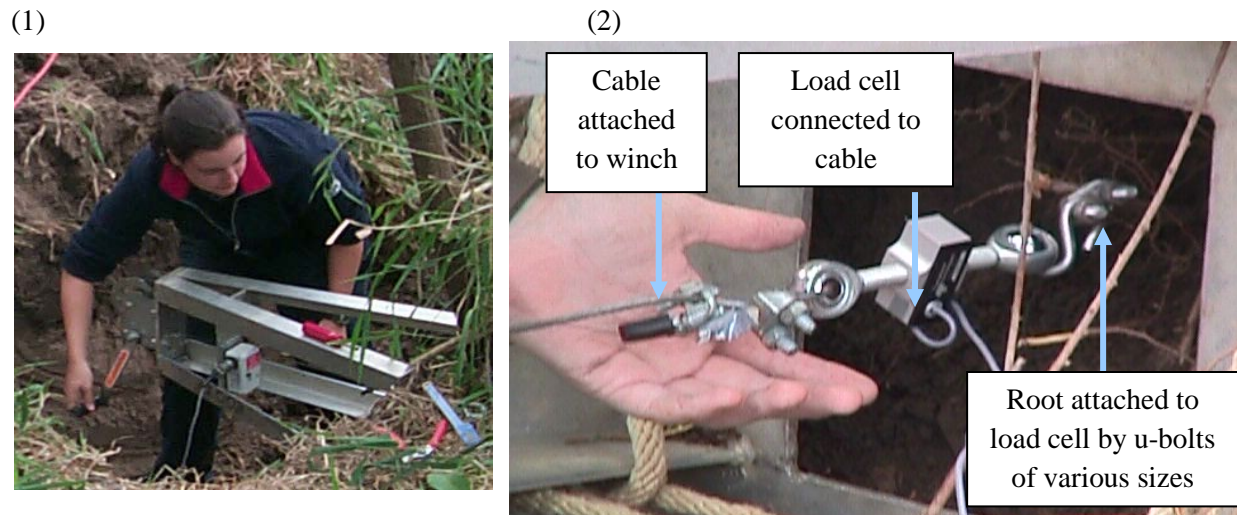


Figure 15. Photos of the Root-Puller constructed at the USDA-ARS-NSL. (1) original large puller built by USDA-ARS-NSL being used to measure the strength of riparian tree roots. (2) close-up of the way that the load cell and roots are connected to the winching cable.



Figure 16. Root-puller device being used to measure the strength of excavated *Phragmites* roots and rhizomes, in a sandbar along the Elm Creek reach of the Platte River, NE.



Figure 17. Plant-pulling device being used to measure the force required to extract young phragmites stems from a sandbar in the Elm Creek reach along the Platte River, NE.

3.3.4 Numerical modeling: root network resistance to removal

Field measurements of whole plant removal will likely yield a relatively small sample size that only represents part of the population of plant resistances that are actually present in a given reach. To account for parameter variability and to estimate the full range of plant resistances to removal, the RipRoot model was executed within a 25,000-run Monte Carlo framework (modified from Thomas and Pollen-Bankhead, 2010). Data requirements are shown in Table 2. Field measurements provided the data necessary to parameterize simulations for the three species investigated in the present study. For each species, the measured minimum and maximum numbers of roots per plant, minimum and maximum root diameters, tensile strength-diameter curve, and the range of typical rooting depths (obtained from direct measurements and from the images of extracted plant networks) were used as input to the model. In addition, plant areal densities (number of stems per unit area) were also input so that the resistance of patches of plants could be estimated in addition to that of individuals. Average bulk unit weight (19.2 kN) and friction angle (27°) were determined from samples collected at the fieldsites. In all of the RipRoot simulations, soil cohesion was set to be just 1 kPa to be representative of the saturated sand substrates that would most likely be present during a SDHF event.

RipRoot modeling provided predictions of mean plant and patch resistances, with upper and lower bounds for:

- 1) Different species
- 2) Different ages of each species where applicable
- 3) Different densities of plants growing on a given bar
- 4) Different depths of burial and scour

Model results were then validated using rooting depth and plant pullout data collected in the field.

Table 2. Summary of the input parameters that are required for the Monte Carlo version of the RipRoot model (modified from Thomas and Pollen-Bankhead, 2010), reasons each parameter is required and method of measurement.

Variable to measure	Reason for measuring	Method of measurement
Root tensile strength	Each species has a characteristic relationship between root tensile strength and root diameter that plays a critical role in determining plant resistance to removal; parameter was required in RipRoot	Used Root-Puller device shown in Figures 14 and 15, on the roots of plants that were excavated from sandbars along the study reaches of the Platte River, NE.
Root diameter distribution	Because root tensile strength is related to root diameter, knowledge of the range of root diameters and their frequency distribution for each species was required; parameter was required in RipRoot	Measured the root diameters of plants that had been pulled out of the substrate using WinRhizo root scanning software.
Root lengths	Knowledge of root lengths allows calculation of root pullout forces; parameter was required in RipRoot	Measured maximum extent of root length of plants that had been pulled out of the substrate, using a tape measure.
Rooting depth/ burial depth	Required input for the RipRoot model to allow determination of plant and patch resistance to pullout after scour or deposition of sediment	Rooting depth was estimated in the field from measurement of root lengths added to any burial measured above the initiation point of root growth at the base of the stem
Soil bulk unit weight	Required to calculate root or rhizome pullout forces in RipRoot	Bulk density samples were taken at various field locations to obtain the typical range of bulk unit weights of the substrate in each study reach.
Particle size data	Required to calculate rates of scour under different flow magnitudes and durations	Samples were collected at each field sites to allow characterization of minimum and maximum rates of scour under different flow conditions. Particle size samples were transported to USDA-ARS-NSL, Oxford, MS for analysis in the soils lab.
Plant pullout force	These values were used to compare with RipRoot model predictions of plant pullout based on root and rhizome parameters collected in the field. This data was also used to test changing plant resistances with different burial/scour depths.	Plant pullout forces were measured using a plant-pulling device (Figure 16).

4 RESULTS

4.1 Driving forces

To calculate the flexural stiffness of the three species tested, and be able to simulate them in flume experiments a number of field measurements were required. The results of these measurements are given in sections 4.1.1 through 4.1.4.

4.1.1 Basic geometric properties

The basic geometric properties measured in the field for the species being tested are shown graphically in Figures 18 and 19, and provided in Table 3.

Table 3. Basic geometric properties of stems tested for flexibility.

Species	Mean external stem diameter (mm)	Number of tests	Mean internal stem diameter (mm)	Number of tests	Mean stem length (m)	Number of tests	Mean areal density (m ⁻²)	Number of surveys
<i>Phragmites</i>	6.0 ± 1.94	91	3.27± 0.67	55	0.86± 0.64	90	200 ± 50	8
Reed canarygrass	3.21 ± 1.08	69	-	-	0.77± 0.35	69	799± 107	5
Cottonwood (seedlings)	2.92 ± 1.38	66	-	-	0.39± 0.09	63	13 ± 13	4
Cottonwood (3-5 years)	12.45± 2.42	12	-	-	1.58± 0.20	10	-	-

4.1.2 Plant bending forces

Figure 20 shows the maximum force observed during each bending test plotted against the stem diameter. Upon inspection, there appears to be a positive trend between maximum force and stem diameter for cottonwoods ($R^2 = 0.62$), but it is difficult to discern a trend between the two variables for both *Phragmites* and Reed canarygrass (Figure 20). Minimum, maximum and mean values for stem bending are shown in Table 4.

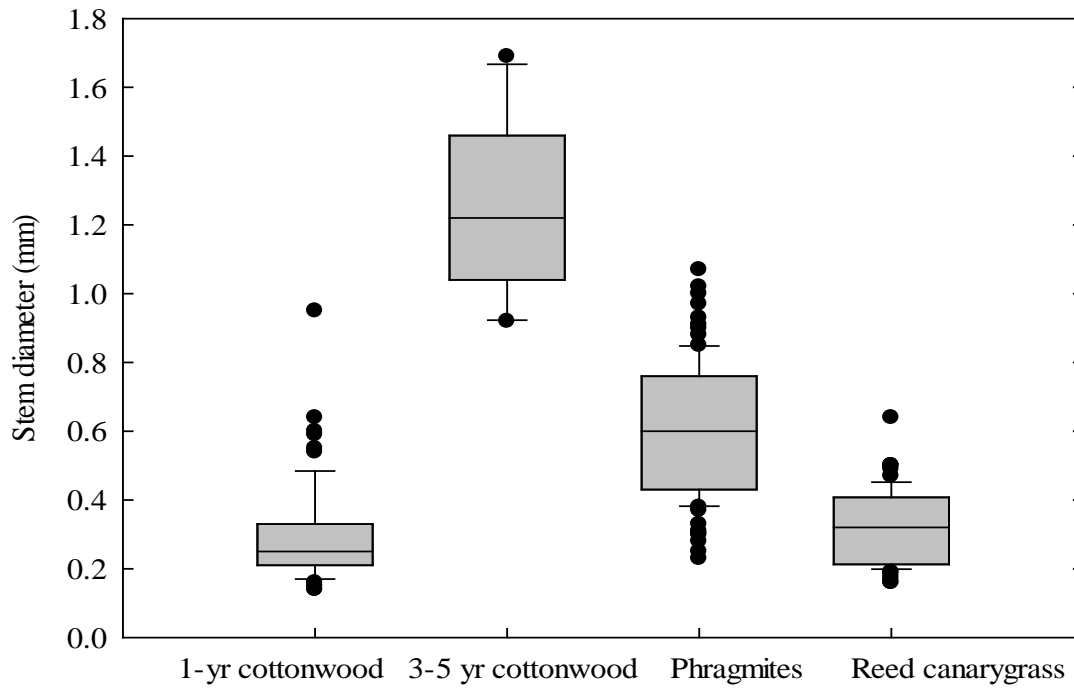


Figure 18. Distributions of measured stem diameters.

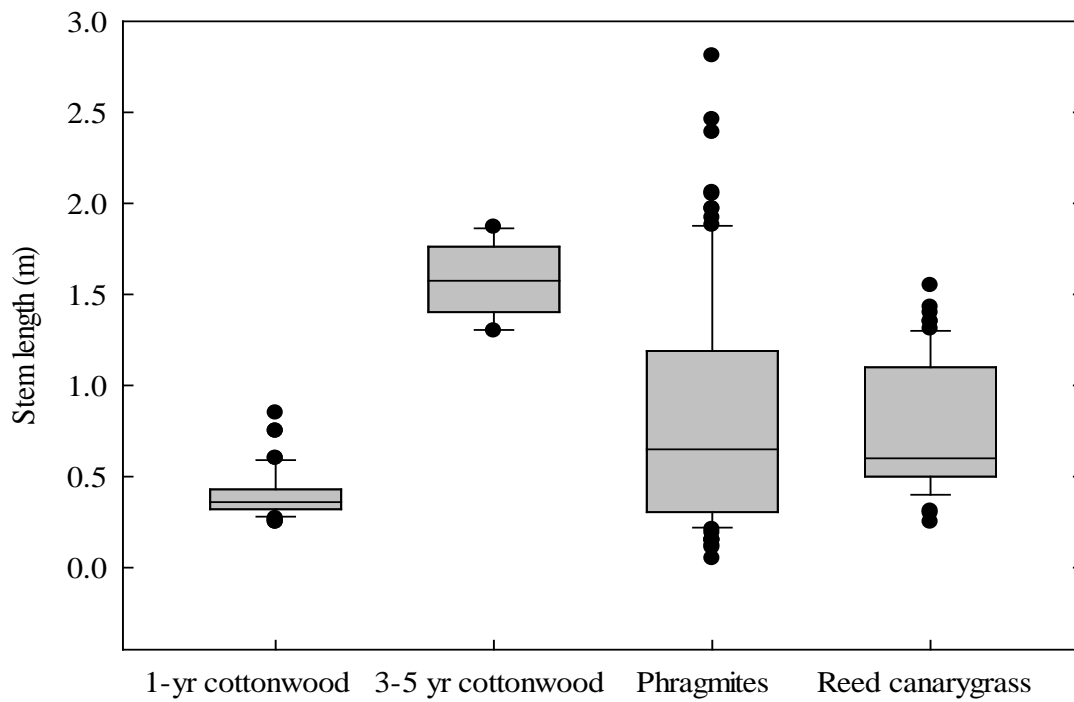


Figure 19. Distributions of measured stem lengths.

Table 4. Minimum, maximum and mean forces for stem bending measured in the field.*Greater than 20 samples were tested but some were removed from the analysis where orientation of bending and direction of flow did not match.

Species	Minimum force (N)	Maximum force (N)	Mean force (N)	Number of tests
<i>Phragmites</i>	3.07	68.6	24.3±18.5	21
Reed canarygrass	3.56	44.4	22.4±11.3	16*
Cottonwood	1.78	122	42.1±37.2	20

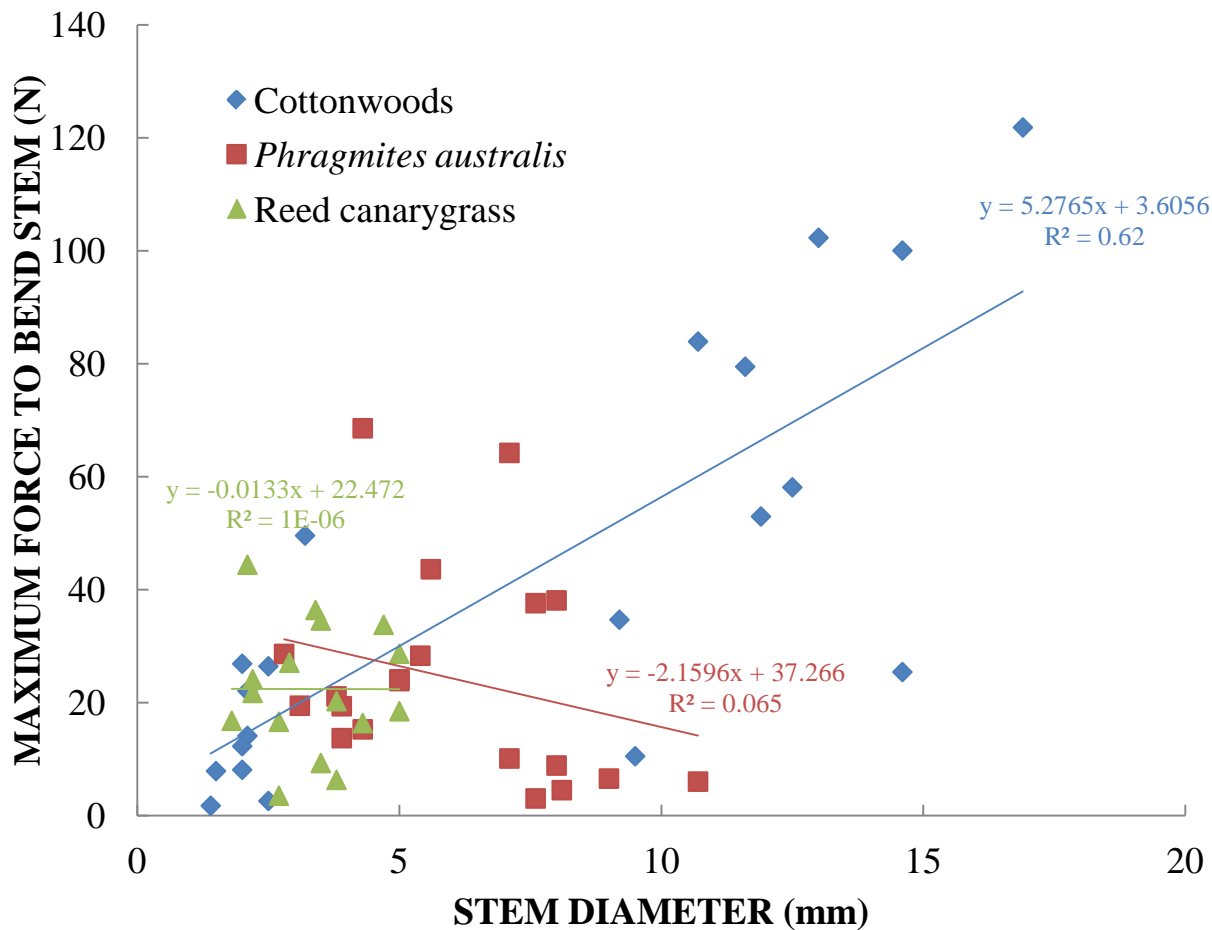


Figure 20. Maximum force to bend stem against stem diameter.

4.1.3 *Plant flexural stiffness*

The mean flexural stiffness of cottonwood seedlings was $0.0099 \pm 0.0082 \text{ N m}^2$ (number of tests = 10, number of evaluations = 23), that of 3-5 year old cottonwoods was $1.53 \pm 1.86 \text{ N m}^2$ (number of tests = 10, number of evaluations = 80), that of *Phragmites* was $0.94 \pm 1.07 \text{ N m}^2$ (number of tests = 21, number of evaluations = 105), and that of Reed canarygrass was $0.18 \pm 0.17 \text{ N m}^2$ (mean \pm 1 standard deviation, number of tests = 16, number of evaluations = 62). Significant variability is evident in the loading curves shown in Figure 21. For this reason, these values were verified by plotting the computed flexural stiffness values against the stem diameter-length ratios and then finding the flexural stiffness associated with the mean stem diameter-length ratio. For both Reed canarygrass and cottonwood seedlings, the resulting flexural stiffness was not statistically different than the computed mean flexural stiffness, but for *Phragmites*, the resulting flexural stiffness was 0.25 N m^2 . As the stems of *Phragmites* displayed similar behavior to those of Reed canarygrass in the field, this value was selected as the target value for artificial material selection for use in the flume experiments. For similar stem diameters, a survey of available materials from a number of manufacturers and suppliers, combined with a literature search, identified fiberglass rods, acrylic tubes, and polypropylene rods as having almost identical flexural stiffnesses (0.0087 , 0.24 , and 0.21 N m^2) to those of cottonwood seedlings, *Phragmites*, and Reed canarygrass, respectively.

4.1.4 *Plant projected area*

Field tests indicated that the projected area of the smallest cottonwood seedlings did not change significantly, with reductions in projected area ranging from 6.2 to 30% (mean = 21.5%, number of tests = 10) (Figure 21A), but as plants become larger, the potential for streamlining increases (Figure 22A), with reductions in projected area ranging from 30.6 to 68.4% (mean = 52.0%, number of tests = 10). Observations made during laboratory flume experiments of the behavior of artificial cottonwood seedlings constructed to match flexural properties measured in the field, differed from field tests, in that streamlining of leaves was significant in the flume experiments, but not seen in the field methodology where flow was absent. The projected area of *Phragmites* was initially smaller than that of cottonwoods because of the slender nature of the leaves and stems (Figure 22B) but, perhaps surprisingly, also declined in response to drag. Reductions in projected area ranged from 0 to 99.7% (mean = 47.8%, number of tests = 21) (Figure 22A), The maximum loss of projected area is again of the order of 50%. Results of tests on Reed canarygrass were similar to those conducted on *Phragmites*, with reductions in projected area ranging from 18.2 to 95.9% (mean = 53.2%, number of tests = 16) (Figure 22C).

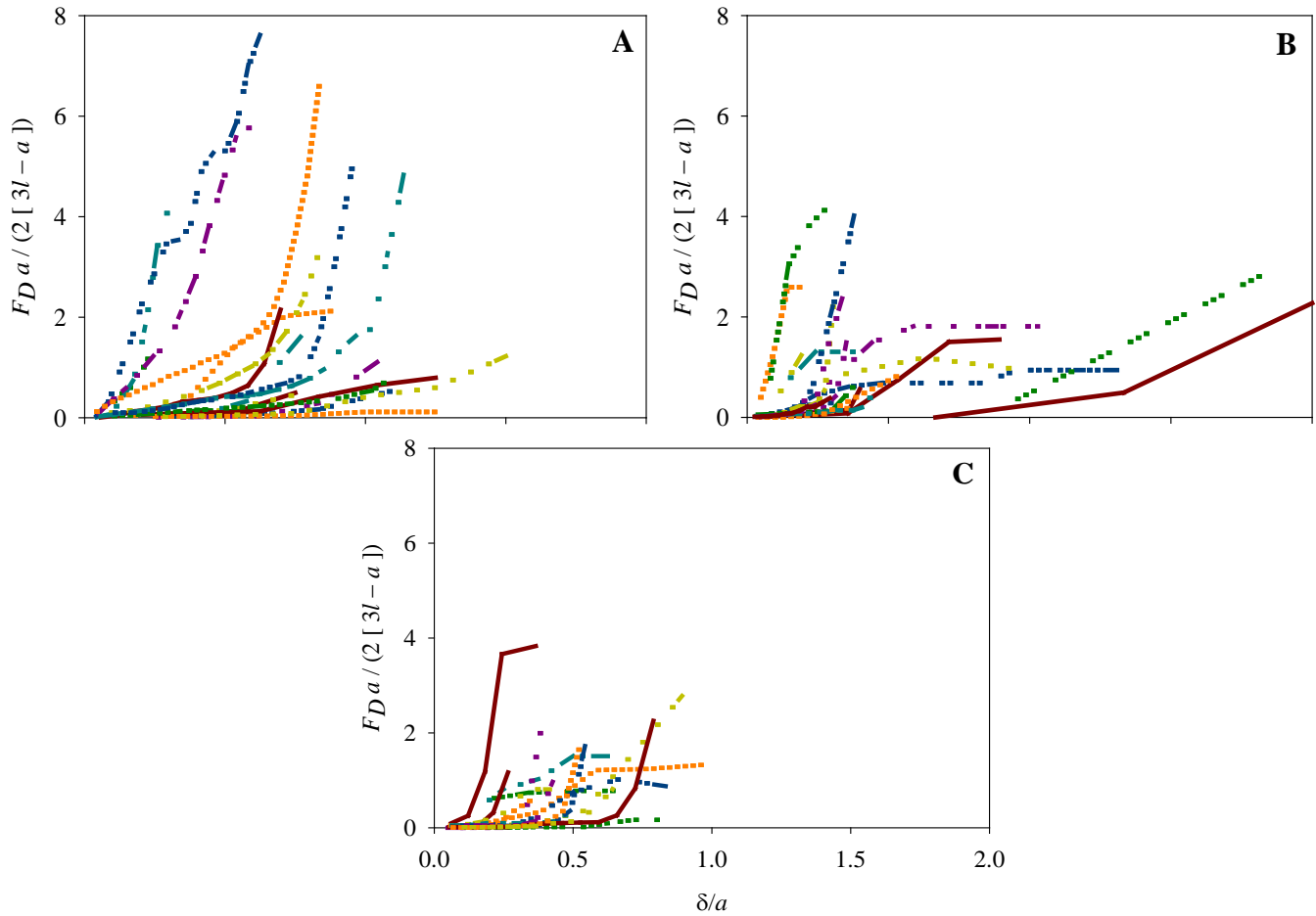


Figure 21. Loading curves for bending tests on: A) Cottonwoods, B) *Phragmites*, and C) Reed canarygrass. Flexural rigidity is defined as the slope of these curves. Following equation 30, the y-axis is the applied force normalized by $2(3L - a)/a$ and the x-axis is the deflection of the stem normalized by the distance from the base of the stem to the point at which the force is applied. Flexural rigidity is defined as the slope of these curves.

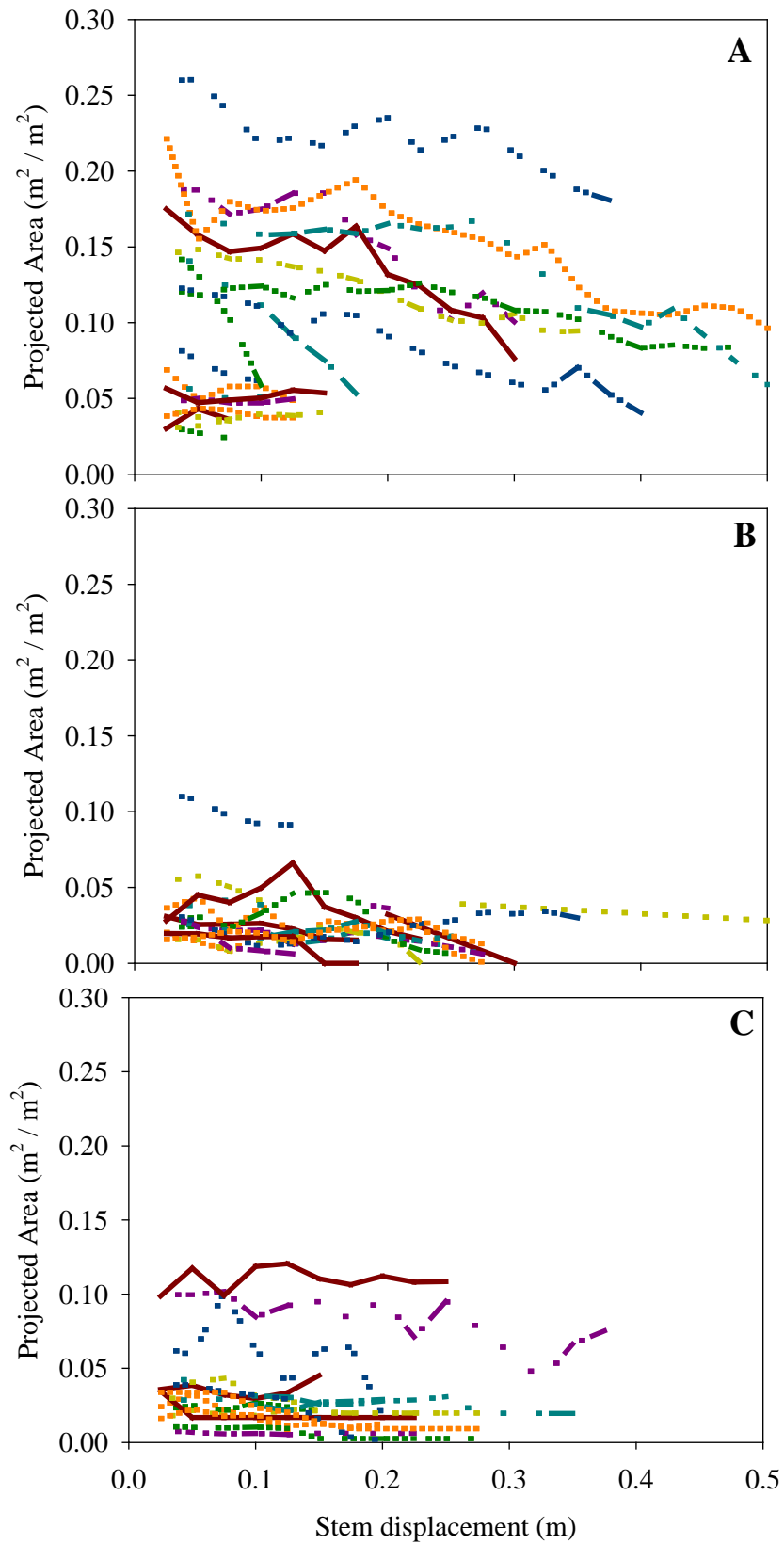


Figure 22. Plant projected area against horizontal displacement for bending tests on: A) Cottonwoods, B) *Phragmites*, and C) Reed canarygrass.

4.1.5 Drag coefficients and drag forces

Drag coefficients, C_D , were computed using data collected during the laboratory flume experiments and Equation 6. At low discharge ($0.0285 \text{ m}^3\text{s}^{-1}$), drag coefficients were found to vary from 16.8 to 18 for artificial cottonwood seedlings with an areal density of 13 stems m^{-2} , from 11.9 to 16.9 for artificial cottonwood seedlings with an areal density of 26 stems m^{-2} , from 8.81 to 13.0 for artificial *Phragmites* plants with an areal density of 200 stems m^{-2} , from 17.8 to 26.1 for artificial Reed canarygrass plants with an areal density of 400 stems m^{-2} , and from 10.4 to 15.8 for artificial Reed canarygrass plants with an areal density of 800 stems m^{-2} . At high discharge ($0.0478 \text{ m}^3\text{s}^{-1}$), drag coefficients were found to vary from 11.5 to 11.9 for artificial cottonwood seedlings with an areal density of 13 stems m^{-2} , from 13.2 to 15.5 for artificial cottonwood seedlings with an areal density of 26 stems m^{-2} , from 7.27 to 10.8 for artificial *Phragmites* plants with an areal density of 200 stems m^{-2} , from 16.2 to 21.1 for artificial Reed canarygrass plants with an areal density of 400 stems m^{-2} , and from 9.73 to 13.1 for artificial Reed canarygrass plants with an areal density of 800 stems m^{-2} . These values seem high relative to those reported previously (e.g., García et al., 2004 for a discussion), although they are similar to those reported by James et al. (2008), who studied drag forces on *Phragmites* for a variety of submergences and velocities. James et al. (2008) noted that C_D -values are sensitive to the method used to characterize the projected area, and Li and Shen (1973; see also associated discussion), noted that errors in computing projected area values would result in higher mean drag coefficients. Of interest is the finding that the drag coefficient acting upon artificial cottonwood seedlings displays the opposite trend to that on both artificial *Phragmites* and artificial Reed canarygrass: for constant areal densities and discharges, shallower flow depths yielded smaller drag coefficients than deeper flow depths. In other words, higher velocities yielded smaller drag coefficients. This confirms that streamlining is important in limiting drag on cottonwood seedlings, because the reduction in velocity, U , is approximately balanced by the reduction in projected area. This conclusion is reinforced by comparing the drag coefficients obtained when varying discharge for constant areal densities and weir heights. Conversely, both artificial *Phragmites* and artificial Reed canarygrass were stiff enough that their projected areas did not change during the flume experiments and therefore for constant areal densities and discharges, drag was larger at shallower flow depths and faster velocities.

Parameterizing Equation 4 with the computed drag coefficients, C_D , and projected areas, the drag forces acting upon the artificial plants can be computed (Figure 23). At low discharge ($0.0285 \text{ m}^3\text{s}^{-1}$), drag forces were found to vary from 1.02 to 1.27 N for artificial cottonwood seedlings with an areal density of 13 stems m^{-2} , from 1.07 to 1.28 N for artificial cottonwood seedlings with an areal density of 26 stems m^{-2} , from 1.20 to 1.78 N for artificial *Phragmites* plants with an areal density of 200 stems m^{-2} , from 1.22 to 1.78 N for artificial Reed canarygrass plants with an areal density of 400 stems m^{-2} , and from 1.41 to 2.16 N for artificial Reed canarygrass plants with an areal density of 800 stems m^{-2} . At high discharge ($0.0478 \text{ m}^3\text{s}^{-1}$), drag forces were found to vary from 1.67 to 2.16 N for artificial cottonwood seedlings with an areal density of 13 stems m^{-2} , from 2.22 to 2.47 N for artificial cottonwood seedlings with an areal density of 26 stems m^{-2} , from 2.78 to 4.13 N for artificial *Phragmites* plants with an areal density of 200 stems m^{-2} , from 3.10 to 4.04 N for artificial Reed canarygrass plants with an areal density of 400 stems m^{-2} , and from 3.72 to 5.00 N for artificial Reed canarygrass plants with an areal density of 800 stems m^{-2} . These values are commensurate with those obtained by previous researchers. For example, Schnauder and Wilson

(2009) assembled datasets obtained by a number of researchers and showed that drag forces acting upon various willow species ranged from 0.5 to 12 N for the range of flow velocities measured herein.

A number of trends are evident in our experimental results. First, in all cases, for a given discharge the drag force is higher for shallower flow depths and faster velocities. Second, in all cases, for a given flow depth, the drag force is higher for larger discharges and faster velocities. Third, in all cases, for a given species, the drag force is higher for larger areal densities (stems m^2). Fourth, the drag force acting upon the stand of artificial *Phragmites* plants with an areal density of 200 stems m^2 , is almost identical to that acting upon the stand of artificial Reed canarygrass plants with an areal density of 400 stems m^2 . This is because the stem diameter of the artificial *Phragmites* plants is exactly double that of the artificial Reed canarygrass plants. Therefore, the projected areas of these two cases are identical.

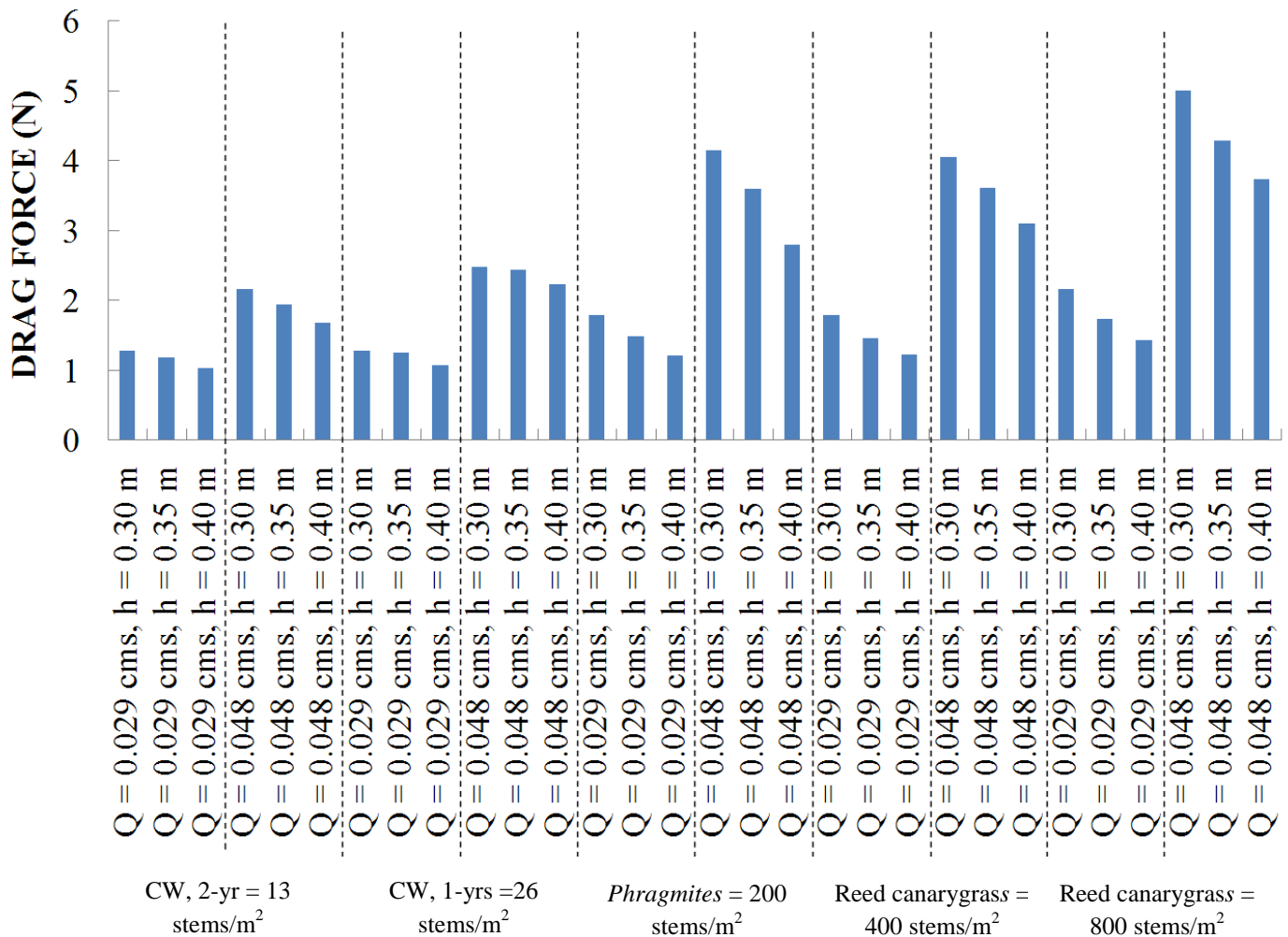


Figure 23. Drag forces computed using Equation 4 for the species and experimental parameters tested herein.

4.2 Resisting forces

4.2.1 Root architecture

Excavation of the plant species included in this study revealed dramatically different rooting architectures and extents. Reed Canarygrass exhibited a very dense, fibrous root network that extended to approximately 0.5 m deep in places, with the densest rooting being seen in the upper 0.3 m of the soil profile (Figure 24A). Root densities were seen to be in the order of tens of thousands of roots per square meter, ranging from 0.1 to 2 mm in diameter.

Young cottonwood seedlings (up to 2-years) were seen to have a much sparser root network, composed of roots that were more woody in texture (Figure 24B). The one-year-old seedlings had already developed a distinct, woody taproot that extended up to 0.25 m into the soil profile, with a mean rooting depth of 0.14 m. Smaller, lateral roots extended from the upper portion of the taproot to assist in anchoring the seedlings. For two-year-old seedlings the maximum rooting depth measured was 0.48 m, but again the mean rooting depth was 0.14 m, indicating that in some cases seedlings had preferentially thickened the taproot over lengthening, and in other cases lengthening rather than thickening of the taproot had occurred. In most cases the maximum rooting width was less than the rooting depth of a given cottonwood sapling, indicating that more of the plant's energy is spent on development of the taproot than the lateral roots. During our study, several five-year-old cottonwood trees were also excavated to see how development continues over the next few years of growth. The taproot continued to dominate the root architecture, extending up to 1.5 m in some cases, or to whatever depth was necessary for the plant to reach sufficient moisture. These trees therefore exhibit rapid taproot growth over the first few years of their development, which has important implications for the timing of any potential removal of these trees, be it by mechanical or hydraulic means.

The sandbar willow trees excavated showed consistently different root architectures to the cottonwood seedlings (Figure 25A). Willow seedlings were dominated by long horizontal roots. Within the first year of growth these lateral roots may be separate from other plants (if the plants have grown from seed), or may be connected to other willow seedlings via runners (if they have grown vegetatively). Over time these lateral runners develop into interconnected systems of roots that spread between neighboring seedlings. Mean rooting depth for these seedlings was just 0.12 m whilst mean rooting width was 0.35 m, extending to over 1.5 meters in some cases. Older willows were not studied so changes in root-architecture beyond the first few years of growth cannot be discussed here. However, as members of the Salicaceae family are taprooted phreatophytes (Karrenberg et al., 2002), a vertical taproot may grow and influence uprooting of older willows. The depth of this taproot is highly dependent on groundwater depth (Amlin and Rood, 2002; Stella and Battles, 2010), and where this is shallow, the majority of roots will remain concentrated near the soil surface. At the sites samples in this study, the shallow rooting of young willow seedlings suggests that erosion or removal of the upper 0.2 meters of a soil profile would successfully remove many of these younger plants.

Phragmites stands tended to be dominated by interconnected networks of rhizomes, with fine roots growing from them (Figure 25B). Excavation revealed deeply rooted rhizomes, extending depths of greater than 1.5 m in places. Even where stands of phragmites had been sprayed, the buried rhizome

networks seemed healthy and capable of regenerating above-ground biomass in the following growing season. Rhizomes were even seen to have grown vertically through the soil profile from old buried stems of phragmites. Each individual stem of phragmites had a rhizome, commonly 1 cm or more in diameter with multiple fibrous roots growing at nodes along the rhizomes (Figures 25B and 25C). As the most deeply rooted plant studied, and the plant with the greatest ability to regenerate from buried rhizomes and stems, it is likely the hardest of the species studied to remove from sandbars in the Platte River.



Figure 24. A) Rootball of Reed canarygrass B) 1-year-old cottonwood seedling



Figure 25. A) Young willow seedling, B) Young *Phragmites* stems with vertical rhizome attached to deeper horizontal rhizome, C) Mature *Phragmites* rhizome

4.2.2 Root and rhizome strengths

Root and rhizome strengths varied considerably between the species studied. As can be seen in Figure 26, the Reed canarygrass roots tested were 1mm in diameter or less, and exhibited very low breaking forces of up to just 5.60 N. These low breaking forces help to explain why during uprooting tests, the Reed canarygrass stems almost always broke right at the base of the stem where root growth had initiated; even though many roots were seen to grow from each stem, the force required to break all of the roots was still less force than was required to break the stem, or to pull the roots out of the ground intact. *Phragmites* roots and rhizomes were shown to be relatively strong, requiring forces of up to 456 N for breakage. Cottonwood roots were shown to be the strongest of the three species tested (as indicated by the regression line with the steepest gradient, indicating that for a root of the same diameter, a greater force was required to break a cottonwood root, compared to a *Phragmites* root/rhizome and a Reed canarygrass root), with the forces measured for breakage reaching a maximum value of 398 N. The strength of the cottonwood roots helps to explain why entire root networks of cottonwood seedlings were extracted from the soil during uprooting tests; the force required to pull them out of the soil was less than the force that would have been required to break them. Statistical analyses (Kruskal-Wallis One Way Analysis of Variance on Ranks) showed that the difference in the median root breaking forces of the three species were greater than would be expected by chance and that there is, therefore a statistically significant difference between all three data sets ($P < 0.001$).

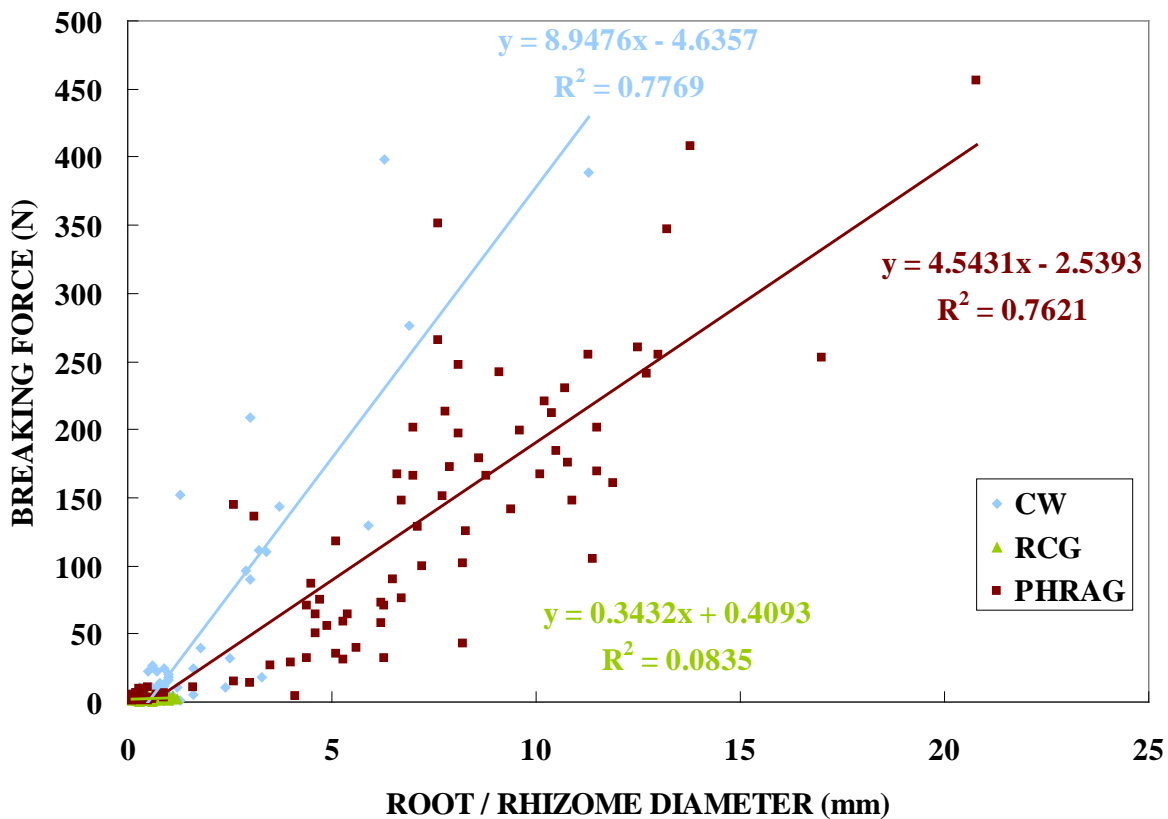


Figure 26. Breaking forces for roots and rhizomes of the three species tested for root strength.

4.2.3 *Plant resistance to pullout*

In this section we discuss the range of forces measured in the field that were required to remove individual plants of each species from their substrates, and the dominant failure modes seen for each species during pullout tests.

The one-year-old cottonwood seedlings (or seedlings in their first year of growth) had the lowest removal forces, ranging from 8.2 to 64.3 N (mean value of 32.0 N) (Figure 27). In the case of these plants (sample size, $n = 50$) in every test the plant was removed smoothly as the stem was winched upwards, no breaking was heard, or any evidence of breaking seen when each plant root network was examined. The plant root networks were therefore considered to have been extracted intact, largely as a result of the simple structure of the root networks dominated by a single taproot and at this young age, and very few lateral roots whose force had to be overcome during vertical pulling. The two-year-old cottonwood seedlings required greater force for removal, ranging from 6.4 to 474 N (mean value of 139 N, sample size, $n = 30$) (Figure 27). Similar to the one-year-old seedlings the majority of the root network of each plant was removed during each test, but in some cases the main taproot showed evidence of breaking. The higher breaking forces compared to the one-year-old cottonwoods were a result of increased numbers of lateral roots growing in the additional growing season, and thickening of lateral roots as the plant developed. The greater number of lateral roots and their increased surface area both increased the force required to remove the plant in these vertical uprooting tests. Statistical tests (Mann Whitney Rank Sum) showed a significant difference existed between the median values for uprooting of 1 and 2-year old cottonwoods ($P < 0.001$). One and two year old cottonwood uprooting forces were also found to be statistically significantly different from those measured for Reed canarygrass, *Phragmites*, and Sandbar willow (Mann Whitney Rank Sum; $P < 0.001$).

Sandbar willow seedlings (approximately one-year-old) were harder to remove during uprooting tests than cottonwood seedlings of a similar age, with pullout forces ranging from 19.6 to 189 N (mean value of 65.5 N, sample size, $n = 30$; Figure 27) This was as a result of their root-architecture, dominated by long lateral roots. These lateral roots provided a large, horizontal surface area over which resistance to vertical uprooting occurred. Examination of the uprooted plants indicated that in some cases the lateral roots/runners had snapped during the uprooting test, but the vertical roots were commonly removed intact. Statistical tests showed that a significant difference existed between pullout forces for Sandbar willow and 1-year cottonwoods, 2-year cottonwoods and *Phragmites* (Mann Whitney Rank Sum; $P < 0.001$). Resistance to removal for Reed canarygrass stems was within a similar range to the Sandbar willow seedlings (Figure 27), ranging from 2.5 to 192 N (mean value of 58.3 N, sample size, $n = 100$). Indeed, statistical analysis showed no significant difference between the median values for pullout of Sandbar willow and Reed canarygrass ($P = 0.385$). However, different to the willows, in almost all uprooting tests for this species, failure of the grass stem occurred right at the base of the stem where the roots initiate. The fibrous roots of the Reed canarygrass were dense and highly connected, but each individual root was small and easy to break. In some tests a short length of root was extracted from the substrate, but there was always evidence of rupture of roots, with the majority of roots thus being left in the ground.

Finally, *Phragmites* stems provided the largest uprooting forces out of the four species tested. Forces required for failure of the *Phragmites* stems ranged from 8.9 to 740 N (mean value of 254.5 N, sample

size, n = 115). Statistical tests showed that the median value of the uprooting forces for *Phragmites* was significantly different than all the other species tested (Mann Whitney Rank Sum; $P < 0.001$). The large range of values is likely due to sampling of a range of stem ages and sizes. In addition, some stems that had been sprayed the previous growing season but had not been removed were also tested, and these stems were particularly brittle, resulting in many of the lower forces measured for this species. During uprooting tests for this species the part of the plant that most often failed was the main rhizome attached to each stem, indicating that when pulling on the plants in an upward motion, each stem was stronger than its rhizome. It was interesting to notice, however, that the rhizomes were rarely pulled from the ground intact, with signs of breakage visible, and audible in almost every test. This suggests that even when the force applied to *Phragmites* stems is great enough to cause the rhizome to break, parts of the rhizome network will still be left in the ground, and the plant will thus be able to regenerate in following growing seasons. A few dead *Phragmites* stems that had been sprayed were also tested for pullout resistance. These stems were very brittle and broke easily at the soil surface, leaving the root and rhizome networks in the substrate. These tests suggested that SDHFs may be capable of breaking and removing these dead stems, but the rhizomes left in the substrate may be capable of regeneration the following growing season if not also killed by the spraying process. Seedling mortality may also be affected by sedimentation and inundation in certain locations; these dead stems are also likely to be removed during SDHF events.

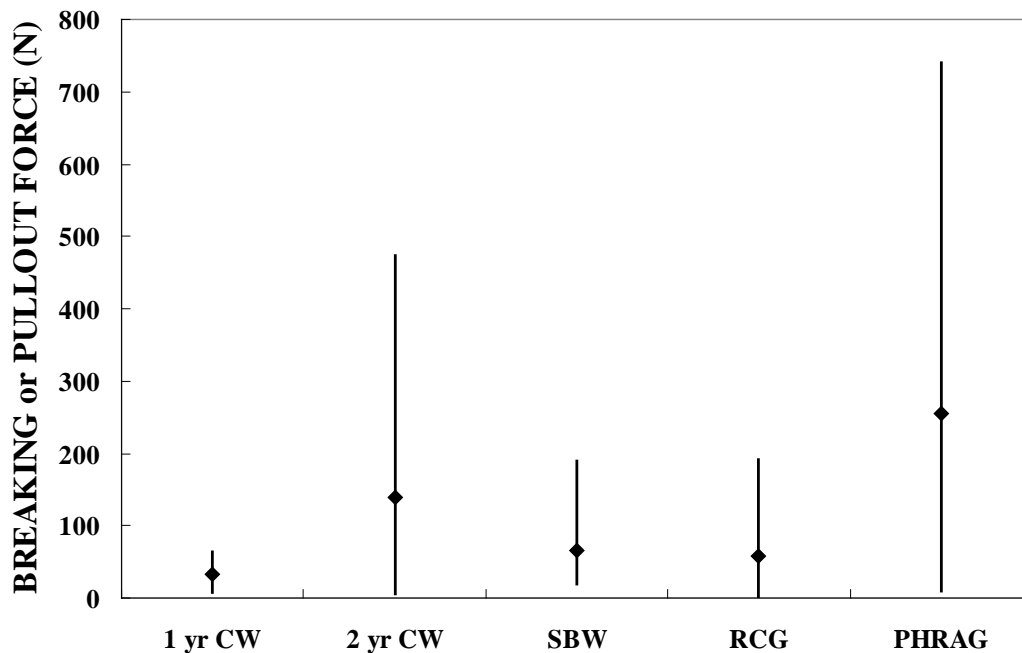


Figure 27. Full range of breaking or pullout forces for each of the four species studied in uprooting tests on sandbars of the Platte River, NE. Diamonds represent mean values.

The data shown in Figures 28 and 29 are the vertical and horizontal rooting extents of plants of each species measured after uprooting tests. As such, they indicate either the full rooting extent (in the case of cottonwood seedlings), or rooting extent to the point of rupture (Reed canarygrass and *Phragmites*). Therefore, although the two-year-old cottonwood seedlings had the longest vertical rooting measurements after the uprooting tests, in their case this length was almost always the full extent of the plant's rooting.

Conversely, *Phragmites* rhizomes broke at depths of up to 0.4 m but these values do not represent the full rooting extent of this species, which, as discussed earlier, was found through full excavation to extend as deep as 1.5 m and greater in some sand bars on the Platte River, NE.

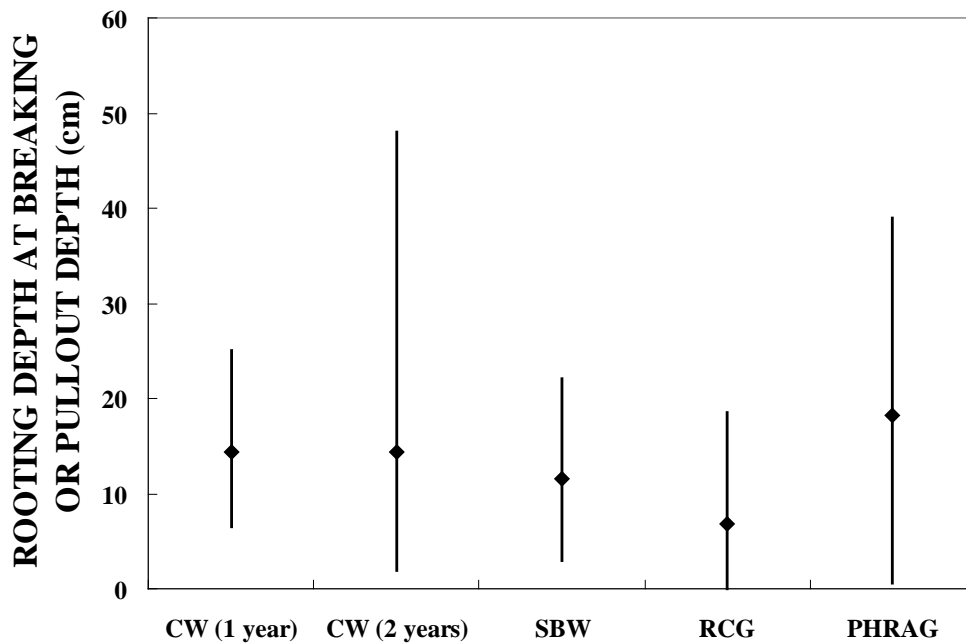


Figure 28. Vertical rooting extent measured after uprooting tests. Diamonds represent mean values with full ranges measured.

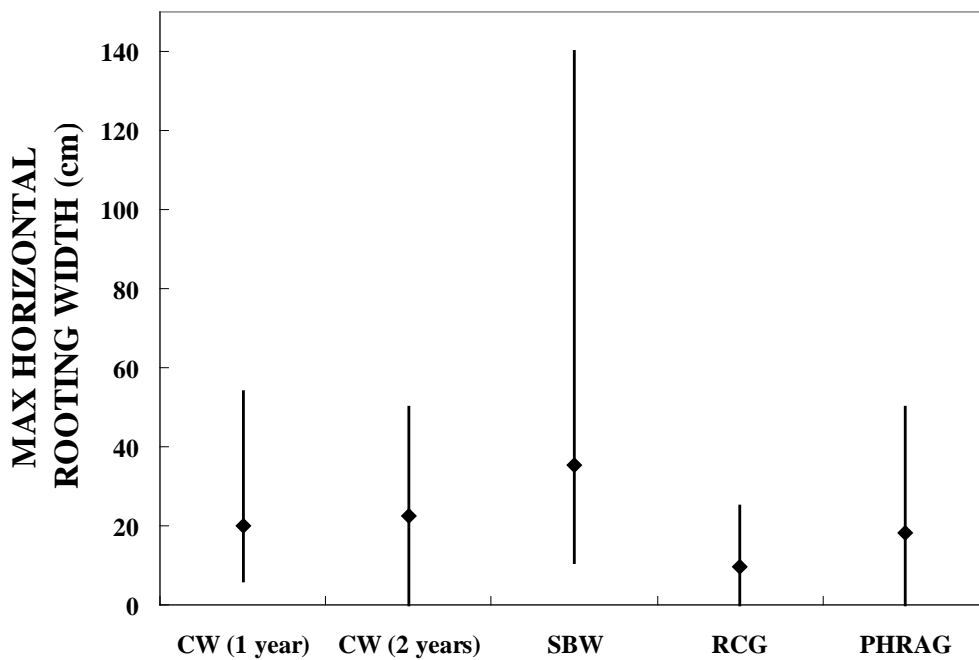


Figure 29. Horizontal rooting extent measured after uprooting tests. Diamonds represent mean values with full ranges measured.

4.3 Comparing root strength, uprooting resistance and plant bending forces

As stated in preceding sections, the stems of *Phragmites* were shown in vertical uprooting tests to be stronger than their rhizomes, and when force was applied to a given stem, in almost all cases the rhizome broke at a certain depth within the substrate. However, when force is applied to *Phragmites* from flow, the resulting effect on the plant stems will depend not only on the breaking strength of the stems and rhizomes, but also the force required to bend stems over. In the case of *Phragmites* stems, field data showed that bending forces were lower than either the stem or rhizome breaking forces, suggesting that when a force is applied to stems of this species, the first “failure” mechanism is likely to be bending of the stems in the direction of flow, rather than stem breaking or uprooting. Figure 30 illustrates the field data collected for plant pullout, root/rhizome tensile strength testing, and bending tests for each species. For *Phragmites*, the populations of data for rhizome breaking and plant pullout showed some overlap because in most cases for the plant to pullout the rhizome had to break. In contrast, the stem bending forces were much lower (mean value of 24.3 N for stem bending compared to 106 and 254.5 N for rhizome breaking and plant pullout respectively). The higher mean pullout force compared to rhizome breaking force is likely because in some tests more than one rhizome had to break for the stem to be uprooted. Interestingly for this species, all one way ANOVA results showed statistically significant differences between uprooting forces, root breaking forces, and stem bending forces ($P < 0.05$).

For cottonwood seedlings, as stated previously, most of the seedlings were uprooted in pullout tests with their entire root-networks intact, indicating that their stems were stronger than the sum of the root strengths, especially when young. Larger roots were shown from the field data collected to be stronger than stems, so as seedlings get older, stem breakage rather than root breakage would be more common during uprooting, leaving roots left in the substrate. In Figure 29 it can be seen, however, that for one-year-old cottonwood seedlings, the range of forces required to bend plant stems overlapped with the population of data for uprooting forces. It is therefore possible to suggest that as flow is applied to these plants more than one predominant failure mechanism might be seen, including plant uprooting or plant bending. Statistical tests confirmed these findings, with one way ANOVA tests indicated that for cottonwood seedlings, uprooting forces were significantly different to root breaking forces ($P < 0.05$), and root breaking forces were significantly different to stem bending forces ($P < 0.05$), but uprooting forces were not significantly different to stem bending forces ($P > 0.05$). Indeed, the mean stem bending force for all of the cottonwood seedlings tested (1 to 2 years combined) was 42.1 N compared to a mean uprooting force for 1-year old seedlings of 31.9 N. As the cottonwood seedlings get older, the force required for uprooting increases rapidly, and differences between data populations for stem bending versus plant uprooting start to emerge. For the two-year-old seedlings the mean pullout force was 139 N, considerably higher than the mean bending force of 42.1 N. This suggests that as the seedlings get older and their resistance to uprooting increases, the primary “failure” mechanism of these plants in flow becomes more likely to be stem bending rather than uprooting.

The roots of Reed canarygrass were much weaker than the plant stems, and thus, during most of the uprooting tests for this species, the roots broke and just the stem was removed. The data in Figure 30 show that the bending and “uprooting” forces for this grass had some overlap in their populations. This suggests that when a flow is applied to this plant species both stem breaking and stem bending are possible outcomes. It is unlikely however, that the roots of this species can be removed from their

substrate unless scour occurs around the dense rootball. For Reed canarygrass all one way ANOVA results showed statistically significant differences between uprooting forces, root breaking forces, and stem bending forces ($P < 0.05$).

4.3.1 Measurement uncertainty and modeling implications

In terms of measurement uncertainty, field measurements using the load cell (plant bending, pullout, root breaking) were all accurate to within 0.1 lbs. Any uncertainty in measurements taken in the field will perpetuate through the RipRoot modeling. Any error in the range of field data measurements would first impact predictions of individual plant uprooting values, and would then multiply up when these values were applied to patch resistances. The assumption was therefore made here that the field data collected accurately represented the full range of possible pullout, bending or root breaking values, for the ages and species tested. We tried to ensure this was the case by sampling a large enough population of plants, and by selecting bars that were representative of the study reach.

Another assumption made in this study, was that the uprooting forces for individual plants were the same vertically as the forces required to pull the plant out by the horizontal force of the flow of water. Whilst in reality the resolution of forces, and root orientations of each plant would likely result in different pullout forces for varying pullout angles, there was insufficient time and funds within this current study to test pullout forces at a range of angles. This also relates to another assumption that all of the force from the flow is transferred to the root ball when drag force is applied. In reality there is some loss of energy through bending of the stems, and only a proportion of the force will be transferred to the roots of each stem.

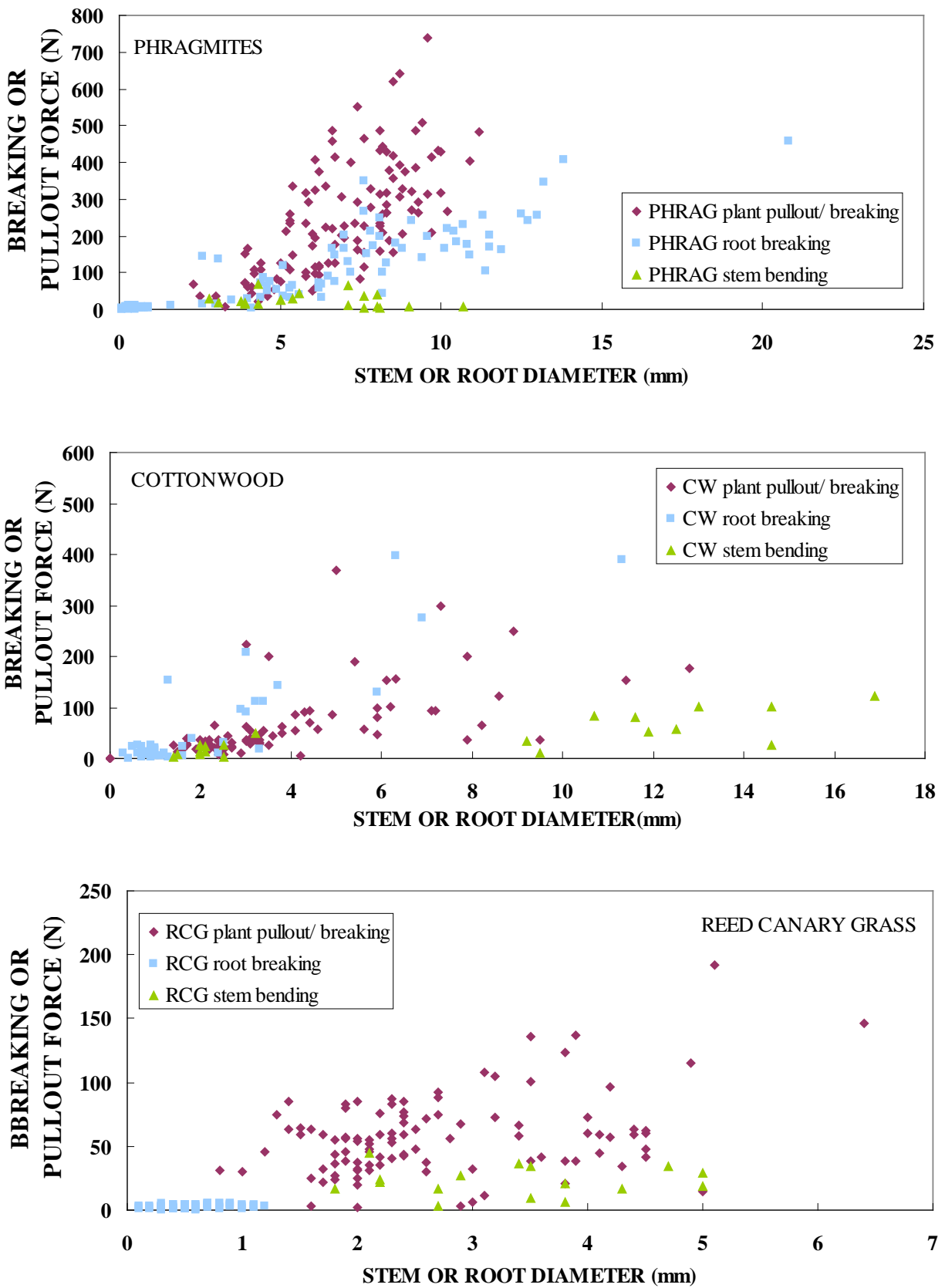


Figure 30. Plots comparing plant pullout forces with root breaking and stem bending forces.

4.3.2 Results of laboratory experiments to test pullout forces under controlled soil moisture conditions

Plants transported from sandbars of the Platte River, NE were used in controlled laboratory experiments to test the effect of antecedent soil moisture on the range and magnitude of uprooting forces for young cottonwood seedlings (Figure 31). Tests were conducted at three different soil moisture contents, the driest being 16.8 %, the wettest being 34.8 % (saturated). Results showed that the mean force required for uprooting increased slightly from 19.2 to 23.8 N as soil moisture decreased, indicating that as the soil dried it became harder to remove plants from their substrate. Statistical tests showed, however, that there was not a significant difference between the tests between the highest and lowest soil moisture contents (Mann Whitney Rank Sum Test; $P = 0.879$). The most noticeable difference between the three sets of tests however, were the maximum forces required for plant removal under different soil moisture conditions. The maximum uprooting force measured at the highest soil moisture was 28.8, which more than doubled under the driest antecedent soil moisture content to 61.1 N. The implication of the results of this set of tests is that plant removal from sandbars of the Platte River, NE, through hydraulic forces and scour, is more likely to occur when the antecedent soil moisture content is higher. At the onset of a flow event the potential for plant removal will likely be lower than later in the same storm event, even if flow depth and discharge remains unchanged, because as the bar material wets up, uprooting resistance decreases. During a SDHF of 2 to 3 days it is very likely that the bars in the central Platte River would become saturated, allowing uprooting resistance to decrease slightly over time during the high flow event.

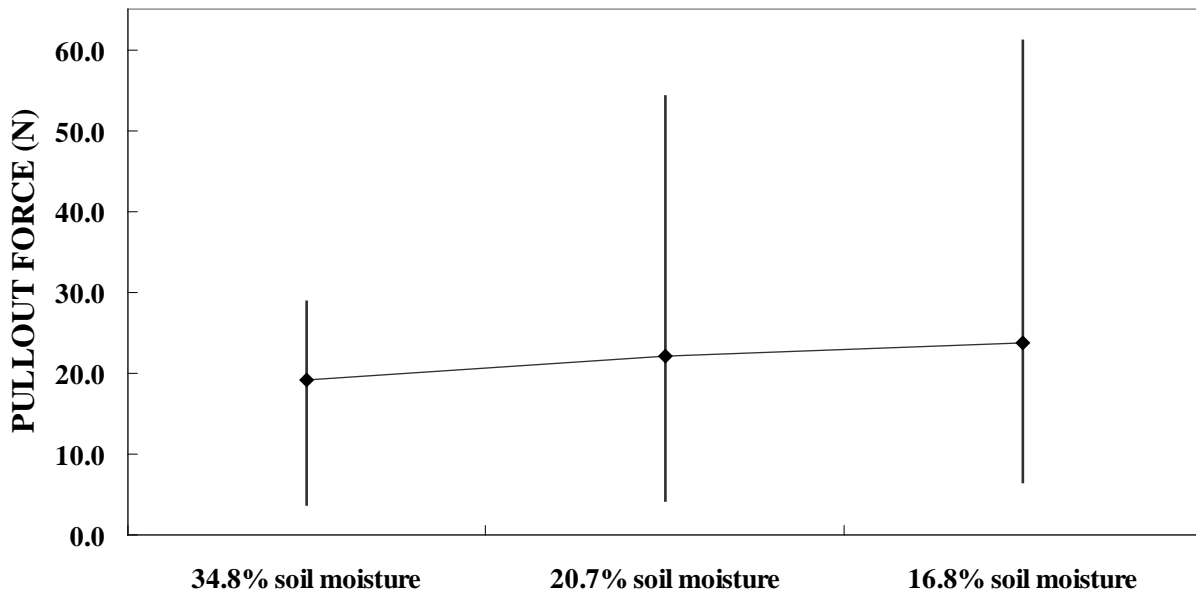


Figure 31. Minimum, maximum and mean pullout forces for one-year-old cottonwood seedlings under controlled soil moisture conditions.

4.3.3 *Modeling plant pullout forces using RipRoot*

To model plant uprooting forces in the RipRoot Model, field data collected for the previous sections were used to parameterize the model. Input parameters are shown in Table 5. The RipRoot model can take into account both breaking and pullout of roots as failure mechanisms. Observations made in the field suggested that the dominant root/rhizome failure process varied according to the species being tested; in the case of *Phragmites* and Reed canarygrass the dominant failure mechanism noted was root/rhizome breaking, whereas for the young cottonwood seedlings the dominant root failure mechanism was pullout. The reason for the difference in dominant root failure mechanisms between species is the way in which the root systems grow and the plants propagate. In the case of *Phragmites* and Reed canarygrass, stems are interconnected by a network of roots, and in the case of *Phragmites*, thick rhizomes, and these interconnections must be broken for a stem to be removed. Cottonwood seedlings tended to have separate root networks, so during pullout most of the roots were removed intact. The exception to this was the observation that deeper taproots of the cottonwood seedlings did break in some uprooting tests; as roots become both bigger in diameter, and grow deeper into the soil, the frictional force required to remove them becomes larger than the force required to break them (Pollen, 2007).

To model each species, the species-specific failure mechanisms noted in the field were applied to the RipRoot code (Figure 32). In the case of *Phragmites* and Reed canarygrass, the code was modified so that breaking was the dominant root/rhizome failure mechanism, whereas for the cottonwood seedlings the code was left unmodified so that pullout *or* breaking could be calculated in the model using the diameter of the roots and the frictional strength of the substrate material; for each root or rhizome modeled the model then selected the mechanism with the lesser force.

Comparing the modeling results with the field data collected for the Platte River, NE, we can see that the model does a good job of estimating the range of potential uprooting forces for each species, when the correct failure mechanisms of the roots are accounted for (Figure 33). Additional runs were carried out to confirm these results, in each case allowing the model to select for pullout or breaking; for *Phragmites* if the model was allowed to select between breaking and pullout, the low frictional resistance of the sandy substrate material led to preferential root pullout rather than breaking, leading to large underestimations of the field measured values for uprooting forces of *Phragmites* stems. This is because the rhizomes of each *Phragmites* stem are connected to those of other stems. Pullout of an individual rhizome is thus very unlikely, and the only way these plants can be uprooted is if the rhizomes actually break. Similar results were seen with the runs for Reed canarygrass. For cottonwood seedlings, if the model selected breaking as the only potential failure mechanism for root failure, large overestimations in uprooting forces were seen. This is because the roots of an individual cottonwood plant are separate from other plants and when uprooted, pullout of the majority of roots occurred, and only the largest/longest roots broke.

Table 5. Input parameters for RipRoot modeling.

Input Parameter	<i>Phragmites</i>	Reed Canarygrass	Cottonwood (1 yr-old seedlings)	Cottonwood (2 yr-old seedlings)
Minimum root/rhizome diameter (mm)	1	0.1	0.3	0.3
Maximum root/rhizome diameter (mm)	20.8	1.2	3	9
Tr a parameter*	16.2	3.63	15.05	15.05
Tr b parameter*	-0.91	-1.68	-0.52	-0.52
Minimum plant density	96	348	1	1
Maximum plant density	272	912	28	28
Soil friction angle	27	27	27	27
Soil bulk density	19.2	19.2	19.2	19.2
Maximum rooting length (m)	0.39	0.19	0.48	0.48
Number of roots/rhizomes failing by breaking	1 to 3	125	0 to 1	0 to 2
Number of roots/rhizomes failing by pullout	0	0	20	20

*Where root tensile strength equations are generally of the form $Tr = ax^{-b}$ and Tr = tensile strength, x = root diameter, a and b are regression parameters.

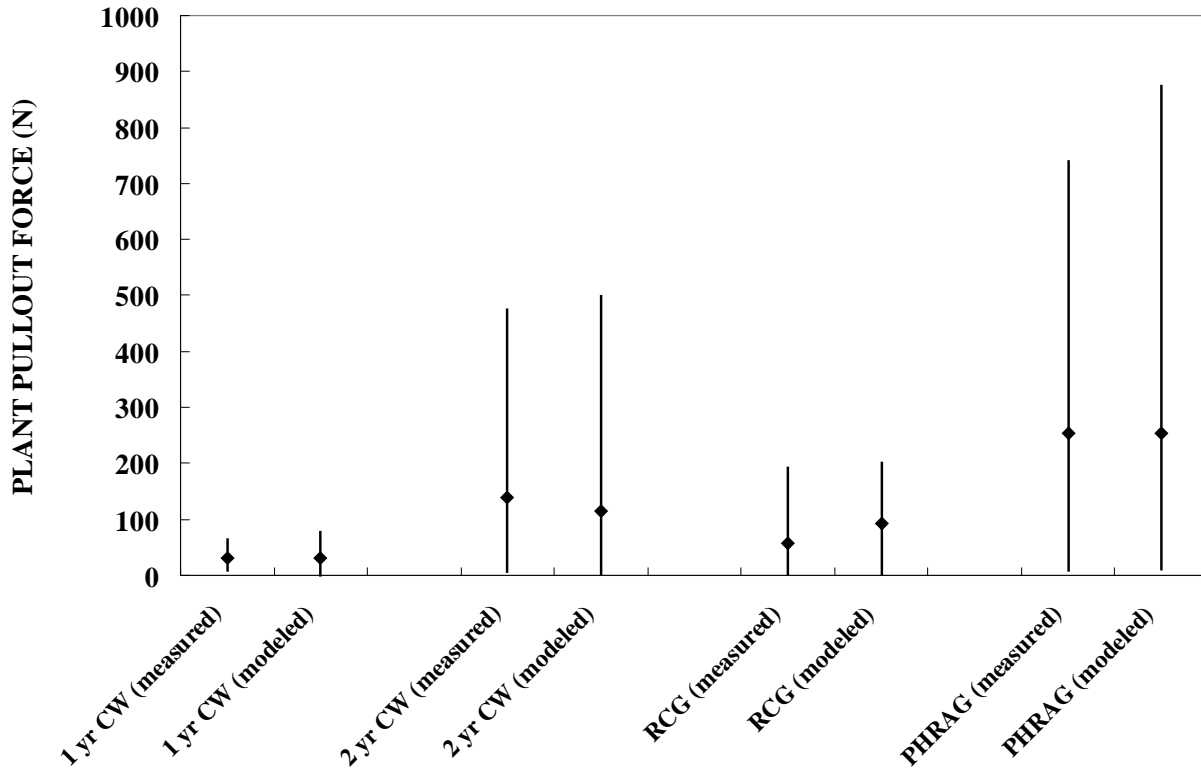


Figure 32. Measured versus modeled values for each species. The vertical lines represent minimum and maximum values, the diamonds represent mean values.

Once the RipRoot model had been validated against our field measurements by incorporating the correct root failure mechanisms, the model could then be used to model potential changes in uprooting forces with increasing scour around the stems (ie. decreased rooting length). In the case of *Phragmites* and Reed canarygrass because the roots and rhizomes of these species were found to break rather than pullout of the substrate during uprooting, any change in rooting length had no effect on the force required to uproot these plants (i.e. root or rhizome breaking forces are independent of burial depth) (Figure 33). For cottonwood seedlings, because the predominant failure mechanism for their roots was pullout rather than breaking, and because pullout forces are affected by root surface area in contact with the soil, changes in rooting length, or scour around the root network was predicted by RipRoot to affect plant pullout forces (i.e. the force at which some plants start to be uprooted). The plot in Figure 33 shows the minimum force required for pullout of the three main species tested. It can be seen for cottonwood seedlings there was a difference in the force required for initiation of uprooting of these species according to plant age (one or two years of growth), and that the response to scour/deposition was non-linear. Therefore, a change in rooting depth, or scour depth of say, 0.1 m had a greater effect when the plant was deeply rooted, than when the plant was shallowly rooted. At shallow rooting depths (< 0.5 m) scour of material from around the roots had very little effect on the force required to start uprooting cottonwood plants.

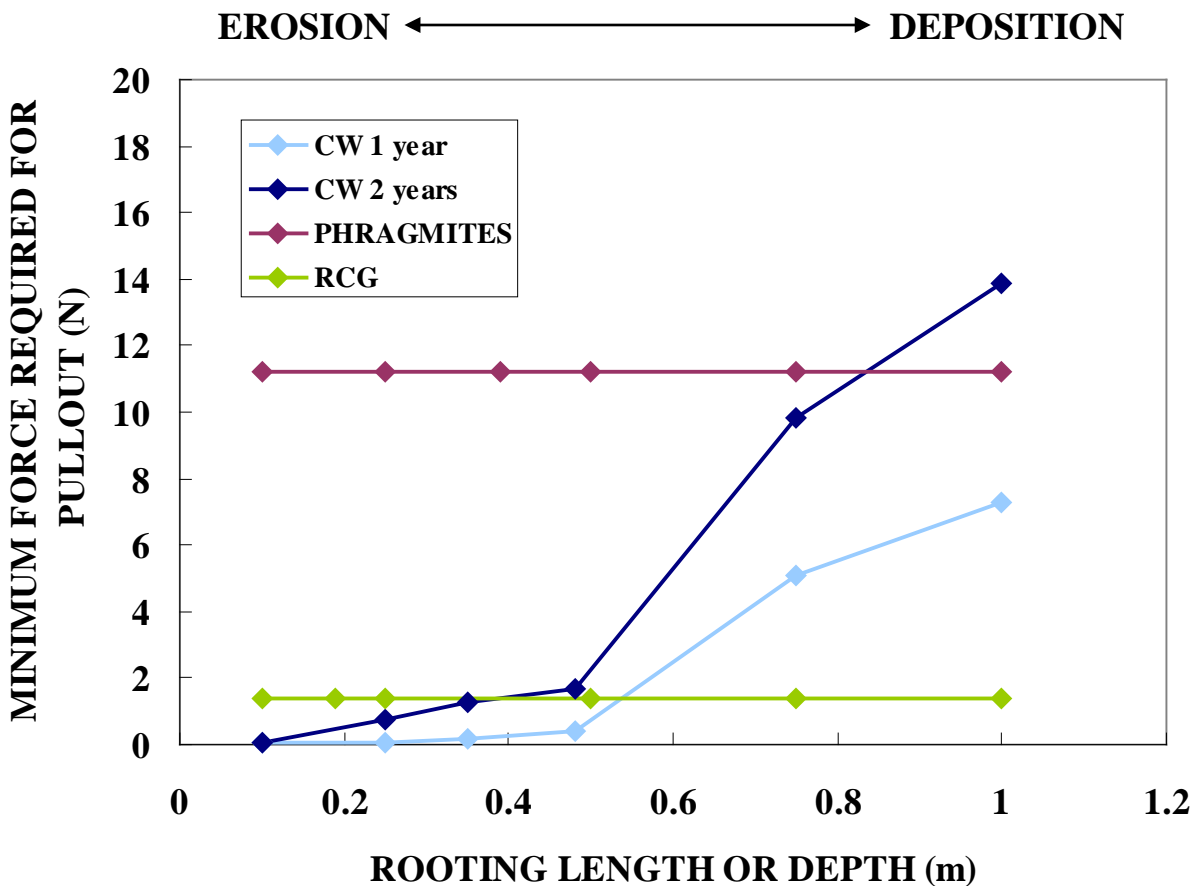


Figure 33. Minimum force required to initiate uprooting of plants, at varying rooting depths.

The data in Figure 34 shows only the model results for the forces required to initiate uprooting of each plant species from sandbars of the Platte River, NE. In the following plots (Figures 34A and 34B), the modeled minimum, maximum and mean forces required for uprooting at a given rooting depth are shown for both one and two-year-old cottonwood seedlings; field data are also shown as a validation of the model results. As with the minimum force required to uproot the cottonwood seedlings, the mean and maximum forces also show distinct non-linearity. Most of the one-year-old cottonwoods uprooted in the field had shallow rooting depths of < 0.3 m, but the implication from the non-linearity in the modeling results is that if these young seedlings were to experience deposition around them, the force required to remove them would increase dramatically. Within the range of rooting depths noted for both one and two year old cottonwoods, the change in uprooting forces with rooting depth or scour depth changed very little, suggesting that for this species, scouring of material from around the roots would have little effect on the forces that need to be applied to a given cottonwood plant for it to be removed by flow. It is interesting to note that the force required to initiate uprooting of some of these plants (i.e. the minimum force required for removal) was similar for both the one and two-year-old seedlings. However, the mean and maximum values required for plant removal were considerably higher for the two-year old seedlings. This suggests that although initiation of removal of both one and two-year old seedlings may occur under similar flow conditions, the *percentage* of plants removed under a given flow condition will be lower for the two-year-old than the one-year-old seedlings.

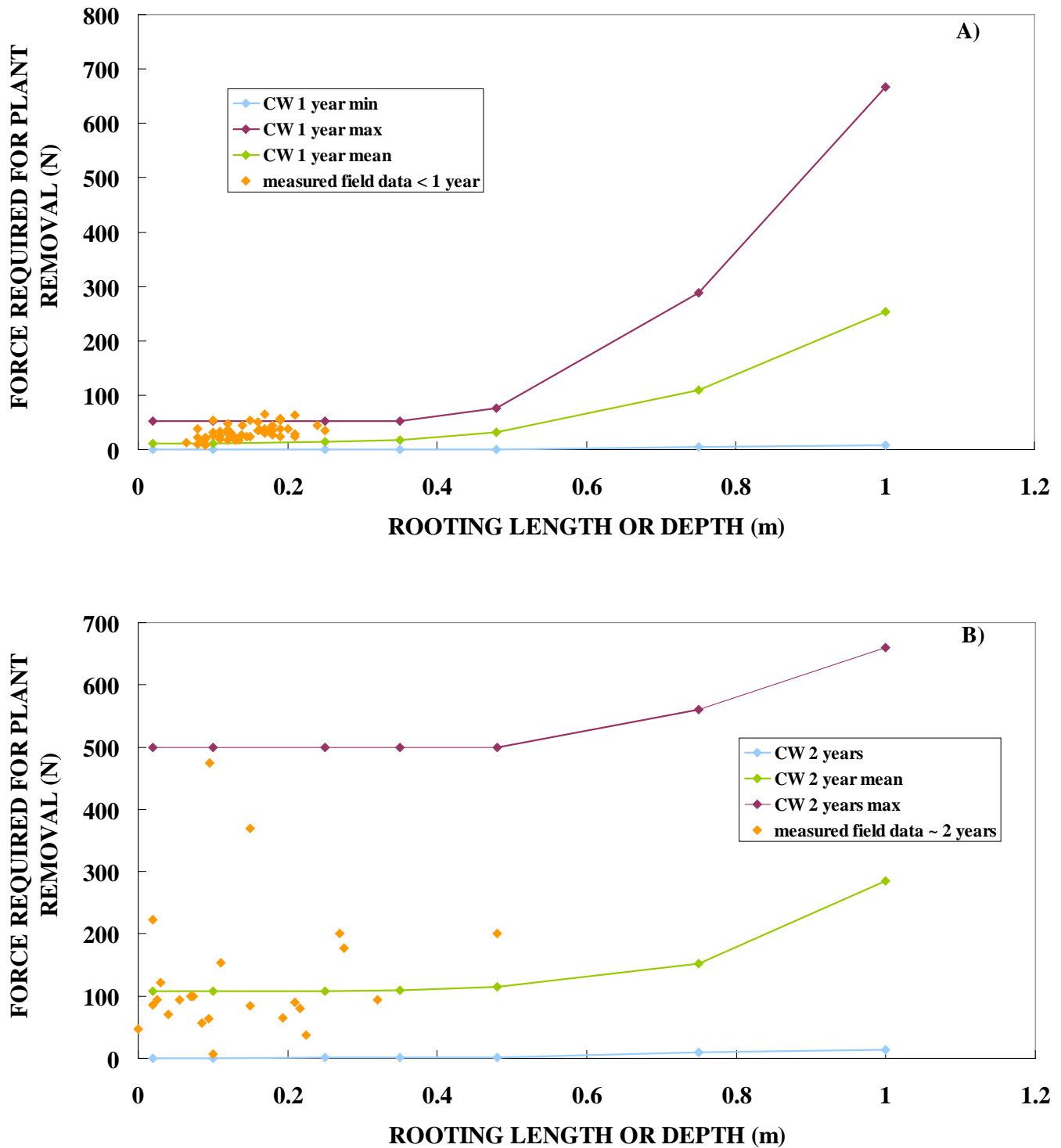


Figure 34. A) Modeled minimum, maximum and mean uprooting forces, and measured uprooting forces for one-year-old cottonwood seedlings B) Modeled minimum, maximum and mean uprooting forces, and measured uprooting forces for two-year-old cottonwood seedlings.

4.3.4 Modeling resistance of plant patches to removal using validated RipRoot model.

The flow acting on a vegetated bar acts over an area, rather than on individual plants. It was necessary, therefore, to calculate the total resisting force of patches of plants over a range of typical stem densities. To accomplish this, once RipRoot had been validated against field data for individual plants, additional Monte Carlo simulations were performed to quantify the range of potential patch resistances for each species. Minimum and maximum stem densities measured on bars of the Central Platte River were used as input to the model (see Table 3; Section 4.2.5). Listed below are the steps taken by the model to calculate the resisting force of the patches of plants:

1. Select a species from the three species tested
2. Select a plant density based on minimum and maximum densities measured in field, and based on a normal distribution.
3. For each plant, select a number of roots or rhizomes, based on minimum and maximum values collected in the field, and a normal distribution.
4. For each root of each plant, select a root diameter, based on diameter-distributions collected in the field (typically more small diameter roots than large diameter roots).
5. Calculate root tensile strength for each root of each plant, based on species-specific results obtained from fieldwork
6. Group roots and rhizomes from all plants together to run progressive breaking algorithm
7. Algorithm calculates which roots break first, and the stress to be redistributed to remaining in-tact roots. This is repeated until all roots have broken, recording the total resisting force supported by remaining roots at each timestep.
8. Repeat steps 1 through 7 25,000 times to establish ranges of patch resistances for each species.

The resistance of a patch of plants is therefore dependent on the number of roots per plant, the strength of those roots, and the density of plants in a given area. RipRoot results for patch resistances showed dramatic differences between the three species tested. Patches of cottonwood seedlings had the lowest patch resistances (Figure 35), ranging from 0.4 (sparse seedling density) to 685 N (highest seedling density) for 1-year old seedlings and from 0.7 to 2,400 N for 2-year old seedlings. Reed canarygrass had the next highest patch resistance to uprooting, with forces ranging from 2.7 to 8,500 N. *Phragmites* had by far the highest resistance to uprooting, with estimated forces ranging from 300 to 42,000 N.

It is important to remind readers here that the range of uprooting resistances for individual plants predicted by RipRoot was slightly larger (in terms of minimum and maximum forces) than the range of measured values in the field. As noted in the methodology, up to 100 plants per species were measured in the field, and these values, along with additional input data measured in the field were used to parameterize the model. When the model was run, 25,000 iterations were performed, resulting in a larger range of output values than that given by the field data; this RipRoot output range reflected the potential upper and lower limits of plant resistances that could have been expected had our sample size in the field been infinitely large. The patch resistances shown in Figure 35 were based on the RipRoot runs for individual plants and as such reflect not only variations in stem density, but also, this larger range of modeled plant pullout forces. The implications of these patch resistance results in terms of plant removal

by flowing water, will be discussed in Section 5 when these forces are compared with the drag forces given in Section 4.1.5.

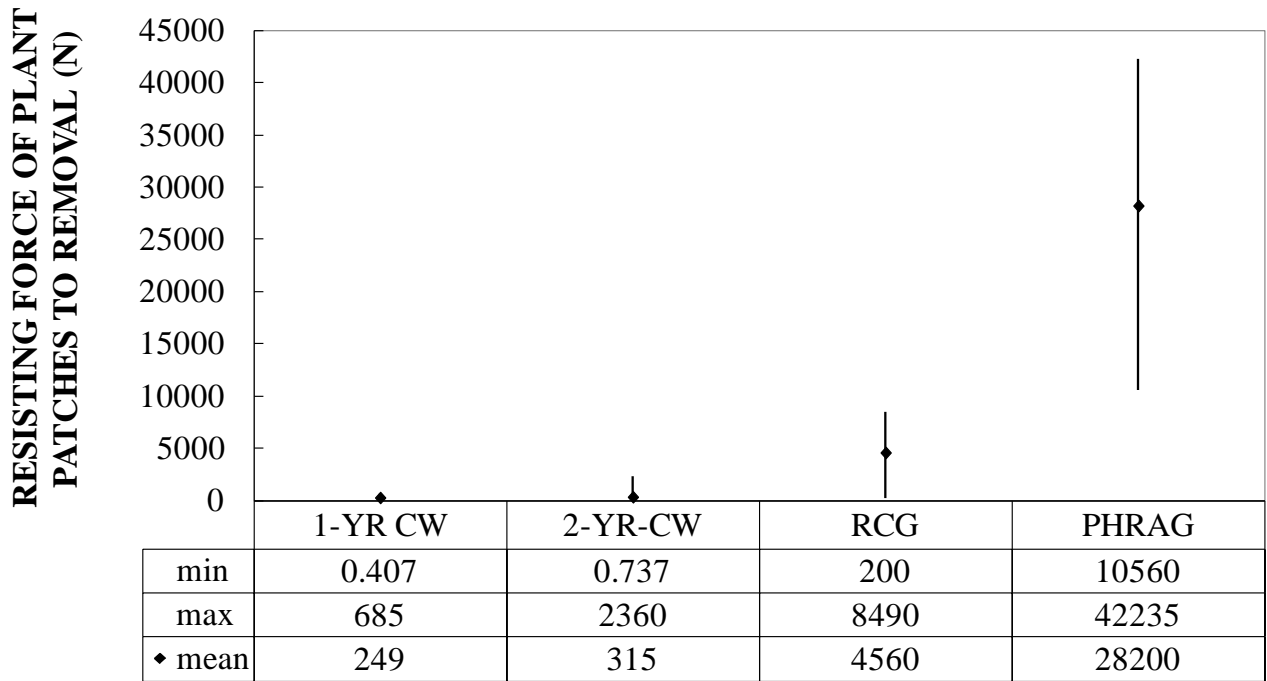


Figure 35. Resistance of plant patches to removal by uprooting. Vertical lines indicate minimum and maximum uprooting force per patch of plants. Diamonds indicate mean values.

5 IMPLICATIONS FOR THE MANAGEMENT OF VEGETATION

In the previous sections we have provided the drag forces acting on each of the three plants species during flume experiments carried out at USDA-ARS-NSL, and the in-field measurements of resistance of the same species to uprooting and bending. In this section, we will draw together those results so that we can evaluate whether PRRIPs target Short Duration High Flow events (SDHFs) of 5,000 to 8,000 cfs are likely to be of sufficient duration and magnitude to remove stands of these study species. In addition, we will discuss predicted values of local scour around plant stems for a range of discharges, and the effect that local scour may have on plant removal alone and in combination with drag forces.

5.1 Comparing drag forces (driving) with uprooting forces (resisting) of vegetation

For plants to be removed from their substrate (in this case, in-channel bars) during a flow event, the driving forces acting on the vegetation must exceed their resisting force. To illustrate how these forces compare for the three species tested herein (cottonwood seedlings < 2 years old, *Phragmites*, and Reed canarygrass), the ranges of driving and resisting forces are shown in Figures 37 to 39. In each figure, two lines indicate where the drag forces (driving) overlap with the resisting forces (uprooting or bending). The first line shows the highest drag force measured for up to 0.25 ms⁻¹ flow velocities measured in our flume study, and the second line shows the estimated increase in drag forces that could be expected for velocities up to 1.5 ms⁻¹. In the case of cottonwood seedlings (Figure 36), drag forces measured during flume experiments overlap with the lower end of the ranges of predicted uprooting forces (i.e. those with less well developed root networks and shallow rooting), and the lower end of bending forces measured in the field. At the range of velocities measured in the flume experiments (up to 0.25 ms⁻¹), it therefore seems likely that only the very youngest and/or, most shallowly rooted seedlings will be removed through drag applied by flow, and some may experience bending. Flow velocities that could be experienced in the field may be as high as 1.5 ms⁻¹ during SDHFs in the Central Platte. At high flows there is also an increasing chance that the weakest seedlings could be removed. To estimate drag forces at higher velocity flows, the following methodology was used:

- 1) A relation was developed between percent change in plant projected area and applied force (from field bending test data)
- 2) The drag force equation was solved using a given velocity, projected area with no bending or streamlining (from flume data), with drag coefficients coming from flume data
- 3) The plant projected area was recalculated for the force calculated in 2) using relation developed in 1)
- 4) The drag force was re-solved using new plant projected area from 3)
- 5) Steps 3) and 4) were iterated through until a solution was reached
- 6) This process was repeated, solving for different flow velocities and different species and stem densities

It should be noted that the approach described above does not account for complex flow patterns and characteristics that can occur during larger flow events, such as avulsions, woody debris transport and lateral erosion of the bank and bar edges. The approach here may therefore underestimate the erosive ability of larger flow events where complex flow elements could develop.

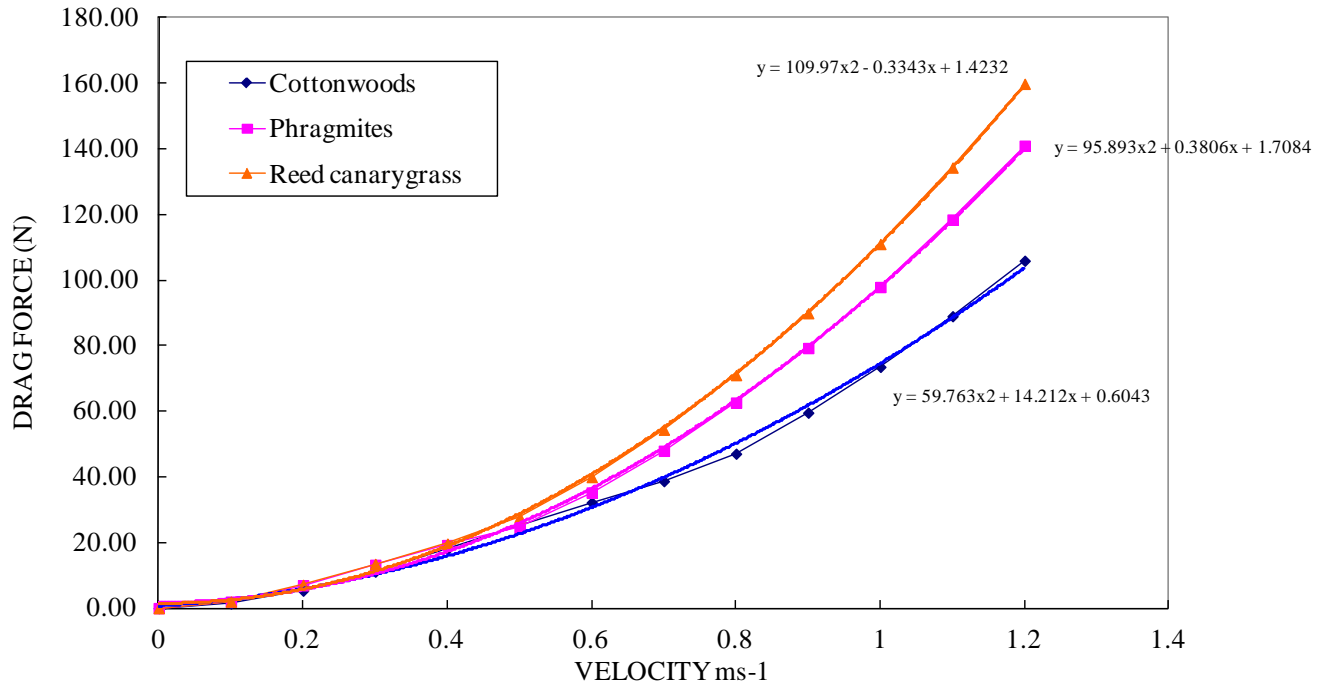


Figure 36. Drag forces calculated for flow velocities beyond those used in the flume experiments.

In each of Figures 37 – 39, minimum, maximum and mean values modeled for patch resistance, and measured for bending resistance of cottonwoods, *Phragmites*, and Reed canarygrass are shown. The statistical distribution of plants within these ranges is unknown, and will vary according to localized variations such as water table height, local plant competition, and substrate composition, to name but a few. Drag forces acting on young cottonwood seedlings were calculated to be up to approximately 156 N at a flow velocity of 1.5 ms⁻¹ (Figure 37), and would be sufficient to bend all young (<2 years old) cottonwood seedlings growing on sandbars affected by a flow of this magnitude. In addition, drag forces at 1.5 ms⁻¹ are likely to be capable of removing the weakest one to two-year old seedlings; the estimated drag force acting at this velocity (156 N) is still well below the mean values for patch resistances of one and two year old cottonwood seedlings, of 249 and 315 N respectively. It should, however, be noted that because these plants are elastic, not rigid, not all of the drag force applied to the stems during a flow will be transferred to the roots. At low flows this loss of energy in the stems will likely result in very few cottonwood seedlings being removed, and even at high flows this elastic energy loss may reduce the likelihood of all but the weakest of these plants being removed by flows, with the majority of plants simply bending over. The lines indicating drag forces in Figure 37A (1-yr-old seedlings) are actually slightly higher than those shown in Figure 37B (2-yr-old seedlings), because the drag forces measured for the lower stem density of 2-yr-old seedlings were slightly lower than for the higher density 1-yr-old seedlings. Furthermore, by the second year of growth, rooting depth for most seedlings will have increased. Therefore, in addition to the decreased drag being applied to these seedlings as stem density decreases, uprooting and bending resistances will increase as the plant invests more energy in above- and below-ground biomass with each additional growing season. The probability of a SDHF removing cottonwoods from channel bars is thus reduced with each season of growth.

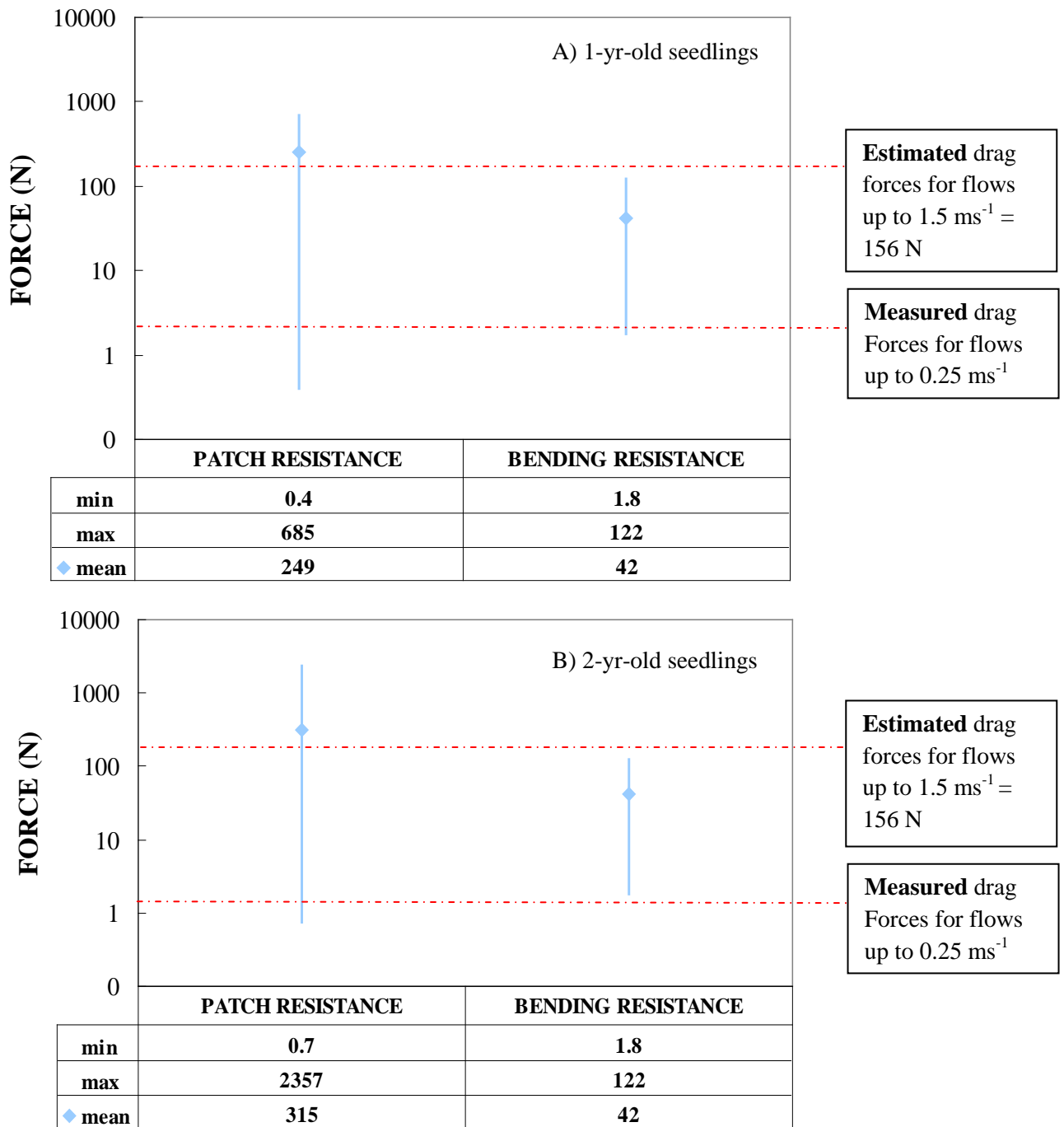


Figure 37. Maximum drag (driving) forces calculated from flume study, and estimated for maximum in-field velocities, compared with patch uprooting resistance, and bending resistance. A) shows results for 1-year-old cottonwood seedlings with stem density of 26 stems per m² and B) shows results for 2-year-old cottonwood seedlings with stem density of 13 stems per m².

For Reed canarygrass (Figure 38), the drag forces measured in the flume (up to 0.25 ms^{-1}) suggest that at this range of flows the driving force acting on the grass is lower than both ranges of forces for uprooting and bending at the lower stem density of 400 stems per square meter. In the case of the higher stem density of 800 stems per square meter, higher drag forces were recorded, and under these conditions, some bending of grass stems may occur. As previously discussed for cottonwoods, the grass stems are not rigid, and as such, some of the drag force is absorbed by the stems and leaves of the grass, with only a portion of that force being transferred to the roots. It is therefore very unlikely that stems of this plant will be removed by flows in the range of the flume experiments. At a flow velocity of 1.5 ms^{-1} , drag forces were estimated to be approximately 248 N, therefore always exceeding the force required for stem bending. At these drag forces, some weaker, more exposed stems may experience breaking or uprooting, but this is likely to be limited (the mean patch resistance for Reed canarygrass was 4560 N), and bending will tend to be the dominant process observed. It is also important to note that the log scale can be a little misleading, and the line indicating the maximum drag force recorded for flow velocities up to 1.5 ms^{-1} for 800 stems/m^2 , represents only a very small portion of the total range of uprooting forces for patches of Reed canarygrass.

In the case of *Phragmites* (Figure 39), the drag forces from the flume study (up to 0.25 ms^{-1}) were lower than both the forces required for bending and for uprooting. At the estimated drag forces for flows up to 1.5 ms^{-1} (218 N) drag forces exceed the full range of bending forces, but are still insufficient to initiate uprooting of even the weakest and sparsest patches of *Phragmites*. As with Reed canarygrass, at high flows bending will be the dominant result during SDHFs rather than uprooting or stem breaking.

The results presented in this section therefore suggest that at high flows, limited numbers of cottonwood seedlings may be removed by drag forces, but for Reed canarygrass and *Phragmites* stem bending will dominate over uprooting. For cottonwoods, the likelihood of seedling removal will decrease with each additional year of growth, as rooting depths increase and lower stem density reduces drag forces acting on a stand of seedlings. SDHFs targeted towards the beginning of the growing season, while rooting depths are still shallow, would maximize the chances for removal of cottonwood seedlings, as well as other annual plant species. Established cottonwood trees, Reed canarygrass, and *Phragmites*, do however, from the results of this study, appear to be very resistant to removal through drag forces applied by high flows. The presence of annual plants such as *Eragrostis*, *Cyperus*, *Xanthium* and *Echinochloa* (Johnson, 2000) increases the roughness of the bars and would thus reduce the hydraulic shear stress available for scour and drag around the stems of woody vegetation. The period of time during the year when annuals have not yet vigorously colonized bar locations, therefore provides PRRIP with the best opportunity for SDHFs to scour around, and exert drag on stems of woody vegetation.

In the next section, then, we consider how much scour is likely to occur around plant stems during SDHFs, and what impact this local scour may have on uprooting forces and removal by drag forces.

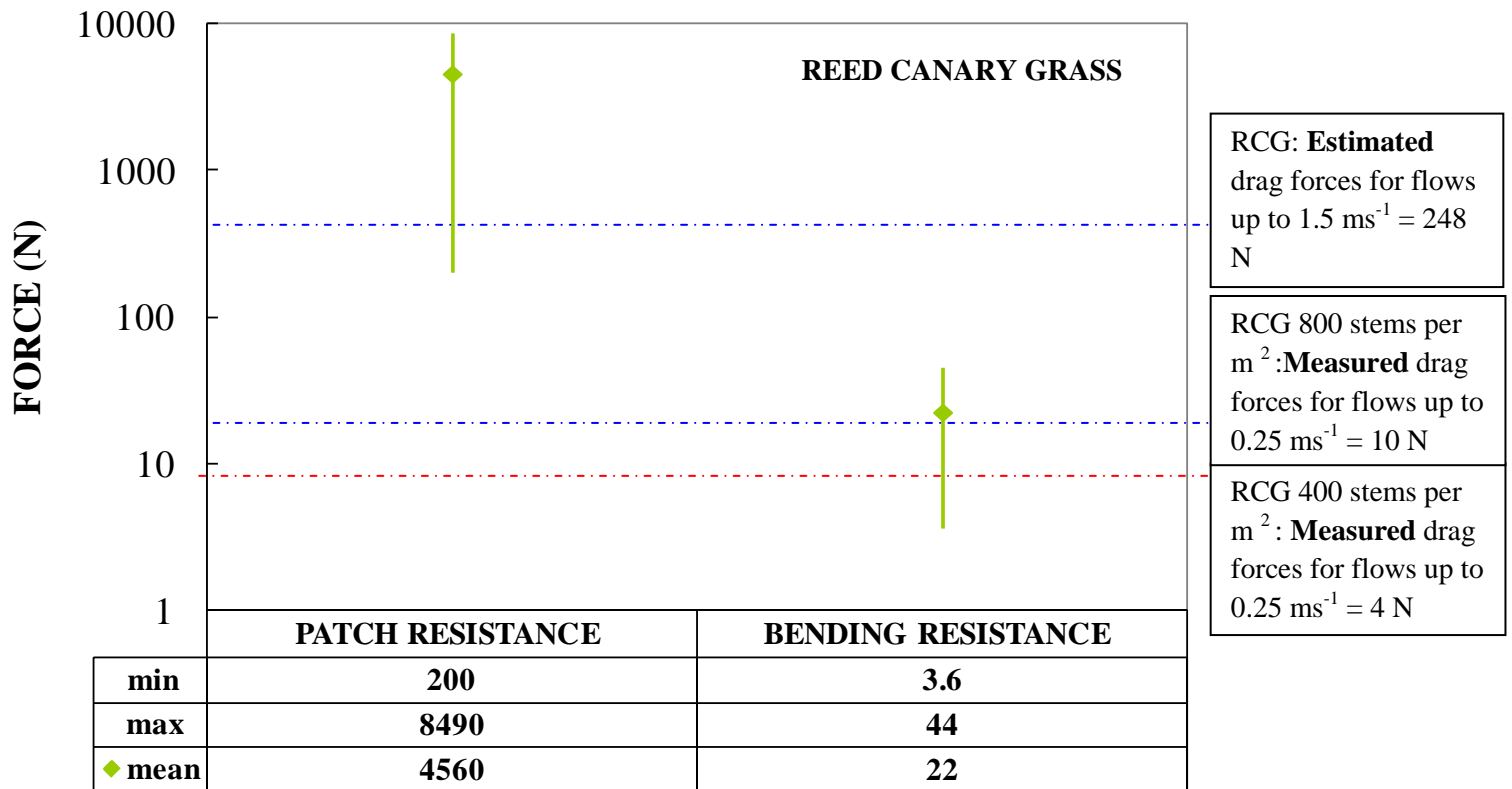


Figure 38. Maximum drag (driving) forces calculated from flume study, and estimated for maximum in-field velocities, compared with patch uprooting resistance, and bending resistance A) shows results Reed canarygrass with a stem density of 400 stems per m^2 and B) shows results for Reed canarygrass with a stem density of 800 stems per m^2 .

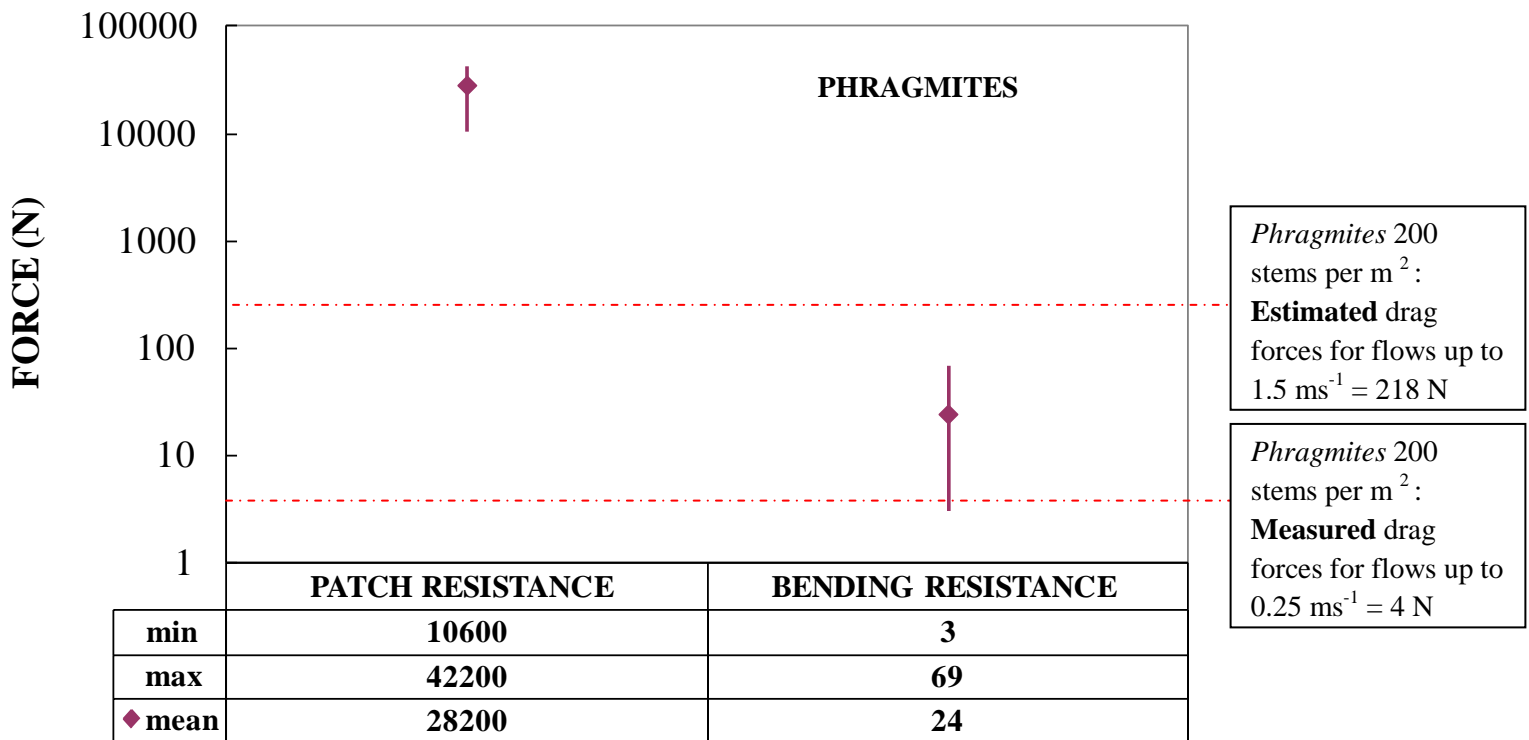


Figure 39. Maximum drag (driving) forces calculated from flume study, and estimated for maximum in-field velocities, compared with patch uprooting resistance, and bending resistance. Data shown are for *Phragmites* stems with a density of 200 stems per m².

5.2 Magnitude and duration of flow events required for scour of bar vegetation on the Platte River, NE

The previous section suggested that drag forces during SDHFs alone are insufficient to clear the bars of the three vegetation species studied here, especially once the vegetation has established. It is therefore necessary to consider how much local scour can be expected around the base of the plant stems during flows of various magnitudes and durations, and whether this local scour can affect uprooting forces enough to increase uprooting by drag forces. To calculate local scour for each of the three plant species, it was first necessary to develop discharge-depth rating curves for sections along the study reach. Three cross section geometries corresponding closely (at or within 0.1 miles) to our three field sites were selected from a report by Holburn et al (2006), at river miles 230.8, 228.7 and 210.6. The blue water line mark on each cross section represents an estimation of flow elevation at 8,000 cfs through the main channel alone (Figure 40).

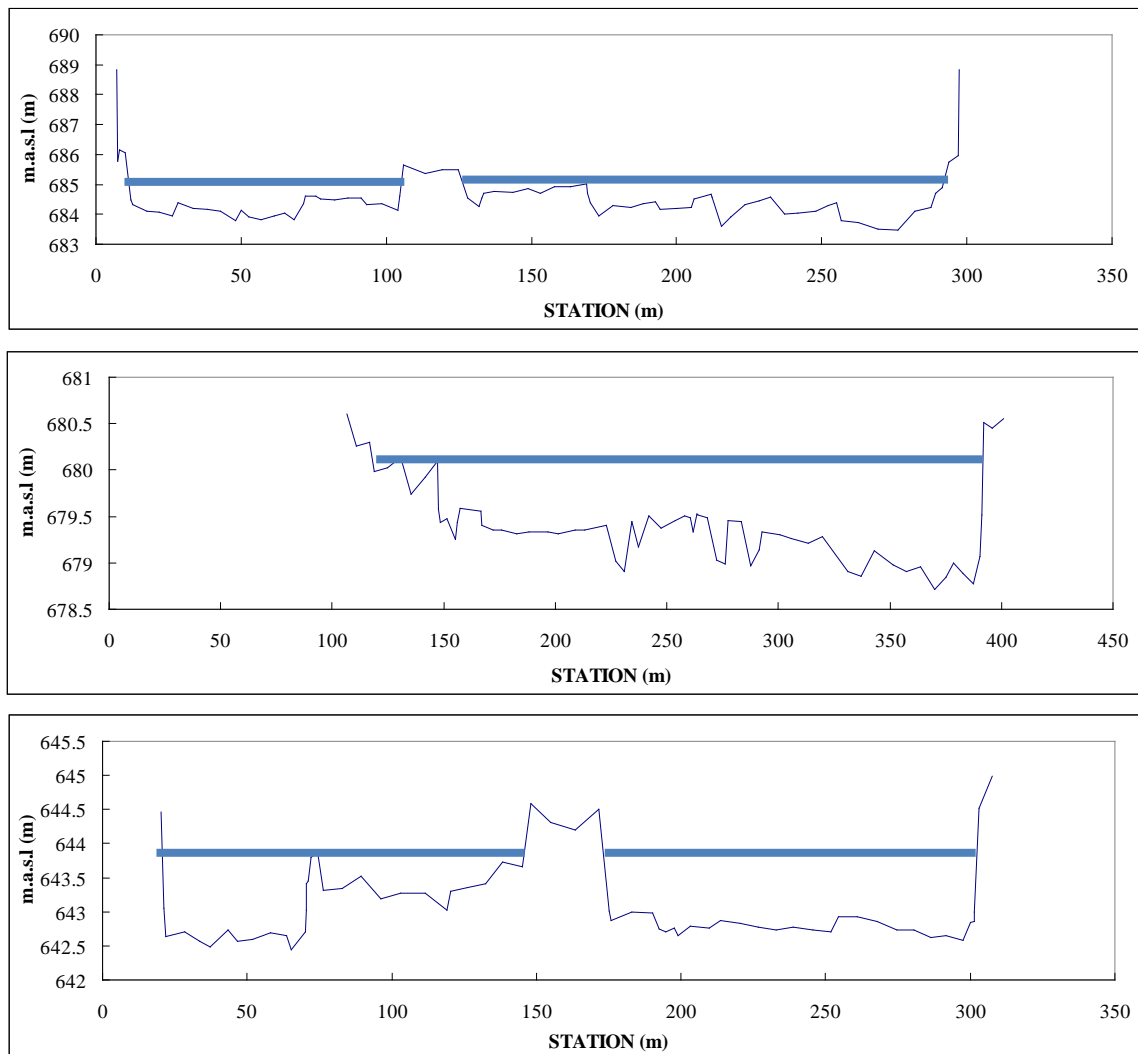


Figure 40. Cross sections at river miles 230.8, 228.7 and 210.6 as given by Holburn et al. (2006), and used in this study to estimate discharge at different flow stages.

First, a normal depth approximation method was used to calculate discharge values for incremental values of stage in each of the three main stem cross sections. Normal depth approximation assumes uniform flow conditions. Therefore, in a one-dimensional frame of reference, the uniform flow equation (Manning's equation) can be used to estimate the cross-sectional average velocity ($U = R^{2/3}S^{1/2}/n$). A Manning's n value of 0.035 was used in these calculations. Discharge and slope values (0.013) were then used to estimate the depth of local scour around vegetation stems, as predicted by a range of bridge-pier scour equations (See Section 2.2.1). In the following two sections we will discuss first, the equilibrium scour depths reached around vegetation stems at the three sites, at a range of discharges/flow depths/flow velocities (i.e. flow magnitude), and then second, the time taken to reach these equilibrium scour depths (i.e. flow duration).

5.2.1 Maximum (equilibrium) scour depths at the base of plant stems

As stated in Section 2.2.1 four bridge-pier scour equations were used to provide a range of predicted scour depths. The equations of Melville and Sutherland (1988), HEC-18 (Richardson and Davis, 2001) and Superposition of Components (Richardson and Davis, 2001), all produced consistent results within the same order of magnitude; as HEC-18 is generally considered to be one of the most reliable bridge-pier scour equations, the results from these three equations were used to compare possible ranges of equilibrium scour depths. Indeed, comparison of results from a range of bridge-pier scour equations by Chase and Holnbeck (2004) showed that bridge pier-scour depths calculated with the HEC-18 equation were rarely smaller than measured pier-scour depths. In addition, pier-scour depths calculated using the HEC-18 equation were closer to measured scour than for the other equations that did not underestimate pier scour. In this current study, the equation of Froehlich (1988) gave scour depths that were consistently an order of magnitude higher than the other three equations and are omitted in the plots in Figures 41 - 43 so that differences between the remaining three equations can be seen more easily. Figure 41 shows results for the site at River Mile 230.8, Figure 42 shows results for River Mile 228.7, and Figure 43 shows results from River Mile 210.6. The results for the three species are separated out as their average stem diameters, as measured in the field, were considerably different, and this is an important parameter in the scour depth equations. Mean stem diameter for *Phragmites* was 6.0 mm. Results for Reed canarygrass and cottonwood were the same as their mean stem diameters were both 3.1 mm.

Results for the site at RM 230.8 (Figure 41) showed equilibrium scour depths calculated using HEC-18 were higher than for the Superposition of Components Equation which were higher than the Melville and Sutherland equation. This same pattern also existed at the other two sites tested. Equilibrium scour depths ranged from 0.005 to 0.055 m for *Phragmites* at RM 230.8, from 0.01 to 0.05 m at RM 228.7 (Figure 42), and from 0.015 to 0.055 m at RM 210.6 (Figure 43). Local scour in the range of 0.5 to 5.5 cm was therefore predicted for *Phragmites* at these three sites. For Reed canarygrass and cottonwood seedlings, the equilibrium scour depths ranged from from 0.005 to 0.035 m at RM 230.8, from 0.005 to 0.033 at RM 228.7, and from 0.005 to 0.033 m at RM 210.6. Local scour in the range of 0.5 to 3.5 cm was therefore predicted for Reed canarygrass and cottonwood seedlings at these three sites. These scour depths cover a range of flow depths up to 1.7 m, with associated discharges of up to the planned SDHFs of 8,000 cfs and velocities of up to 1 ms^{-1} . The results show that equilibrium scour depth increases with flow depth, discharge and/or flow velocity, but the trends are non-linear at low flow depth/discharge/velocity. It can also be seen that as discharge increases, initially local scour depth equilibriums around the vegetation

stems increase rapidly, but at higher discharges, further increases in flow rate have less of an effect on local scour depths.

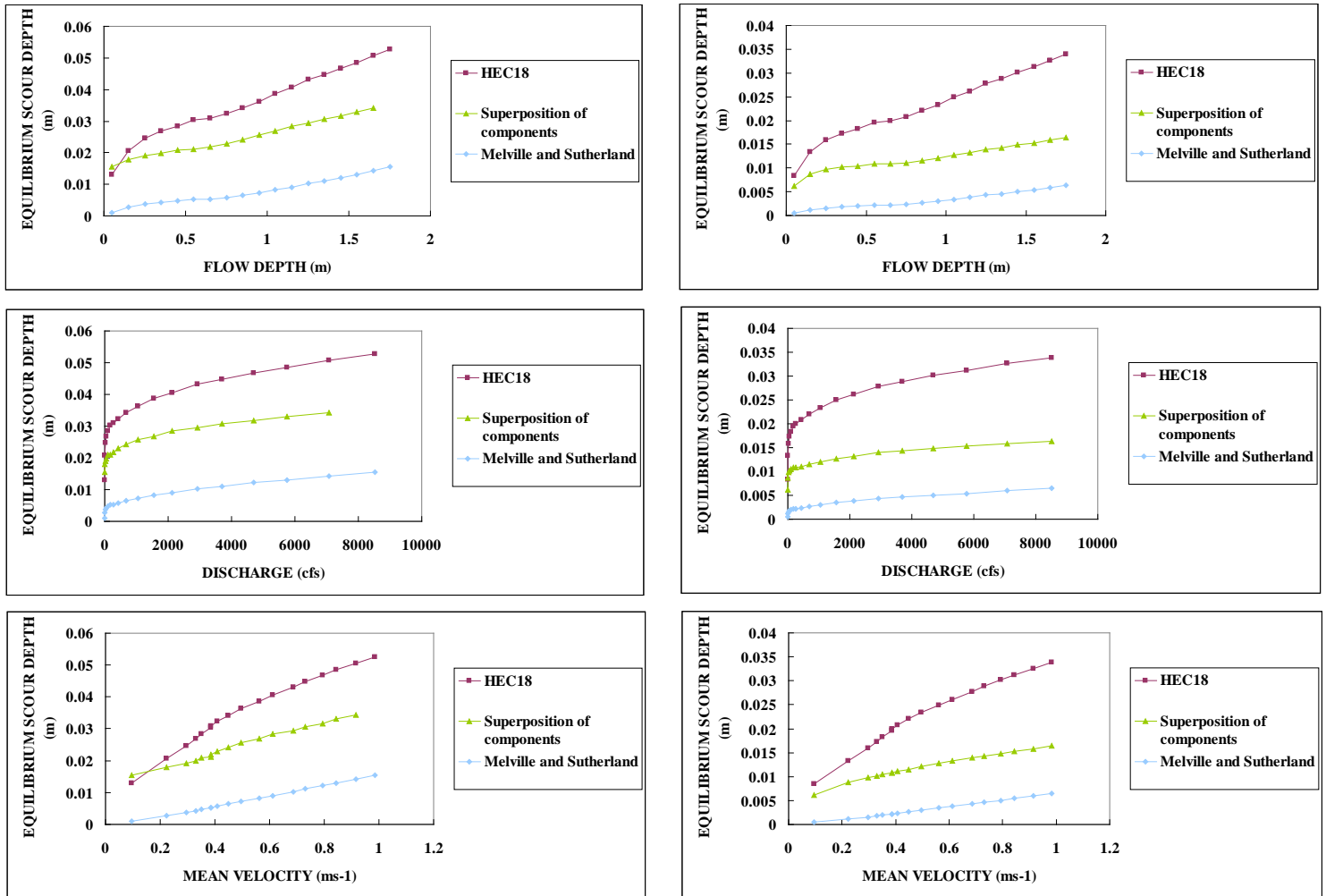


Figure 41. Equilibrium scour depths at RM 230.8 for A) *Phragmites* stems and B) Cottonwood or Reed canarygrass stems.

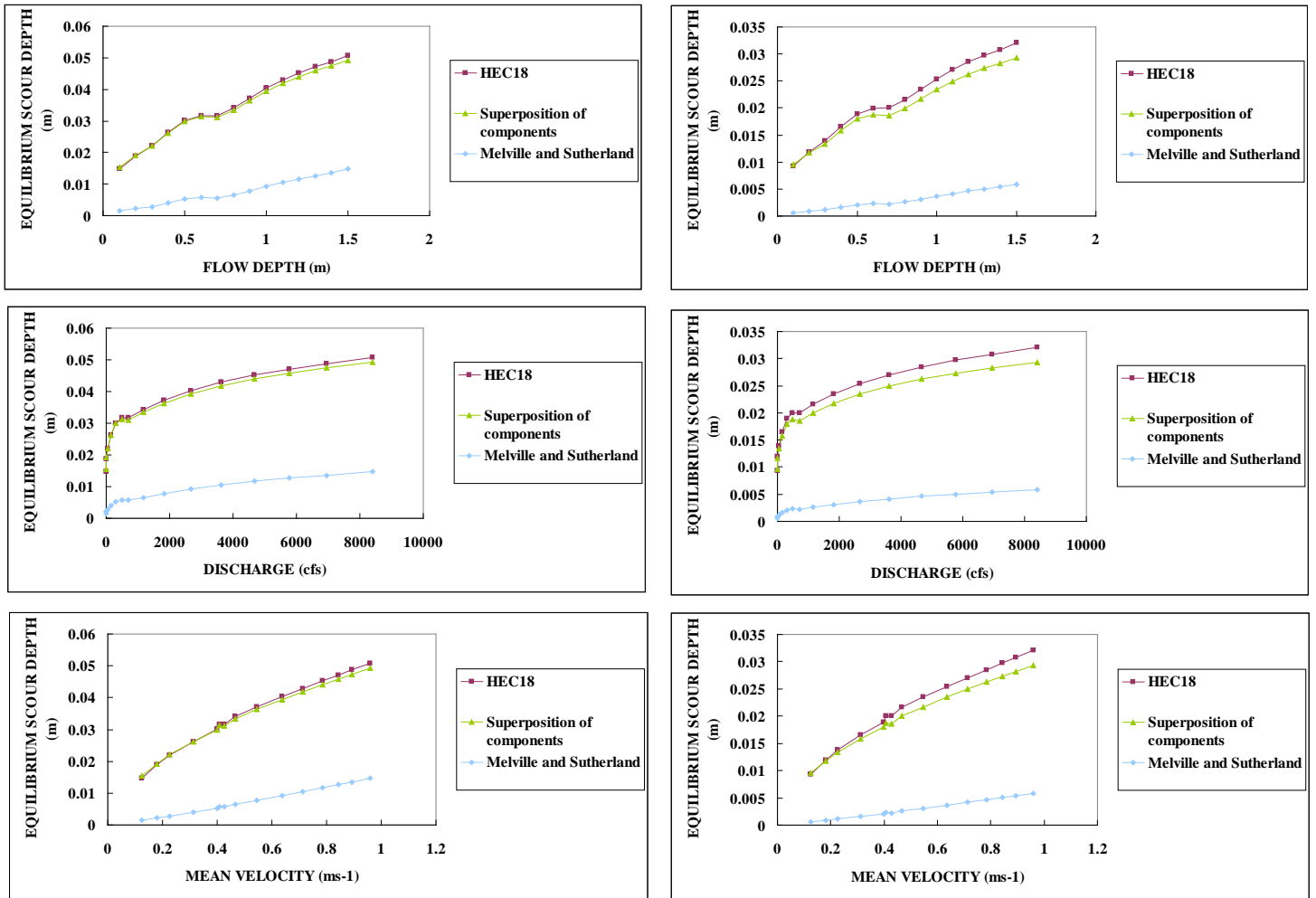


Figure 42. Equilibrium scour depths at RM 228.7 for A) *Phragmites* stems and B) Cottonwood or Reed canarygrass stems.

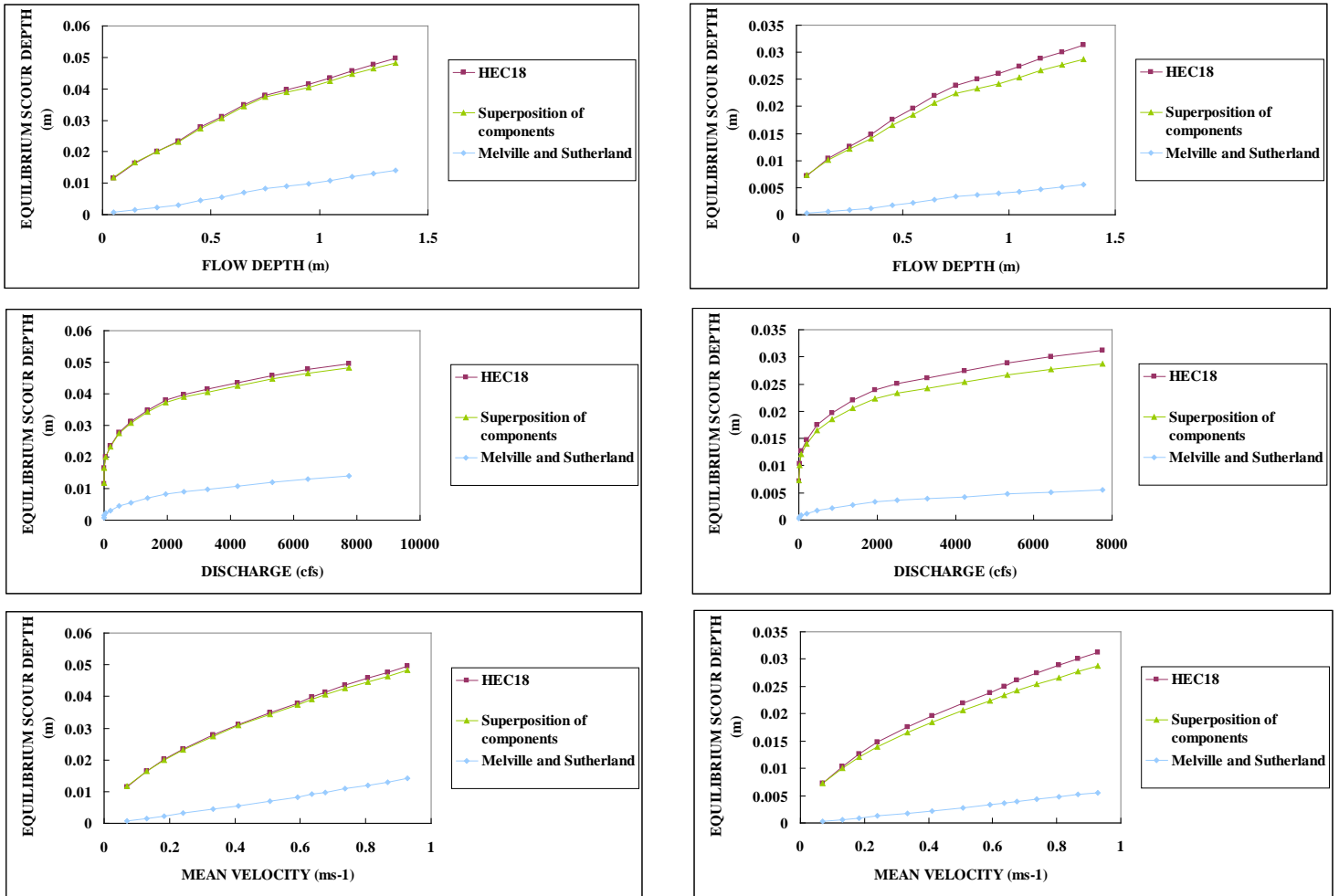


Figure 43. Equilibrium scour depths at RM 210.6 for A) *Phragmites* stems and B) Cottonwood or Reed canarygrass stems.

5.2.2 Time taken to reach Equilibrium scour depths

In the previous section we addressed the maximum extent of scour that could be expected to occur locally around the stems of vegetation growing on bars in the Central Platte River, under flows of various magnitudes. In this section we discuss the predicted duration of a given flow that is required to achieve these maximum scour depths (Figures 44 – 46 show HEC18 results; results from the other scour equations are shown in Appendix B). To accomplish this analysis the equations for local equilibrium scour depths were combined with the method of Melville and Chiew (1999) to calculate scour at certain increments of time.

Two trends can be seen in the plots which separate out results by species (or stem diameter), and by study site (Appendix B). The first trend confirms the results of the previous section, in which, equilibrium scour depth increases with flow depth. The second trend is that in all cases, regardless of flow depth/discharge/velocity, the equilibrium scour depth had been reached within 3,600 seconds, or one hour.

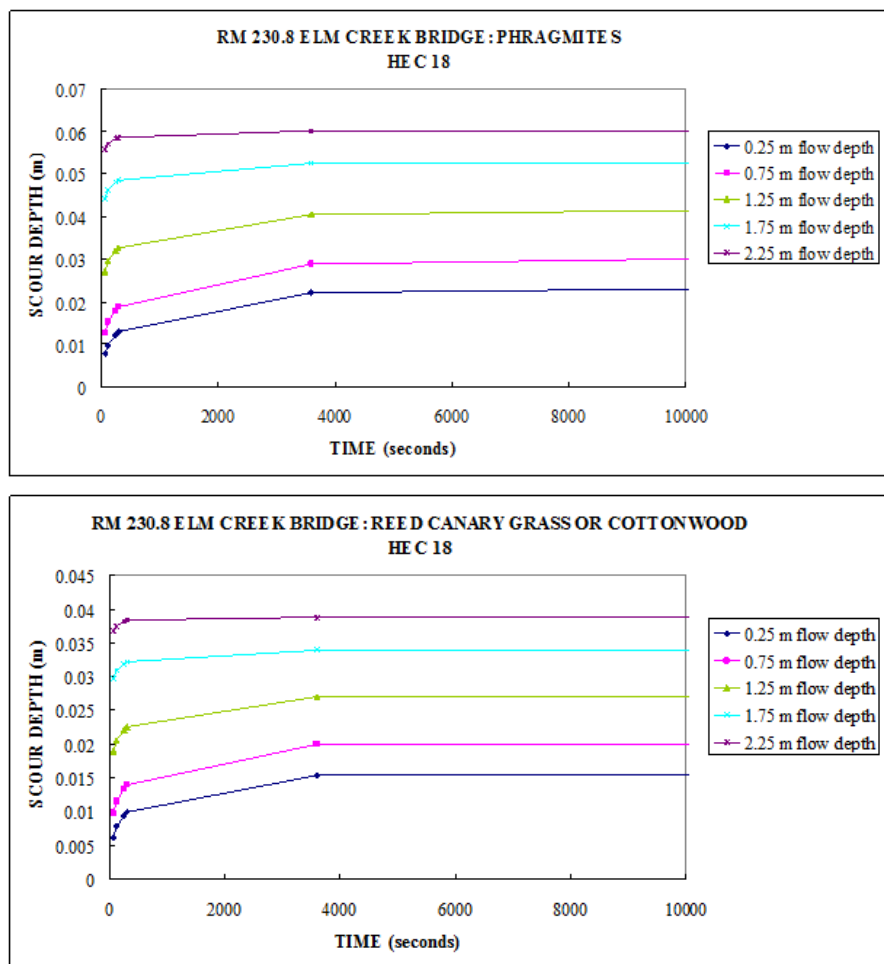


Figure 44. Time to reach equilibrium scour depth for A) *Phragmites* stems and B) Cottonwood or Reed canarygrass stems at RM 230.8.

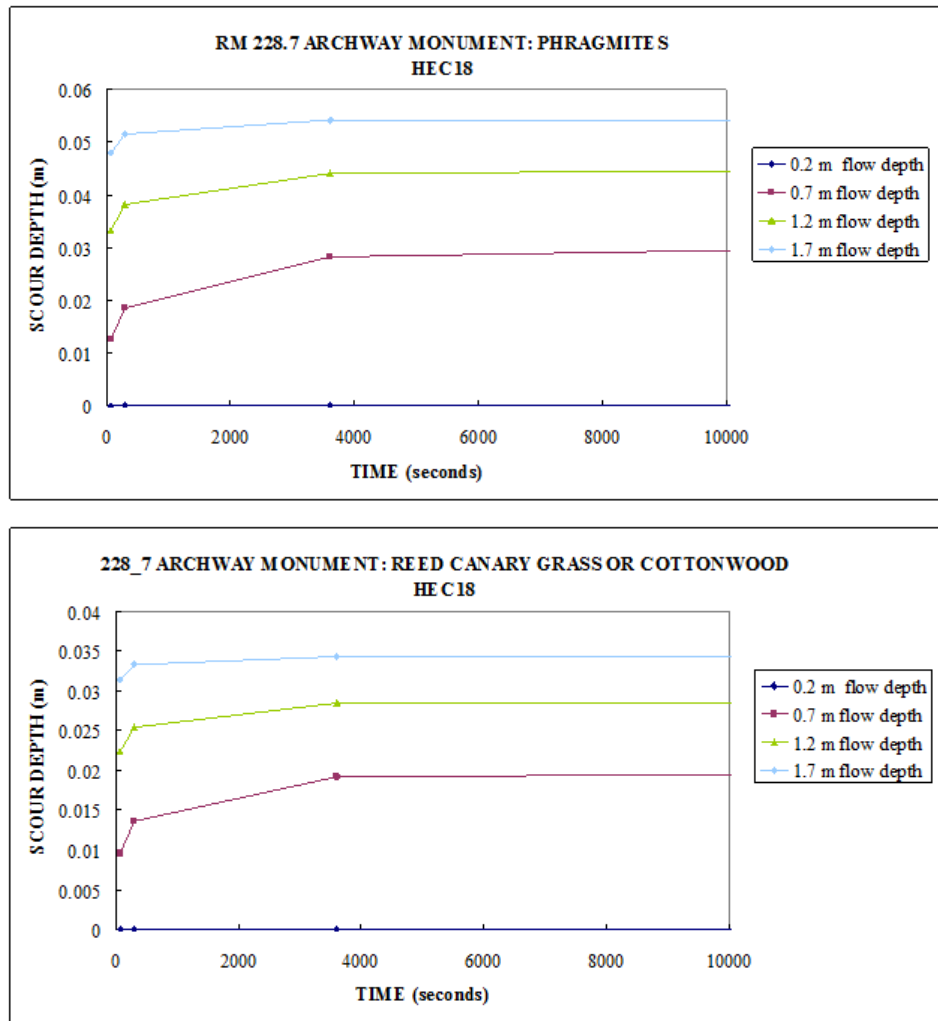


Figure 45. Time to reach equilibrium scour depth for A) *Phragmites* stems and B) Cottonwood or Reed canarygrass stems at RM 228.7

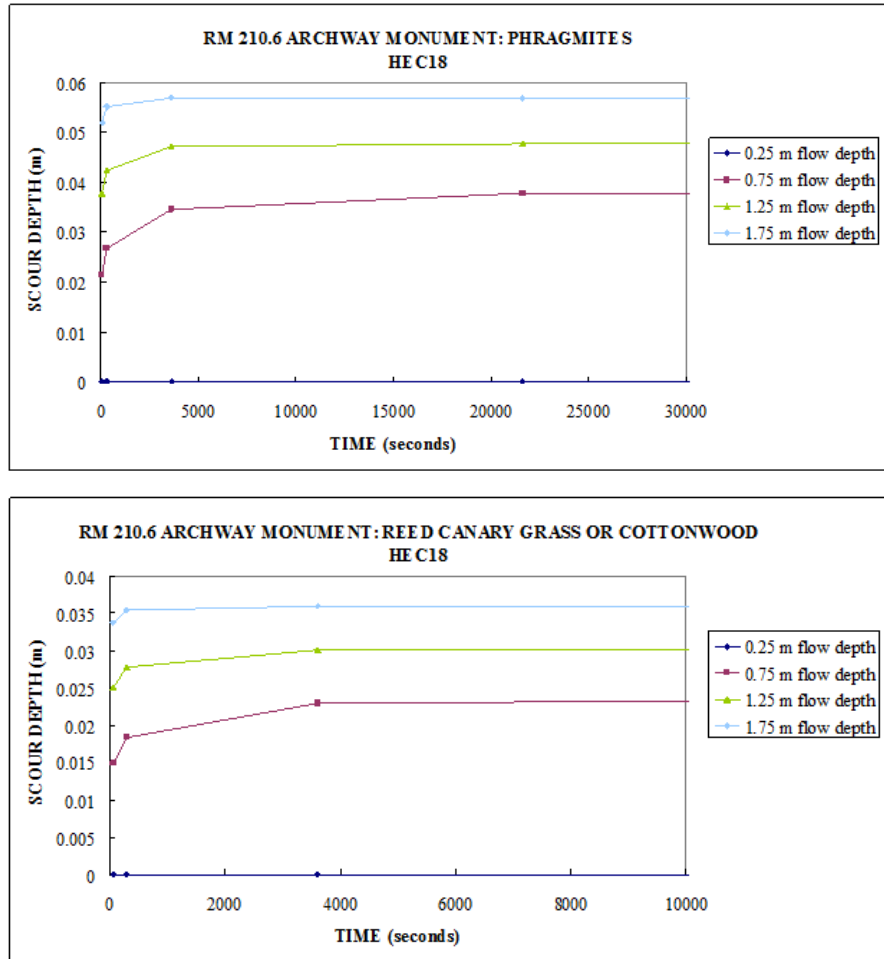


Figure 46. Time to reach equilibrium scour depth for A) *Phragmites* stems and B) Cottonwood or Reed canarygrass stems at RM 210.6

5.2.3 Recurrence Interval analysis of local scour around plant stems

The previous sections have shown the range of local scour depths that could be expected to occur over a range of flow depths/discharges/velocities around the stems of vegetation growing on bars in the Central Platte River. In this section we analyze flow records from the three closest USGS gages to our study sites (06768000 near Overton, 06770200 near Kearney, and 06770000 near Odessa) to determine recurrence intervals for flows of given magnitudes and associated local scour depths. The results presented thus far have suggested that local scour depths around the stems are likely to be much lower than the rooting depths measured in the field, therefore having little effect on removal of all but the shallowest rooting plants. Here we examine the largest flows on record to see if a flow magnitude large enough to scour established *Phragmites*, Reed canarygrass and cottonwood seedlings is possible in this river.

The values listed in Table 6 provide recurrence intervals for the three gage flow records studied. For the 100-year recurrence interval discharge calculated at the Odessa gage (27,600 cfs), local equilibrium scour depths were estimated to range from 0.8 to 6.7 cm across the three cross sections at RM 230.8, 228.7 and 210.6.

5.2.4 Local scour summary

Predicted values of local scour around stems of bar vegetation were thus shown to be relatively small compared to the rooting depths of the plants measured in the field, in particular *Phragmites*. The results from the analysis presented here suggest that equilibrium (maximum) scour depths, even at very high discharges would be insufficient to scour out all but the shallowest rooted vegetation. Indeed, as noted in the methodology section, the scour values predicted using these equations, designed for rigid object, rather than flexible plant stems, actually provide upper estimates of scour depths; scour depths around multiple plants are likely lower because the flexible stems can bend to protect the substrate beneath them. Newly germinated cottonwood seedlings and other annual species could be scoured at high flows where rooting depths have not yet greatly exceeded the potential scour depths of up to 5.5 cm at 8,000 cfs and up to 6.7 cm at the 100-year recurrence interval of approximately 27,600 cfs at the gage at Odessa (Table 6; Figure 44). Similar to the discussion in the section on drag forces, the implication of these results is that the timing of any SDHFs proposed by PRRIP should take into account the onset of the growing season, and potential time for root growth between SDHF events. The scour results also suggest that once bar vegetation has established, and rooting depths have exceeded potential local scour depths, even at high flows at the 100-year recurrence interval, the combination of drag and scour are unlikely to remove the three species tested in this study. There is therefore, likely no magnitude and duration of flow that can remove established bar vegetation through drag and vertical local scour of bars in the Central Platte River.

Table 6. Recurrence intervals of flows at USGS gages 06770000, 06770200, and 06768000 calculated by the authors using Log-Pearson III analysis.

Recurrence Interval (years)	06770000 Platte River near Odessa (Q in cfs)	06770200 Platte River near Kearney (Q in cfs)	06768000 Platte River near Overton (Q in cfs)
1.01	1200	1065	1416
1.11	2500	2054	2618
1.5	4400	3679	4609
2	5800	5003	6253
2.33	6500	5701	7128
5	10200	9444	11901
10	13600	13450	17147
20	17500	18224	23551
50	23000	25932	34186
100	27600	32945	44125

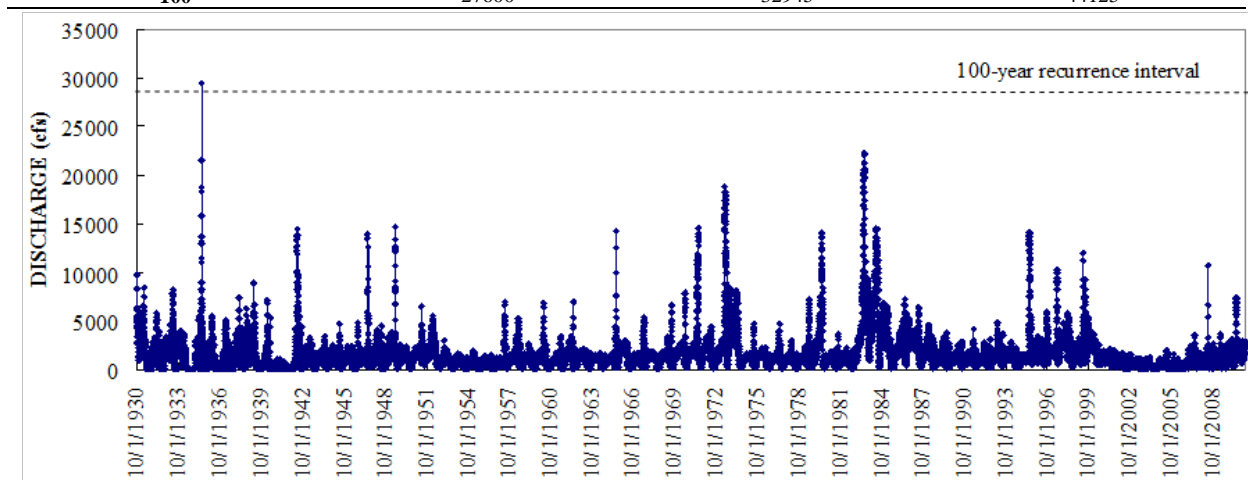


Figure 47. Flow record from gage 06700000 Platte River near Odessa.

6 LINKING EXPERIMENTAL RESULTS TO REAL WORLD MANAGEMENT OF THE CENTRAL PLATTE RIVER

6.1 Flow velocities capable of uprooting plants through drag forces

To better understand the real-world significance of the experimental and modeling results presented in this study, an attempt has been made to determine the spatial patterns of flow velocities capable of uprooting patches of each plant species studied. PRRIP provided the authors with SRH-2D model output for a flow event of 8,000 cfs. The velocity required to initiate plant uprooting (minimum patch resistances modeled in RipRoot runs) and to remove all plants of that species (maximum patch resistance modeled in RipRoot runs) were calculated by taking the minimum and maximum forces in Figures 37-39 and solving for velocity in the quadratic equations shown in Figure 36. Maps were then created to indicate the likelihood of plant uprooting within the Elm Creek reach. Flow velocities that were too low to remove any plants are shown in dark green. Locations where velocities are sufficient to initiate the uprooting of the weakest plants, are indicated in light green. The color scale then transitions through yellow, to orange indicating higher flow velocities and zones where a greater percentage of the plants might be expected to be uprooted during an 8,000 cfs flow. Areas shaded red indicate parts of the channel where velocities are high enough to uproot all plants of that species. Finally, a shapefile showing 2010 bar delineations (also provided by PRRIP) has been plotted over the flow velocities so that velocities on and around bars where vegetation is a management concern, can be isolated from the channels.

Each species studied is discussed in the following pages with an accompanying map. Note that for each map, maximum patch resistance was set to be red, and minimum patch resistance set to be mid-green. Each map therefore has a different velocity scale and the maps should not be directly compared to each other as, for example, yellow on the cottonwood map does not indicate the same velocities as yellow on the Reed canarygrass map. As stated in earlier sections of this report, when considering the velocities required for uprooting, it is assumed that all of the drag force applied to each plant is transferred in full to the roots. In reality, some of the applied force would be absorbed through elastic energy losses in stems and limited transfer of lateral stress to vertical stress. This was confirmed during the bending tests carried out in the field, during which uprooting of a plant never occurred. The results presented here may, therefore, overestimate the ability of SDHFs to remove vegetation, as bending may simply occur.

In the first map (Figure 45) the uprooting velocities for 1-year old cottonwood are shown. It can be seen that there is only one location in this reach where no uprooting is predicted during an 8,000 cfs flow (dark green; area has a higher elevation). The majority of the channel margins indicate velocities where only the weakest cottonwood seedlings could be uprooted (mid-green). The velocities over bar areas mostly suggest the potential for flow to uproot a higher proportion of one year cottonwood seedlings than at channel margins (light green), but the deepest rooted, strongest seedlings will be hard to remove from most bar locations through drag forces alone (indicated by an absence of yellow to red zones overlaying bar regions). The exact percentage of plants removed would be site specific and would vary, for example, according to plant density, typical water table depths and resulting rooting depths. For 1-year old cottonwood seedlings the only areas where flow velocities are indicated to be high enough to remove all cottonwood seedlings of this age, as predicted by the modeling results presented earlier, are in the deepest part of the channel upstream of the diversion, and directly downstream of the diversion; neither of these locations however, correspond to locations where there are vegetated bars. Overall, the map suggests that partial removal of the weakest and most exposed 1-year old cottonwood seedlings is likely on vegetated bars in the Elm Creek reach during an 8,000 cfs flow event. In general, flow velocities over the bars were higher downstream of the diversion, as indicated by the presence of greater proportions of light green compared to mid-green upstream of the diversion. As such, more one-year old cottonwoods could be expected to be removed downstream compared to upstream of the diversion.

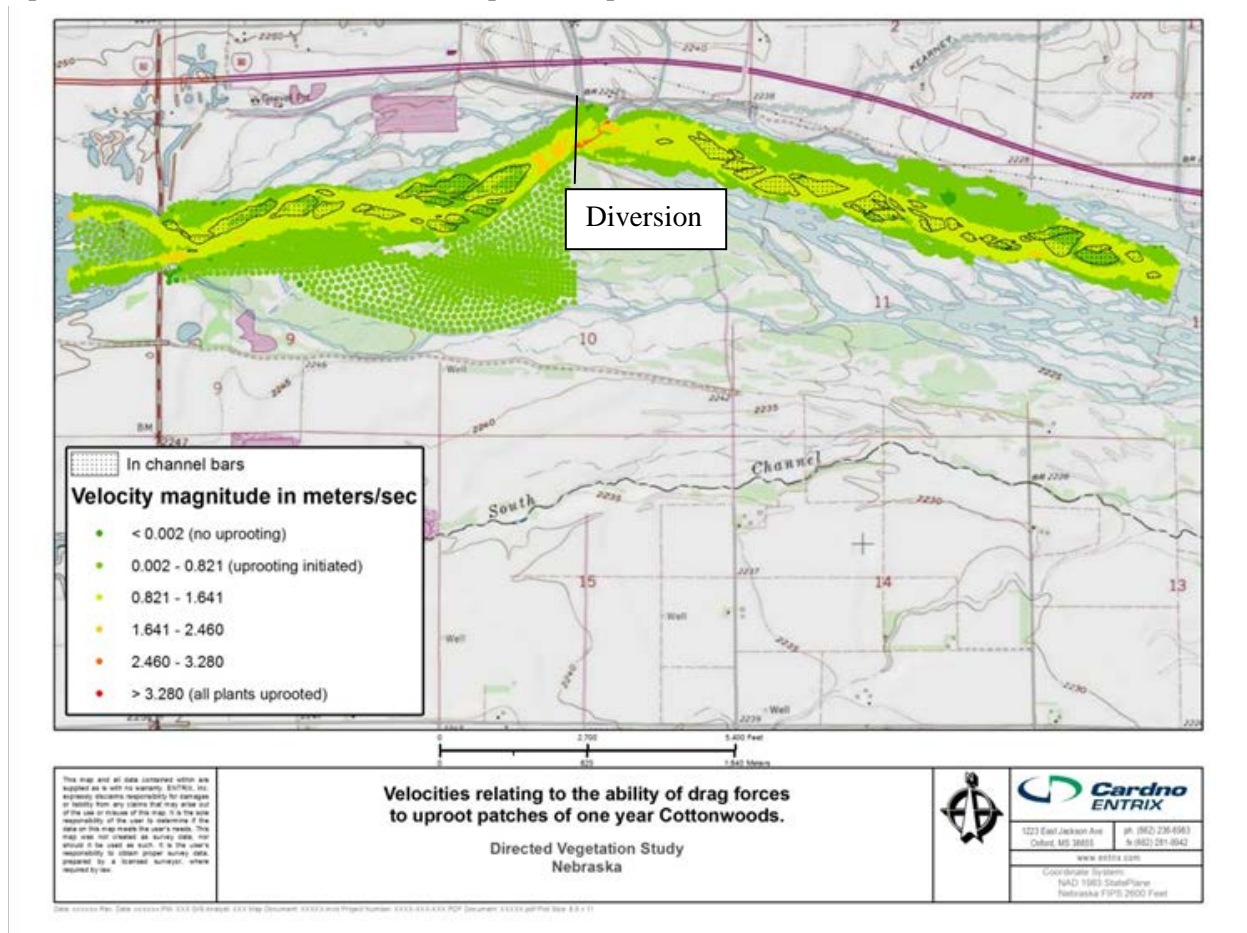


Figure 48. Velocities relating to the ability of drag forces to uproot patches of one-year old cottonwoods.

The map showing uprooting velocities for two-year old cottonwood seedlings (Figure 46) shows similar results to the map for one-year cottonwood seedlings; the flow velocities over the bar areas during and 8,000 cfs flow event are sufficient to uproot the weakest and/or most exposed seedlings (areas indicated in mid to light green). For two-year old cottonwoods, velocities capable of removing all plants, as predicted by RipRoot patch modeling, do not exist anywhere in this reach at 8,000 cfs, even around the diversion. Again, velocities over the bars are generally higher downstream of the diversion, suggesting higher potential for uprooting of two-year old cottonwood seedlings in this part of the reach.

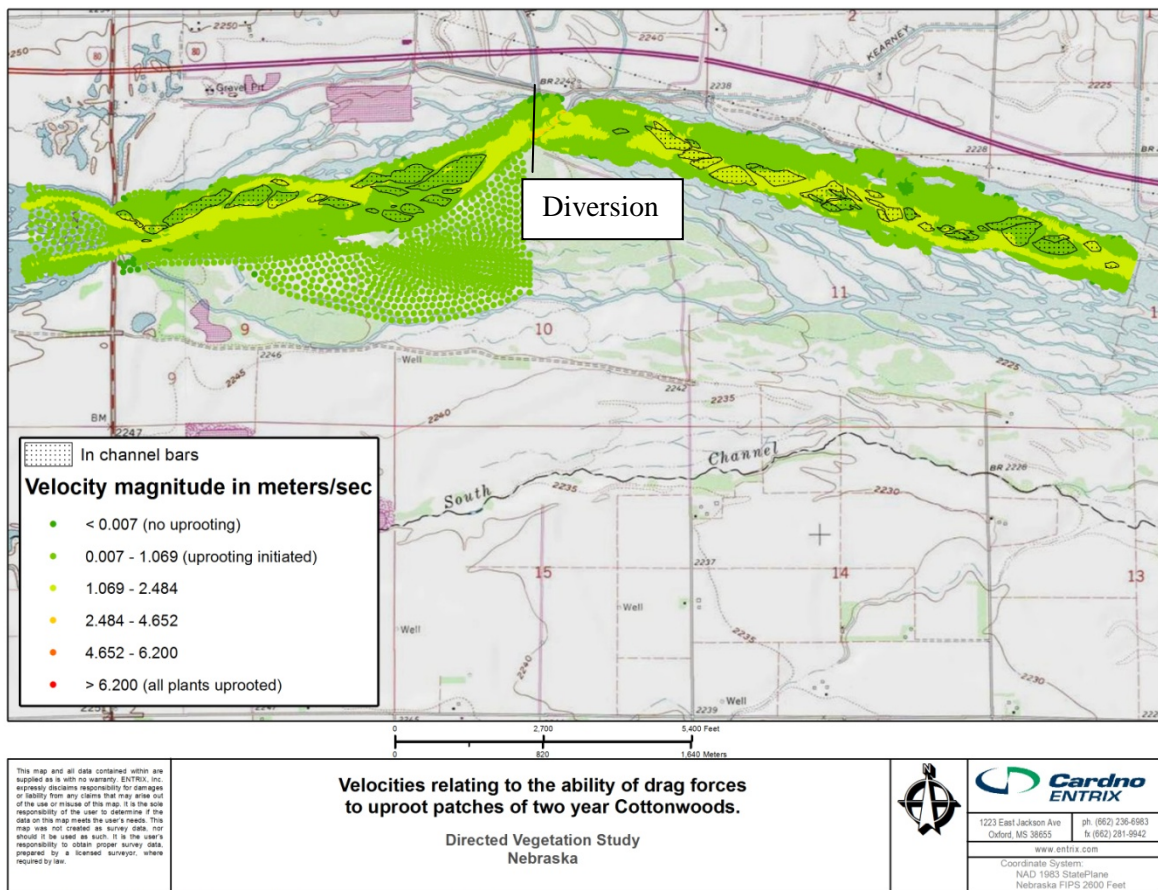


Figure 49. Velocities relating to the ability of drag forces to uproot patches of two-year old cottonwoods.

The distribution of flow velocities capable of uprooting patches of Reed canarygrass are shown in Figure 47. Almost all parts of the channel are shaded in dark green, indicating that velocities are too low to remove even the weakest patches of grass in these locations. Areas of mid-green (indicating initiation of uprooting of the weakest stems) can be seen in some parts of the reach, but these correspond to deeper parts of the channel, rather than bars. Removal of Reed canarygrass through drag forces alone is therefore very unlikely once this species has established on bars, both upstream and downstream of the diversion. When it is also considered that bending will occur before uprooting occurs, the likelihood of uprooting of this species once established can be further decreased.

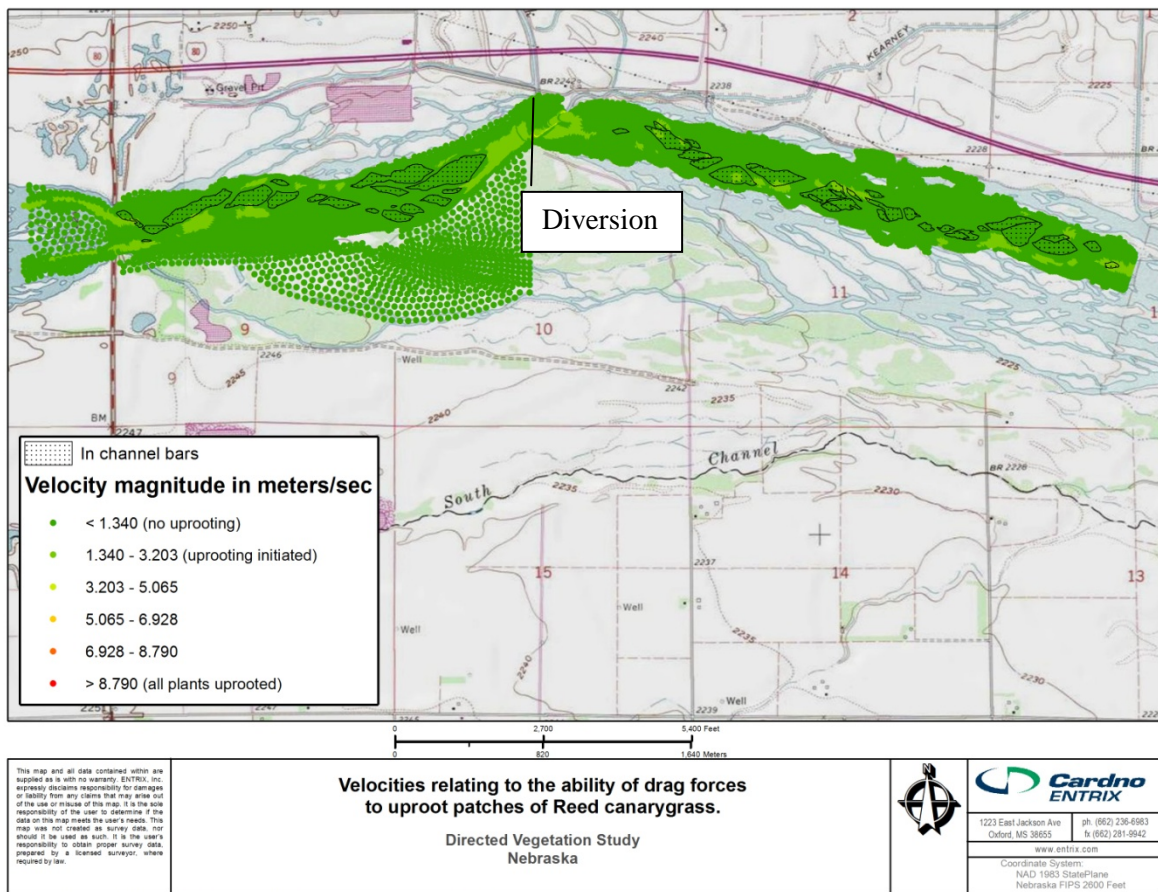


Figure 50. Velocities relating to the ability of drag forces to uproot patches of Reed canarygrass.

The map of flow velocities capable of uprooting *Phragmites* stems in the Elm Creek reach (Figure 48) shows that there are no locations where uprooting is likely to occur through drag forces alone, even during an 8,000 cfs flow event. For removal of this species to occur, once established, either other fluvial processes must also be at work, for example lateral scour and undercutting at bar edges or ice scour, or human intervention must take place. Management techniques such as spraying and diking are probably necessary to remove established stands of *Phragmites*, but SDHF events may then be able to maintain vegetation free bars once mature vegetation is cleared.

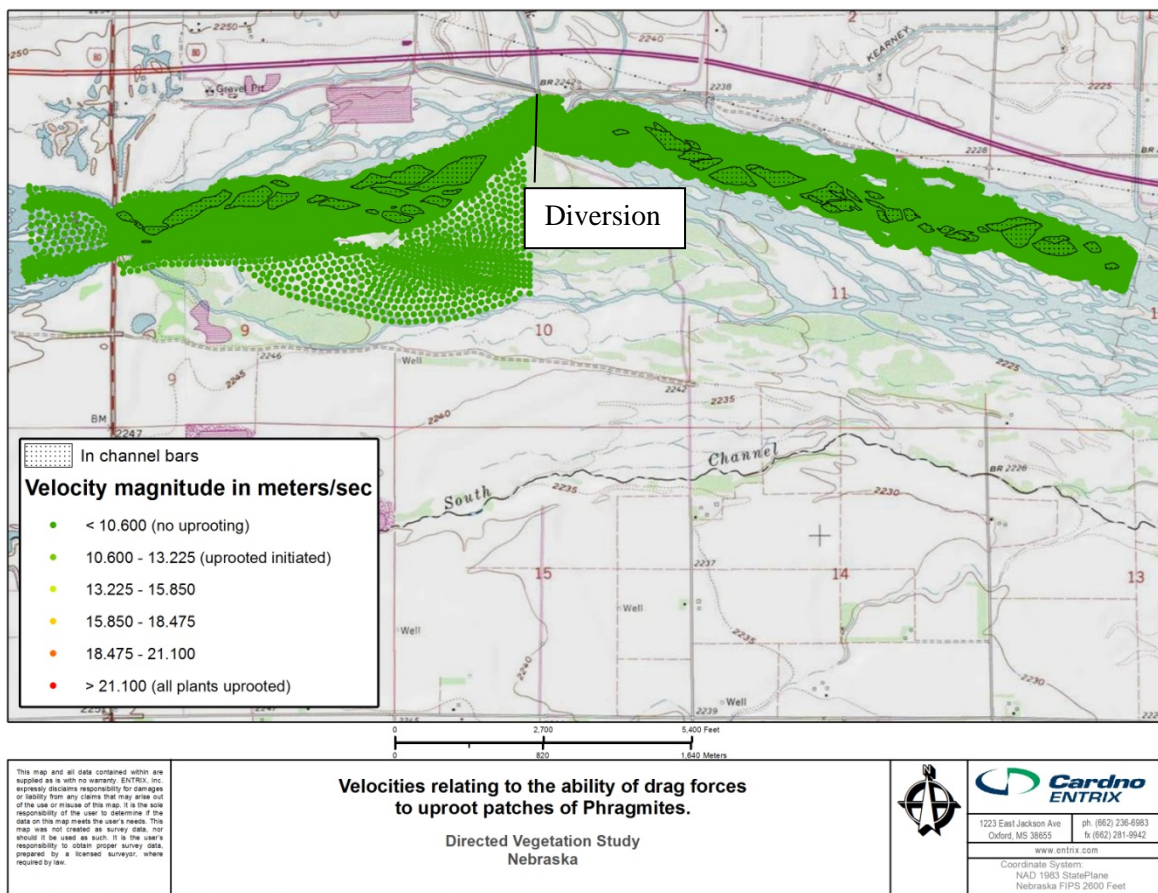


Figure 51. Velocities relating to the ability of drag forces to uproot patches of *Phragmites*.

6.2 Discussion of directed vegetation study findings, in light of 2012 Elm Creek FSM Annual Monitoring Report (Tetra Tech, 2012).

The results presented in this report, including the maps in section 6.1, suggest certain patterns and locations of velocities capable of uprooting each plant species studied, through drag forces alone. In this section these patterns, and other findings during fieldwork are compared to monitoring data collected as part of the 2012 Annual Monitoring Report for the Elm Creek reach, to assess whether the findings of this study accurately represent what is happening in the reach.

The 2012 monitoring report stated that the average height of green lines were similar between the May and Aug/September surveys, with, “*a slight, but statistically insignificant increase in the upstream part of the reach, and a somewhat larger (1.7 feet in May to 1.8 feet in Aug/Sept), but still statistically insignificant increase in the downstream part of the reach.*” (Tetra Tech, 2012). This finding confirms the suggestion made in the previous section, that more vegetation removal is likely downstream of the diversion than upstream (green line increased more downstream than upstream). This is in part a result of higher flow velocities, but other factors such as plant submergence may also affect survival rates. The monitoring report also notes that some bars had experienced significant erosion, indicating that other processes other than drag forces, also play a role in determining plant survival on bars.

Another interesting finding of the 2012 monitoring report was that although discing in Fall 2010 had been successful in breaking up the *Phragmites* root mat, rhizome fragments still present in the bars were able to regenerate and form dense stands the following growing season. The field notes collected as part of this study also suggested that rhizomes of sprayed areas looked healthy, even where the above ground biomass was dead and brittle. As *Phragmites* can regenerate in the growing season following discing and/or spraying, and velocities are insufficient, even during SDHFs to uproot this plant, the continued need for management through discing and spraying seems likely.

Comparison of frequency of occurrence of each species between the May and August/September 2011 surveys, with the results suggested by the maps in 6.1, showed generally similar trends. For example, the monitoring report found that there was a decline in cottonwood frequency in some areas (the 1,200 to 3,000 cfs elevations) between the May and August/September surveys, suggesting that flows during this period created velocities high enough to remove the weaker seedlings of this species. The most commonly occurring species during the August/September survey in all elevation ranges were *Phragmites* and cottonwood confirming that 1) *Phragmites* is very hard to remove through drag forces and 2) even though the weaker cottonwood seedlings can be removed, a large proportion of seedlings remained on the bars even after high flows. The report also notes a substantial cover of Reed canarygrass in the 3,000 to 5,000 cfs range, again confirming that once established this species is difficult to remove even during SDHFs. The map in Figure 47 suggests that no removal of Reed canarygrass is likely at any bar elevations during an 8,000 cfs SDHF, so decreased prevalence of this species below 3,000 cfs elevations may be a result of other processes, such as a lack of tolerance of this species for prolonged wet rooting conditions, or scour of these plants at bar edges.

7 CONCLUSIONS

This study combined several approaches to try to determine whether SDHFs of up to 8,000 cfs through the central Platte River, would be capable of removing cottonwood, *Phragmites* and Reed canarygrass stands of various ages and densities from in-channel bars. First, fieldwork was carried out to measure the rooting extents of each of the species, and to study how their root architectures affect resistance to uprooting. In addition, the uprooting resistance of these three species was measured in the field, along with resistance to bending. Field data were then used to parameterize the RipRoot model so that plant and plant patch resistances to uprooting could be modeled under different conditions. The second part of the study was a set of flume experiments carried out to measure the forces exerted on the three species of interest under different flow conditions. The data collected in the field were used to inform the choice of artificial vegetation; results of the flume experiment were compared to field data and RipRoot model results, to determine the balance between driving and resisting forces acting on the vegetation. Finally, analysis of potential local scour depths around vegetation stems on bars was conducted using a range of bridge-pier scour equations, and data collected in the field pertaining to particle size distributions and plant stem diameters.

Excavation of the species included in this study revealed dramatically different rooting architectures and extents. Reed canarygrass exhibited a very dense, fibrous root network that extended to approximately 0.5 m deep in places, with the densest rooting being seen in the upper 0.3 m of the soil profile. Root densities were seen to be in the order of tens of thousands of roots per square meter. Young cottonwood seedlings (up to 2-years) were seen to have a much sparser root network, composed of roots that were more woody in texture. The one-year-old seedlings had already developed a distinct, woody taproot that extended up to 0.25 m into the soil profile, with a mean rooting depth of 0.14 m. For two-year-old seedlings the maximum rooting depth measured was 0.48 m, but again the mean rooting depth was 0.14 m. During our study, several five-year-old cottonwood trees were also excavated to see how development continues over the next few years of growth. The taproot continued to dominate the root architecture, extending up to 1.5 m in some cases, or to whatever depth was necessary for the plant to reach sufficient moisture. These trees therefore exhibit rapid taproot growth over the first few years of their development, which has important implications for the timing of any potential removal of these trees, be it by mechanical or hydraulic means. *Phragmites* stands tended to be dominated by interconnected networks of rhizomes, with fine roots growing from them. Excavation revealed deeply rooted rhizomes, extending depths of greater than 1.5 m in places. Even where stands of *Phragmites* had been sprayed, the buried rhizome networks seemed healthy and capable of regenerating above-ground biomass in the following growing season. As the most deeply rooted plant studied, and the plant with the greatest ability to regenerate from buried rhizomes and stems, it is likely the hardest of the species studied to remove from sandbars in the Platte River.

Uprooting tests showed that the one-year-old cottonwood seedlings had the lowest uprooting forces, ranging from 8.2 to 64.3 N (mean value of 32.0 N). Sandbar willow seedlings (approximately one-year-old) were harder to remove during uprooting tests than cottonwood seedlings of a similar age, with pullout forces ranging from 19.6 to 189 N (mean value of 65.5 N, sample size, $n = 30$). This was as a result of the willow seedling root-architecture, dominated by long lateral roots. These lateral roots provided a large, horizontal surface area over which resistance to vertical uprooting occurred. Resistance

to removal for Reed Canarygrass stems was within a similar range to the Sandbar willow seedlings, ranging from 2.5 to 192 N (mean value of 58.3, sample size, $n = 100$). However, in almost all uprooting tests for this species, failure of the grass stem occurred right at the base of the stem where the roots initiate. Finally, *Phragmites* provided the largest uprooting forces out of the four species tested. Forces required for failure of the *Phragmites* stems ranged from 8.9 to 740 N (mean value of 254.5 N, sample size, $n = 115$). During uprooting tests for this species the part of the plant that most often failed was the main rhizome attached to each stem. This suggests that even if a great enough force could be applied to *Phragmites* stems through drag from flow, parts of the rhizome network would still be left in the ground, and the plant would thus be able to regenerate in following growing seasons. Repeat spraying of *Phragmites* may eventually kill the rhizome network, but it is unclear at this point how many seasons of spraying this might require.

The flume study showed that at low discharge ($0.0285 \text{ m}^3\text{s}^{-1}$), drag forces varied from 1.02 to 1.27 N for artificial cottonwood seedlings with an areal density of 13 stems m^2 , from 1.07 to 1.28 N for artificial cottonwood seedlings with an areal density of 26 stems m^2 , from 1.20 to 1.78 N for artificial *Phragmites* plants with an areal density of 200 stems m^2 , from 1.22 to 1.78 N for artificial Reed canarygrass plants with an areal density of 400 stems m^2 , and from 1.41 to 2.16 N for artificial Reed canarygrass plants with an areal density of 800 stems m^2 . At high discharge ($0.0478 \text{ m}^3\text{s}^{-1}$), drag forces were found to vary from 1.67 to 2.16 N for artificial cottonwood seedlings with an areal density of 13 stems m^2 , from 2.22 to 2.47 N for artificial cottonwood seedlings with an areal density of 26 stems m^2 , from 2.78 to 4.13 N for artificial *Phragmites* plants with an areal density of 200 stems m^2 , from 3.10 to 4.04 N for artificial Reed canarygrass plants with an areal density of 400 stems m^2 , and from 3.72 to 5.00 N for artificial Reed canarygrass plants with an areal density of 800 stems m^2 . These values are commensurate with those obtained by previous researchers. For example, Schnauder and Wilson (2009) assembled datasets obtained by a number of researchers and showed that drag forces acting upon various willow species ranged from 0.5 to 12 N for the range of flow velocities measured herein.

A comparison of drag forces (driving) measured in the flume study, with uprooting forces (resisting) measured in the field, was carried out for each species to determine the likelihood of plant removal by SDHFs. For cottonwood seedlings, drag forces measured during flume experiments (up to 0.25 ms^{-1}) suggested that only the very youngest and/or, most shallowly rooted seedlings could be removed through drag applied by flow, whilst some may experience bending. Flow velocities that could be experienced during SDHFs in the Central Platte River may, however, be as high as 1.5 ms^{-1} . Drag forces at this range of velocities would be higher, and would be sufficient to bend all young cottonwood seedlings, and possibly remove a greater proportion of plants also. It should be noted, however, that because these plants are elastic, not rigid, not all of the drag force applied to the stems during a flow will be transferred to the roots. At low flows this loss of energy in the stems will likely result in very few cottonwood seedlings being removed, and even at high flows this elastic energy loss may reduce the likelihood of all but the weakest of these plants being removed by flows, with the majority of plants simply bending over.

For Reed canarygrass, the drag forces measured in the flume suggested that at this range of flows the driving force acting on the grass was lower than both ranges of forces for uprooting and bending at the lower stem density of 400 stems per square meter. In the case of the higher stem density of 800 stems per square meter, higher drag forces were recorded, and under these conditions, some bending of grass stems

could occur. At higher flow velocities, drag force always exceeded the force required for grass stem bending. Some weaker, more exposed grass stems may experience breaking or uprooting, but this is likely to be limited; bending will tend to be the dominant process observed. In the case of *Phragmites*, the drag forces from the flume study were lower than both the forces required for bending and for uprooting. At the estimated drag forces for flows up to 1.5 ms^{-1} drag forces exceed the full range of bending forces, but are still insufficient to initiate uprooting of even the weakest and sparsest patches of *Phragmites*. As with Reed canarygrass, at high flows bending will be the dominant result rather than uprooting or stem breaking.

The results presented in this study indeed suggest that at high flows, limited numbers of cottonwood seedlings may be removed by drag forces alone, but for Reed canarygrass and *Phragmites* stem bending will dominate over uprooting. For cottonwoods, the likelihood of seedling removal will decrease with each additional year of growth, as rooting depths increase and reduced stem density reduces drag forces acting on a stand of seedlings. Established cottonwood trees, Reed canarygrass, and *Phragmites*, do however, appear to be very resistant to removal through drag forces applied by high flows. Johnson (1997) also noted that even though vegetation mortality on sand bars was also high after flood events, once vegetation had become established, the roots of the most common Platte River riparian species grow sufficiently that the roots of the plants stabilize their substrate and actually resist erosion. The question then becomes, can local scour change this balance between drag and uprooting/bending forces enough to make a difference to vegetation removal?

As noted by Johnson (1994), several different environmental factors affect vegetation growth on sandbars: winter ice scour, June flows following seedling establishment, and summer drought. When winter flows are high enough, and the temperatures are cold enough for ice to form in the river, ice scour can pluck young cottonwood and willow seedlings from sand bars, at affected elevations. Summer low flows allow for establishment of seedlings, but high June flows can inundate sand bars mobilizing the substrate, can wash away the seeds that have been deposited on the bars and/or scour the shallowest, weakest rooted new seedlings. As commented on by Murphy et al. (2004), annual peak flows at other times of the year may also be capable of scouring seedlings whose roots have not yet become established enough, thereby allowing the flow to pull these plants from their substrate with roots intact.

In this study, predicted values of local scour around stems of bar vegetation were shown to be relatively small compared to the rooting depths of the plants measured in the field, in particular *Phragmites*. The results from the analysis presented here suggest that even at very high discharges, equilibrium (maximum) scour depths, would be insufficient to scour out all but the shallowest rooted vegetation. Our results do suggest that newly germinated cottonwood seedlings and other annual species could be scoured at high flows where rooting depths have not yet greatly exceeded the potential scour depths of up to 5.5 cm at 8,000 cfs and up to 6.7 cm at the 100-year recurrence interval of approximately 27,600 cfs at the gage at Odessa. The scour results confirm the idea that once bar vegetation has established, and rooting depths have exceeded potential local scour depths, even at the 100-year recurrence interval discharge, the combination of drag and scour are unlikely to remove the three species tested in this study.

A large caveat of the work presented here is that general scour across the entire channel cross section was not modeled. Indeed, migration of bedforms such as dunes, and lateral erosion of bars and banks could

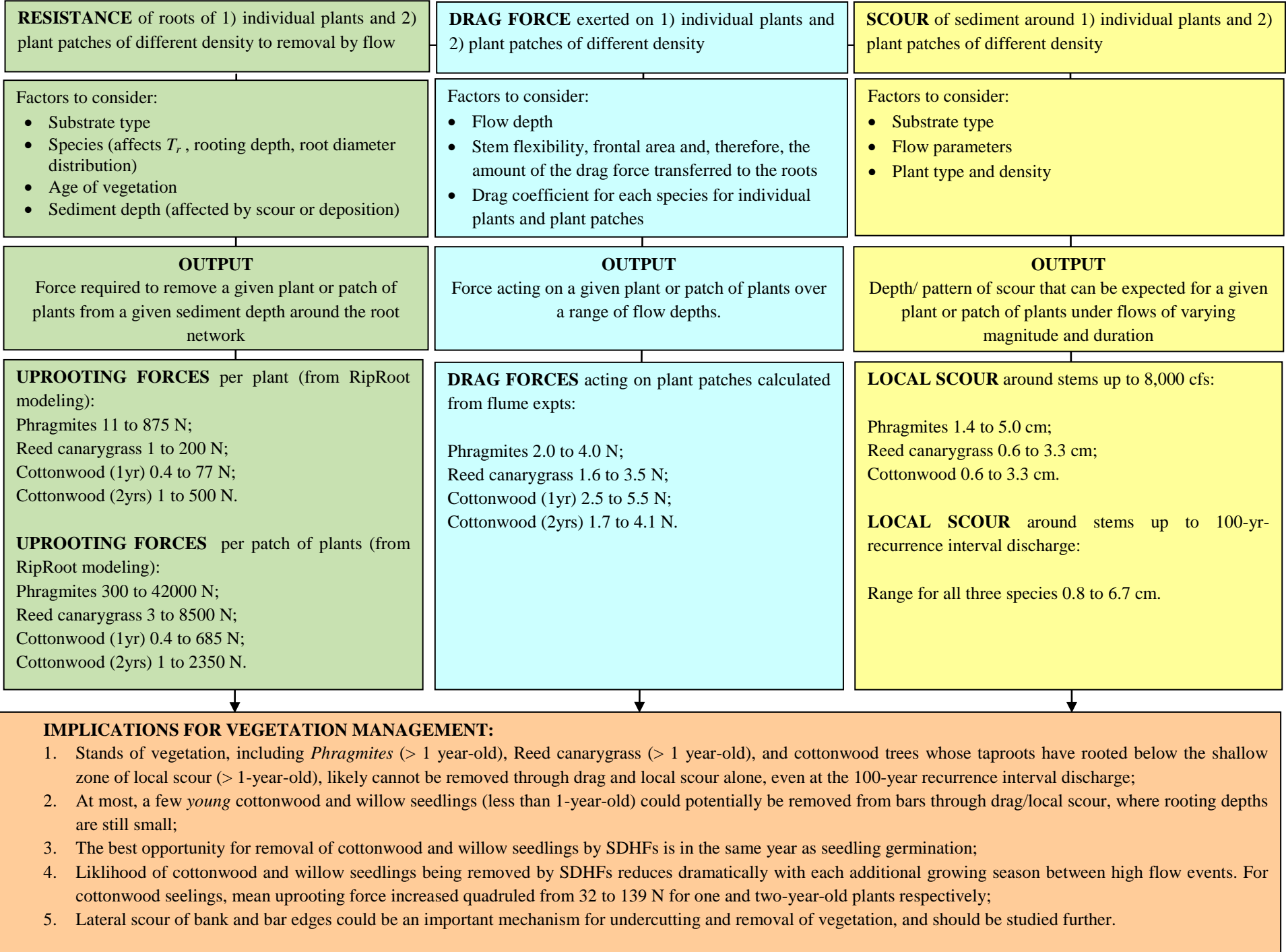
provide an additional, important mechanism because lateral erosion through hydraulic scour and geotechnical mass wasting could enable vegetation removal at channel and bar margins. Future work could focus on this additional mechanism by using the data collected in this study, along with additional information on the geotechnical and hydraulic resistances of the bank and bar materials. Use of the USDA-ARS-NSL's Bank Stability and Toe Erosion Model (BSTEM) combined with the RipRoot algorithm, could then provide PRRIP with estimates of lateral bar and bank retreat under various SDHF scenarios, and for a range of vegetation management options. These model runs would also allow PRRIP to assess the effect of vegetation management strategies on the amount of sediment entering the river from bank and bar edges. As increased bedload is thought to be a requisite for returning the Platte River to a braided planform and increasing habitat for endangered species, knowledge of the impact of vegetation management plans on this aspect of the system would also be beneficial to the Program. Additionally, this report has not discussed ice-scour as a mechanism for plant removal, but this process has been noted, for example by Murphy et al. (2004) to be important for vegetation scour during winter months, when ice levels are high enough relative to elevations of established vegetation. Johnson (1997) in fact found that seedling mortality was highest in the winter as a result of ice scour, and this highlights the importance of this process in the maintenance of vegetation-free bars along the Platte River. Burial of plants by sedimentation and inundation for long periods of time can also cause plant mortality, but were outside the bounds of this study.

As a final point, Johnson (1997) and Murphy et al. (2004) both concluded that the history of flow events during the first years of life for Platte River riparian species, is important for predicting the likelihood of establishment of mature vegetation on sand bars. The quantification of driving and resisting forces measured in this study, certainly support this finding. The importance of the first growing season, and following few years of establishment should therefore be taken into account when PRRIP are planning the magnitude, duration, frequency and timing of potential SDHF events.

Overall the implications of the results of this study for management of vegetation on bars in the central Platte River are:

1. Stands of vegetation, including *Phragmites* (> 1 year-old), Reed canarygrass (> 1 year-old), and cottonwood trees whose taproots have rooted below the shallow zone of local scour (> 1-year-old), likely cannot be removed through drag and local scour alone, even at the 100-year recurrence interval discharge;
2. At most, a few *young* cottonwood and willow seedlings (less than 1-year-old) could potentially be removed from bars through drag/local scour, where rooting depths are still small;
3. The best opportunity for removal of cottonwood and willow seedlings by SDHFs is in the same year as seedling germination;
4. Likelihood of cottonwood and willow seedlings being removed by SDHFs reduces dramatically with each additional growing season between high flow events. For cottonwood seedlings, mean uprooting force increased quadrupled from 32 to 139 N for one and two-year-old plants respectively;
5. Lateral scour of bank and bar edges could be an important mechanism for undercutting and removal of vegetation, and should be studied further.

Finally, the flow diagram used in the Introduction section to illustrate the three separate aspects of this study, and how the results would be drawn together, has been updated and is shown overleaf to summarize the results of the study.



8 REFERENCES

- Abernethy, B., and Rutherford, I.D. 2001. The distribution and strength of riparian tree roots in relation to riverbank reinforcement. *Hydrological Processes*, 15: 63-79.
- Amlin, N.M. and Rood, S.B. 2002. Comparative tolerances of riparian willows and cottonwoods to water-table decline, *Wetlands*, 22(2): 338-346.
- Bennett, S.J., Bridge, J.S., and Best, J.L. 1998. The fluid and sediment dynamics of upper-stage plane beds. *Journal of Geophysical Research* 103: 1239-1274.
- Bennett, S.J., Pirim, T., and Barkdoll, B.D. 2002. Using simulated emergent vegetation to alter stream flow direction within a straight experimental channel. *Geomorphology*, 44: 115-126.
- Bertram, H.-U., 1984. Über die hydraulische Berechnung von Gerinnen mit Uferbewuchs. *Zeitschrift für Kulturtechnik und Flurbereinigung*, 25: 77-86.
- Best, J.L., Kirkbride, A.D., and Peakall, J. 2001. Mean flow and turbulence structure of sediment-laden gravity currents: new insights using ultrasonic Doppler velocity profiling. In: W.D. McCaffrey, B.C Kneller and J. Peakall, eds. *Particulate Gravity Currents*. Blackwell Science, Oxford, UK: 159-172.
- Bischetti, G.B., Chiaradia, E.A., Simonato, T., Speziali, B., Vitali, B., Vullo, P., and Zocco, A. 2005. Root strength and root area ratio of forest species in Lombardy (Northern Italy). *Plant and Soil*, 278: 11-22.
- Briaud, J.L., Chen, H.C., Kwak, K.W., Han, S.W., and Ting, F.C.K., 2001. Multiflood and multilayer method for scour rate prediction at bridge piers. *Journal of Geotechnical and Geoenvironmental Engineering*, 127(2), 114-125.
- Brito, D., Nataf, H.C., Cardin, P., Aubert, J. and Masson, J.P. 2001. Ultrasonic Doppler velocimetry in liquid gallium. *Experiments in Fluids*, 31: 653-663.
- Buckee, C., Kneller, B.C., and Peakall, J. 2001. Turbulence structure in steady solute-driven gravity currents. In: W.D. McCaffrey, B.C Kneller and J. Peakall, eds. *Particulate Gravity Currents*. Blackwell Science, Oxford, UK: 173-188.
- Chase, K.J., and Holnbeck, S.R., 2004, Evaluation of pier-scour equations for coarse-bed streams: U.S. Geological Survey Scientific Investigations Report 2004-5111, 18 p.
- Coppin, N.J., and Richards, I.G. 1990. *Use of Vegetation in Civil Engineering*. Butterworths, London, UK.
- Daniels, H.E. 1945. The statistical theory of the strength of bundles of threads. I. *Proceedings of the Royal Society of London, Series A*, 183(995): 405-435.
- Danjon, F., Barker, D.H., Drexhage, M., and Stokes, A. 2008. Using three-dimensional plant root architecture in models of shallow-slope stability. *Annals of Botany*, 101(8): 1281-1293.
- De Baets, S., Poesen, J., Reubens, B., Wemans, K., De Baerdemaeker, J., and Muys, B. 2008. Root tensile strength and root distribution of typical Mediterranean plant species and their contribution to soil shear strength. *Plant and Soil*, 305: 207-226.
- Docker, B.B., and Hubble, T.C.T. 2008. Quantifying root-reinforcement of river bank soils by four Australian tree species. *Geomorphology*, 100: 401-418.
- Dunn, C., López, F., and García, M.H. 1996. Mean flow and turbulence structure induced by vegetation: Experiments. *Hydraulic Engineering Series No. 50*, UILU-ENG 96-2009, Department of Civil Engineering, University of Illinois at Urbana-Champaign, Urbana, IL.
- Ennos, A.R. 1990. The Anchorage of leek Seedlings: The Effect of Root Length and Soil Strength. *Annals of Botany*, 65: 409-416.

- Falconer, R.A. 1993. An introduction to nearly horizontal flows. In: M.B. Abbott, and W.A. Price, eds. Coastal, Estuarial and Harbour Engineer's Reference Book. Chapman & Hall, London, UK: 27-36.
- Falconer, R.A., Lin, B., and Kashefipour, S.M. 2005. Modelling water quality processes in estuaries. In: P.D. Bates, S.N. Lane, and R.I. Ferguson, eds. Computational Fluid Dynamics: Applications in Environmental Hydraulics. John Wiley & Sons, Chichester, UK: 305-328.
- Fan, C.-C., and Su, C.-F. 2008. Role of roots in the shear strength of root-reinforced soils with high moisture content. *Ecological Engineering*, 33(2): 157-166.
- Fathi-Moghadam, M., and Kouwen, N. 1997. Nonrigid, nonsubmerged, vegetative roughness on floodplains. *Journal of Hydraulic Engineering, ASCE*, 123(1): 51-57.
- Fredlund, D.G., Morgenstern, N.R., and Widger, R.A. 1978. The shear strength of unsaturated soils. *Canadian Geotechnical Journal*, 15(3): 313-321.
- Fredsøe, J. 1978. Meandering and braiding of rivers. *Journal of Fluid Mechanics*, 84(4): 609-624.
- Freeman, G.E., Rahmeyer, W.H., and Copeland, R.R. 2000. Determination of resistance due to shrubs and woody vegetation. USACE Report ERDC/CHL TR-00-25. USACE ERDC, Vicksburg.
- Friedkin, J.F. 1945. A Laboratory Study of the Meandering of Alluvial Rivers. US Waterways Experiment Station, Vicksburg.
- Froehlich, D.C., 1988, Analysis of onsite measurements of scour at piers, *in American Society of Civil Engineers National Conference on Hydraulic Engineering: Colorado Springs, CO, American Society of Civil Engineers*, p. 534-539.
- García, M.H., López, F., Dunn, C., and Alonso, C.V., 2004. Flow, turbulence, and resistance in a flume with simulated vegetation. In: S.J. Bennett and A. Simon, eds. *Riparian Vegetation and Fluvial Geomorphology, Water Science and Application 8*, AGU, Washington, DC: 11-27.
- Genet, M., Stokes, A., Salin, F., Mickovski, S.B., Fourcaud, T., Dumail, J., and van Beek, R. 2006. The influence of cellulose content on tensile strength in tree roots. *Plant and Soil*, 278: 1-9.
- Gray, D.H., and Sotir, R.B. 1996. *Biotechnical and Soil Bioengineering Slope Stabilization: A Practical Guide for Erosion Control*. John Wiley & Sons, Inc., New York, NY.
- Greenway, D.R. 1987. Vegetation and slope stability. In: M.G. Anderson and K.S. Richards, eds. *Slope Stability*. John Wiley & Sons Ltd., Chichester, UK: 187-230.
- Hadley, R.F., Karlinger, M.R., Burns, A.W., and Eschner, T.R. 1987. Water development and associated hydrologic changes in the Platte River, Nebraska, U.S.A. *Regulated Rivers: Research and Management*, 1: 331-341.
- Hales, T.C., Ford, C.R., Hwang, T., Vose, J.M., and Band, L.E. 2009. Topographic and ecologic controls on root reinforcement. *Journal of Geophysical Research*, 114, F03013, doi:10.1029/2008JF001168.
- Hanson, G.J., and Cook, K.R., 1997. Development of excess shear stress parameters for circular jet testing, American Society of Agricultural Engineers Paper No. 97-2227. American Society of Agricultural Engineers: St. Joseph.
- Hidalgo, R.C., Kun, F., and Herrmann, H.J. 2001. Bursts in a fiber bundle model with continuous damage. *Physical Review E*, 64(6), 066122, doi:10.1103/PhysRevE.64.066122.
- Holburn, E.R.; Fotherby, L.M.; Randle, T.J.; Carlson, D.E. (2006). *Trends of Aggradation and Degradation Along the Central Platte River: 1985 To 2005*, U.S. Department of the Interior, Bureau of Reclamation, Technical Service Center, Sedimentation and River Hydraulics Group, Denver, Colorado.

- James, C.S., Goldbeck, U.K., Patini, A., and Jordanova, A.A. 2008. Influence of foliage on flow resistance of emergent vegetation. *Journal of Hydraulic Research*, 46(4): 536-542. doi:10.3826/jhr.2008.3177.
- Järvelä, J. 2002. Flow resistance of flexible and stiff vegetation: a flume study with natural plants. *Journal of Hydrology*, 269(1-2): 44-54.
- Järvelä, J. 2004. Determination of flow resistance caused by non-submerged woody vegetation. *International Journal of River Basin Management*, 2(1): 61-70.
- Johnson, W.C. 1994. Woodland Expansions in the Platte River, Nebraska: Patterns and Causes. *Ecological Monographs*, 64 (1): 45-84.
- Johnson, W. C. 1997. Equilibrium response of riparian vegetation to flow regulation in the Platte river, Nebraska. *Regulated Rivers: Research & Management*, 13: 403-415. doi: 10.1002/(SICI)1099-1646(199709/10)13:5<403::AID-RRR465>3.0.CO;2-U
- Johnson, W.C. 2000. Tree recruitment and survival rates in rivers: influence of hydrological processes. *Hydrological Processes*, 14(16-17): 3051-3074.
- Jones, J.S. 1984. Comparison of prediction equations for bridge pier and abutment scour. *Transportation Research Record*, 950(2): 202-209.
- Jones, J.S. and Sheppard, D.M. 2000. Local Scour at Complex Pier Geometries. In: *Proceedings of the ASCE 2000 Joint Conference on Water Resources Engineering and Water Resources Planning and Management*, July 30 - August 2, Minneapolis, MN.
- Karrenberg, S., Edwards, P.J., and Kollmann, J. 2002. The life history of Salicaceae living in the active zone of floodplains. *Freshwater Biology*, 47(4): 733-748.
- Keevil, G.M., Peakall, J., Best, J.L., and Amos, K.J. 2006. Flow structure in sinuous submarine channels: Velocity and turbulence structure of an experimental submarine channel. *Marine Geology*, 229(3-4): 241-257.
- Knighton, D. 1998. *Fluvial Forms and Processes: A New Perspective*. 383pp.
- Lane, E.W. 1957. A study of the shape of channels formed by natural streams flowing in erodible material. *Missouri River Division Sediment Series 9*. U.S. Army Engineer Division, Missouri River, Omaha, NE.
- Leopold, L.B. and Wolman, M.G. 1957. River channel patterns: braided, meandering and straight. U.S. Geological Survey Professional Paper 282-B. U.S. Government Printing Office, Washington, D.C.
- Li, R.-M., and Shen, H.W. 1973. Effect of tall vegetations on flow and sediment. *Journal of the Hydraulics Division, ASCE*, 99(HY5): 793-814.
- Lin, B., and Falconer, R.A. 1997. Three-dimensional layer-integrated modeling of estuarine flows with flooding and drying. *Estuarine, Coastal and Shelf Science*, 44: 737-751.
- Loades, K.W., Bengough, A.G., Bransby, M.F., and Hallett, P.D. 2009. Planting density influence on fibrous root reinforcement of soils. *Ecological Engineering*, 36(3): 276-284.
- López, F., and García, M.H. 2001. Mean flow and turbulence structure of open-channel flow through non-emergent vegetation. *Journal of Hydraulic Engineering, ASCE*, 127(5): 392-402.
- McBride, M., Hession, W.C., Rizzo, D.M., and Thompson, D.M. 2007. The influence of riparian vegetation on near-bank turbulence: a flume experiment. *Earth Surface Processes and Landforms*, 32(13): 2019-2037.
- Melville, B.W., and Chiew, Y.-M. 1999. Time scale for local scour at bridge piers. *Journal of Hydraulic Engineering, ASCE*, 125(1): 59-65. See also Discussion and Closure, *Journal of Hydraulic Engineering, ASCE*, 126(10): 793-795.

- Melville, B.W., and Sutherland, A.J., 1988, Design method for local scour at bridge piers: American Society of Civil Engineering, Journal of the Hydraulics Division, v. 114, no. 10, p. 1210–1225.
- Met-Flow. 1997. Ultrasonic Velocity Profile Monitor Operation Manual, XW-2-MX Series. Met-Flow SA, Lausanne, Switzerland.
- Mickovski, S.B., Hallet, P.D., Bransby, M. F., Davies, M.C.R., Sonnenberg, R., and Bengough, A.G. 2009. Mechanical Reinforcement of Soil by Willow Roots: Impacts of Root Properties and Root Failure Mechanism. Soil Science Society of America Journal, 73: 1276-1285.
- Mosley, M.P. 2001. Discussion of Paola, C. Modelling stream braiding over a range of scales. In: M.P. Mosley, ed. Gravel-Bed Rivers V. New Zealand Hydrological Society, Wellington: 11-46.
- Murphy et al., 2004 P.J. Murphy, T.J. Randle, L.M. Fotherby and J.A. Daraio, The Platte River Channel: History and Restoration, U.S. Dept. of Int., Bur. of Reclamation report, Denver, CO (2004) 167 pp.
- Nanson, G.C., and Knighton, A.D. 1996. Anabranching rivers: their cause, character and classification. Earth Surface Processes and Landforms, 21: 217-239.
- Nanson, G.C. and Knighton, D. 1996. Anabranching Rivers: Their cause, character and classification. Earth Surface Processes and Landforms: 21(3): 217- 239.
- Nepf, H.M. 1999. Drag, turbulence, and diffusion in flow through emergent vegetation. Water Resources Research, 35(2): 479-489.
- Nikora, V., and Goring, D.G. 2000. Flow turbulence over fixed and weakly mobile gravel beds. Journal of Hydraulic Engineering, ASCE, 126: 679-690.
- Paola, C. 2001. Modelling stream braiding over a range of scales. In: M.P. Mosley, ed. Gravel-Bed Rivers V. New Zealand Hydrological Society, Wellington: 11-46.
- Pasche, E., and Rouvé, G. 1985. Overbank flow with vegetatively roughened flood plains. Journal of Hydraulic Engineering, ASCE, 111(9): 1262-1278.
- Petryk, S., and Bosmajian, G. 1975. Analysis of flow through vegetation. Journal of the Hydraulics Division, ASCE, 101(HY7): 871-884.
- Pollen, N. 2007. Temporal and spatial variability in root-reinforcement of streambanks: Accounting for soil shear strength and moisture. Catena, 69: 197-205.
- Pollen, N., and Simon, A. 2005. Estimating the mechanical effects of riparian vegetation on streambank stability using a fiber bundle model. Water Resources Research, 41: W07025, doi:10.1029/2004WR003801.
- Pollen-Bankhead, N., and Simon, A. 2009. Enhanced application of root-reinforcement algorithms for bank-stability modeling. Earth Surface Processes and Landforms, 34(4): 471-480.
- Pollen, N., Simon, A., and Collision, A.J.C. 2004. Advances in Assessing the Mechanical and Hydrologic Effects of Riparian Vegetation on Streambank Stability. In: S.J. Bennett and A. Simon, eds. Riparian Vegetation and Fluvial Geomorphology, Water Science and Applications 8, AGU, Washington, D.C.: 125-139.
- Pollen-Bankhead, N., Simon, A., and Thomas, R. In Press. The reinforcement of soil by roots: recent advances and directions for future research. In: Hupp, C.R. (ed.), Treatise in Geomorphology. Elsevier. New York.
- Potyondy, J.G., 1961. Skin friction between various soils and construction materials. Geotechnique, 11(4): 339-353.

- Richardson, E.V., and Davis, S.R. 2001. Evaluating Scour at Bridges, Fourth Edition. Hydraulic Engineering Circular 18, Publication Number FHWA NHI 01-001. Federal Highway Administration, U.S. Department of Transportation, Washington, D.C.
- Riestenberg, M., and Sovonick-Dunford, S.S. 1983. The role of woody vegetation in stabilizing slopes in the Cincinnati area, Ohio. *Geological Society of America Bulletin*, 94(4): 506-518.
- Schnauder, I., and Moggridge, H.L. 2009. Vegetation and hydraulic-morphological interactions at the individual plant, patch and channel scale. *Aquatic Sciences*, 71(3): 318-330.
- Schnauder, I., and Wilson, C.A.M.E. 2009. Discussions. *Journal of Hydraulic Research*, 47(3): 384-386. DOI: 10.1080/00221686.2009.9522010.
- Schumm S.A., and Khan, H.R. 1972. Experimental study of channel patterns. *Geological Society of America Bulletin*, 83(6): 1755-1770.
- Schumm, S.A., Mosley, M.P., and Weaver, W.E. 1987. *Experimental Fluvial Geomorphology*. John Wiley & Sons, Inc., New York, NY.
- Schwarz, M., Preti, F., Giadrossich, F., Lehmann, F., and Or, D. 2010. Quantifying the role of vegetation in slope stability: A case study in Tuscany (Italy). *Ecological Engineering*, 36(3): 285-291.
- Shields, A. (1936). Application of similarity principles and turbulence research to bed-load movement. W.P. Ott, and J.C. van Uchelen (translators), *Hydrodynamics Laboratory Publication 167*. USDA Soil Conservation Service Cooperative Laboratory, California Institute of Technology: Pasadena, CA.
- Simon, A., and Collison, A.J.C. 2002. Quantifying the mechanical and hydrologic effects of riparian vegetation on streambank stability. *Earth Surface Processes and Landforms*, 27(5): 527-546.
- Simon, A., Pollen, N., and Langendoen, E.J. 2006. Influence of Two Woody Riparian Species on Critical Conditions for Streambank Stability: Upper Truckee River, California. *Journal of the American Water Resources Association*, 42(1): 99-113.
- Simpson, C.J., and Smith, D.G. 2001. The braided Milk River, northern Montana, fails the Leopold-Wolman discharge-gradient test. *Geomorphology*, 41: 337-353.
- Smith, N.D. 1970. The braided stream depositional environment: comparison of the Platte River with some Silurian clastic rocks, North-Central Appalachians. *Geological Society of America Bulletin*, 81(10): 2993-3014.
- Smith, D.G., and Smith, N.D. 1980. Sedimentation in anastomosed river systems: examples from alluvial valleys near Banff, Alberta. *Journal of Sedimentary Petrology*, 50(1): 157-164.
- Stein, O.R., Julien, P.Y., and Alonso, C.V. 1993. Mechanics of jet scour downstream of a headcut. *Journal of Hydraulic Research*, 31(6): 723-738.
- Stella, J.C., and Battles, J.J. 2010. How do riparian woody seedlings survive seasonal drought? *Oecologia*, 164(3): 579-590.
- Stone, B.M., and Shen, H.T. 2002. Hydraulic resistance of flow in channels with cylindrical roughness. *Journal of Hydraulic Engineering, ASCE*, 128(5): 500-506.
- Tanino, Y. and H. M. Nepf. 2008. Lateral dispersion in a random cylinder array at high Reynolds number. *J. Fluid Mech.* 600, 339-371.
- Tetra Tech. 2012. Elm Creek FSM Annual Monitoring Report. 88pp.
- Terzaghi, K., and Peck, R.B. 1967. *Soil Mechanics in Engineering Practice* (2nd Edition). John Wiley & Sons, Inc., New York, NY.
- Thomas, R.E., and Pollen-Bankhead, N. 2010. Modeling root-reinforcement with a fiber-bundle model and Monte Carlo simulation. *Ecological Engineering*, 36(1): 47-61.

- Thorne, C.R., and Abt, S.R. 1993. Analysis of riverbank instability due to toe scour and lateral erosion. *Earth Surface Processes and Landforms*, 18: 835-843.
- Tosi, M. 2007. Root tensile strength relationships and their slope stability implications of three shrub species in the Northern Apennines (Italy). *Geomorphology*, 87: 268-283.
- Vollsinger, S., Mitchell, S.J., Byrne, K.E., Novak, M.D., and Rudnicki, M. 2005. Wind tunnel measurements of crown streamlining and drag relationships for several hardwood species. *Canadian Journal of Forest Research*, 35: 1238-1249. doi: 10.1139/X05-051.
- Waldron, L.J., and Dakessian, S. 1981. Soil reinforcement by roots: Calculation of increased soil shear resistance from root properties. *Soil Science*, 132(6): 427-435.
- White, B.L., and Nepf, H.M. 2008. A vortex-based model of velocity and shear stress in a partially vegetated shallow channel. *Water Resources Research*, 44(1): W01412. doi:10.1029/2006WR005651.
- Williams, G.P. 1978. The Case of the Shrinking Channel the North Platte and Platte Rivers in Nebraska. *Geological Survey Circular* 781.53pp.
- Wilson, C.A.M.E., Stoesser, T., Bates, P.D., and Batemann Pinzen, A. 2003. Open channel flow through different forms of submerged flexible vegetation. *Journal of Hydraulic Engineering, ASCE*, 29(11): 847-853.
- Wilson, C.A.M.E., Yagci, O., Rauch, H.-P., and Stoesser, T. 2006. Application of the drag force approach to model the flow-interaction of natural vegetation. *International Journal of River Basin Management*, 4(2): 137-146.
- Wu, T.H., McKinnell III, W.P., and Swanston, D.N. 1979. Strength of tree roots and landslides on Prince of Wales Island. Alaska. *Canadian Geotechnical Journal*, 16: 19-33.
- Zong, L. and Nepf, H. 2010. Flow and deposition in and around a finite patch of vegetation. *Geomorphology*, 116(3-4): 363-372.

APPENDIX A

A1.1 Principles of UVP

Ultrasonic Doppler Velocity Profiling (UVP) relies on the transmission of an ultrasonic burst from a piezoelectric transducer (or probe) along a measurement profile. This burst propagates through the fluid and is reflected from the surface of microparticles suspended in the liquid before being received by the same transducer. The spatial and velocity information of the suspended particles assumed to be traveling with the velocity of the fluid flow, and hence the velocity profile, is contained in the reflected waves (echoes). The distance between a suspended particle and the transducer (x) is calculated from the time delay (t) between the start of the burst and the reception signal,

$$x = \frac{ct}{2} \tag{A1}$$

where c is the velocity of ultrasound in the fluid being investigated (assuming the density of the fluid in the measurement area remains constant). If the scattering particle is moving, a Doppler shift of the echo frequency occurs. The velocity component (U) of the particle in the direction of the transducer axis (positive towards the transducer) is derived from the Doppler-shift frequency (f_D) at that instant, given by:

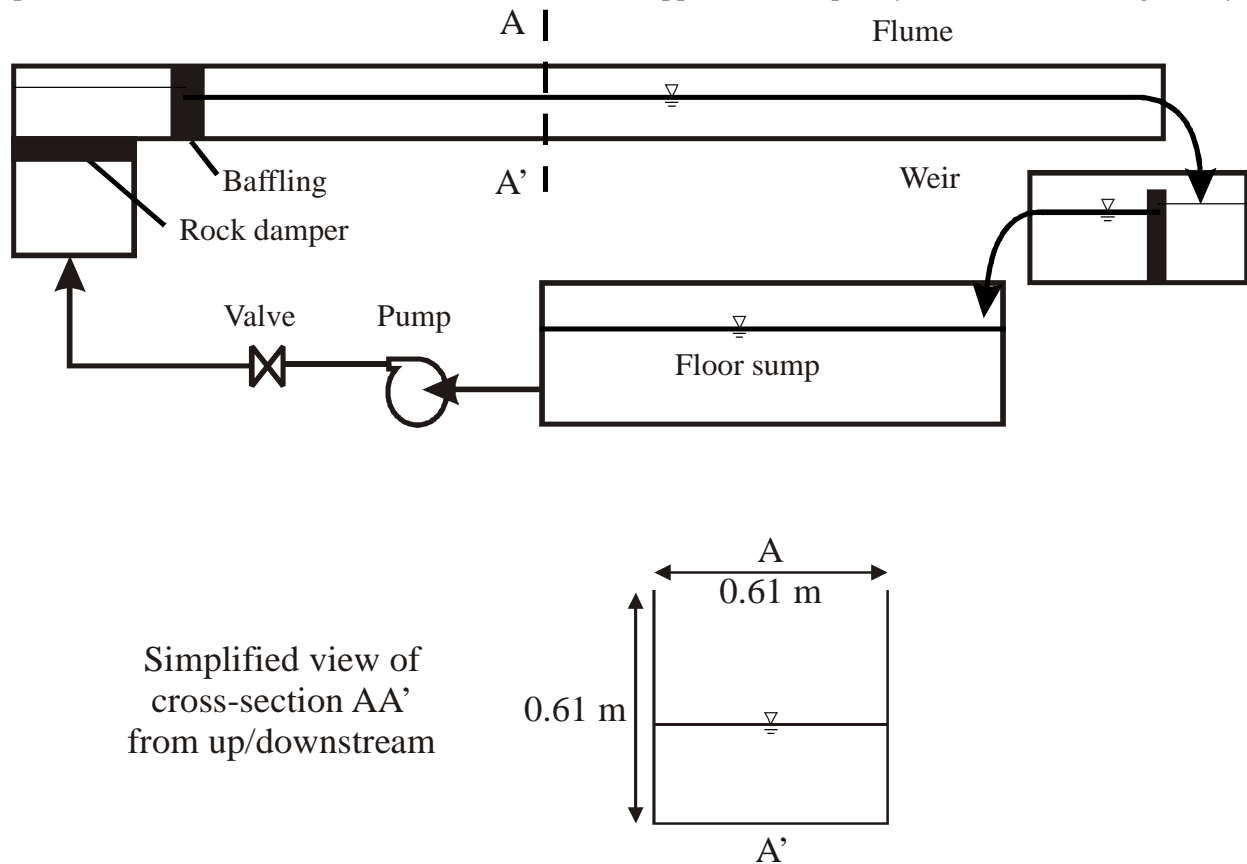


Figure 1A. Schematic diagram of the flume employed in the present study.

$$U = \frac{cf_D}{2f_0} \quad (\text{A2})$$

where f_0 is the transmitting frequency.

Velocities can be established at many different spatial points along the measurement axis to produce a velocity profile. The region along the transducer measurement axis in which velocities are recorded is called the measurement window (Figure 1B), with the maximum width of the measurement window being defined by the minimum and maximum measurable distances. The width of the measurement window, w_w , can be determined as:

$$w_w = \frac{cm}{2f_0} = \frac{m\lambda_0}{2} \quad (\text{A3})$$

where m is the number of cycles per pulse and λ_0 is the ultrasound wavelength, whilst the maximum distance to which the UVP will detect, L_{\max} and the maximum detectable velocity, U_{\max} are determined by:

$$L_{\max} = \frac{c}{2f_{pr}} \quad (\text{A4})$$

$$\text{and } U_{\max} = \frac{cf_{pr}}{4f_0} \quad (\text{A5})$$

respectively, where f_{pr} is the pulse repetition frequency (sampling frequency dictated by the Nyquist sampling theorem such that $f_{pr} > 2f_D$). Within the measurement window, the return signal (echo) is gated at known return times, allowing the measurement of velocity at up to 256 separate, but evenly spaced, positions along the ultrasound emission axis. These positions are referred to as measurement channels or velocity bins (typically 128 velocity bins are used). The distance between two adjacent measurement channels is the channel distance. Increasing the number of cycles (wavelengths) per ultrasonic pulse increases the channel distance, and decreases the spatial resolution. In order to optimise echo versus spatial resolution for a 4 MHz transducer operating in water at 20°C ($c = 1480 \text{ m s}^{-1}$), the default number of four cycles per pulse defines a minimum channel distance of 0.74 mm. During all the experiments presented within this study, the channel width will be equal to the channel distance so that there is no overlap or gap between velocity bins (Figure 1B).

As the frequency of ultrasound is fixed by the choice of transducer, a trade-off exists between the maximum distance of measurement, L_{\max} , and the maximum detectable velocity, U_{\max} , such that (Met-Flow, 1997):

$$L_{\max}U_{\max} = \frac{c^2}{8f_0} = \text{constant} \quad (\text{A6})$$

The on-axis velocity resolution is given by:

$$\Delta U = \frac{U_{\max}}{N} \tag{A7}$$

where $N = 256$ and is the number of Doppler units recorded by the 8-bit UVP-XW system. Therefore, to reduce ΔU and hence ensure that all the velocities are being accurately differentiated, the maximum measurable velocity must be reduced (Equation 35). Consequently, the maximum distance must increase (Equation A6) and the pulse-repetition frequency decrease (Equation A5).

Table A1. Summary of UVP parameters to be used in this study.

Number of bins	128
Number of profiles per transducer	300 – 500
$1/f_{pr}$	$0.37 - 0.59 \times 10^{-3}$ s
Intra-sample delay	15×10^{-3} s
Total sample time	$40 - 70 \times 10^{-3}$ s
Data capture frequency	14.3 – 25.0 Hz
c	1480 m s^{-1}
Velocity range	$313 - 502 \times 10^{-3} \text{ m s}^{-1}$
Minimum velocity	$-157 - -256 \times 10^{-3} \text{ m s}^{-1}$
U_{\max}	$156 - 256 \times 10^{-3} \text{ m s}^{-1}$
ΔU	$1.225 - 1.961 \times 10^{-3} \text{ m s}^{-1}$
Minimum measurement distance	5×10^{-3} m
L_{\max}	0.273 – 0.437 m
Channel distance	$2.04 - 3.33 \times 10^{-3}$ m

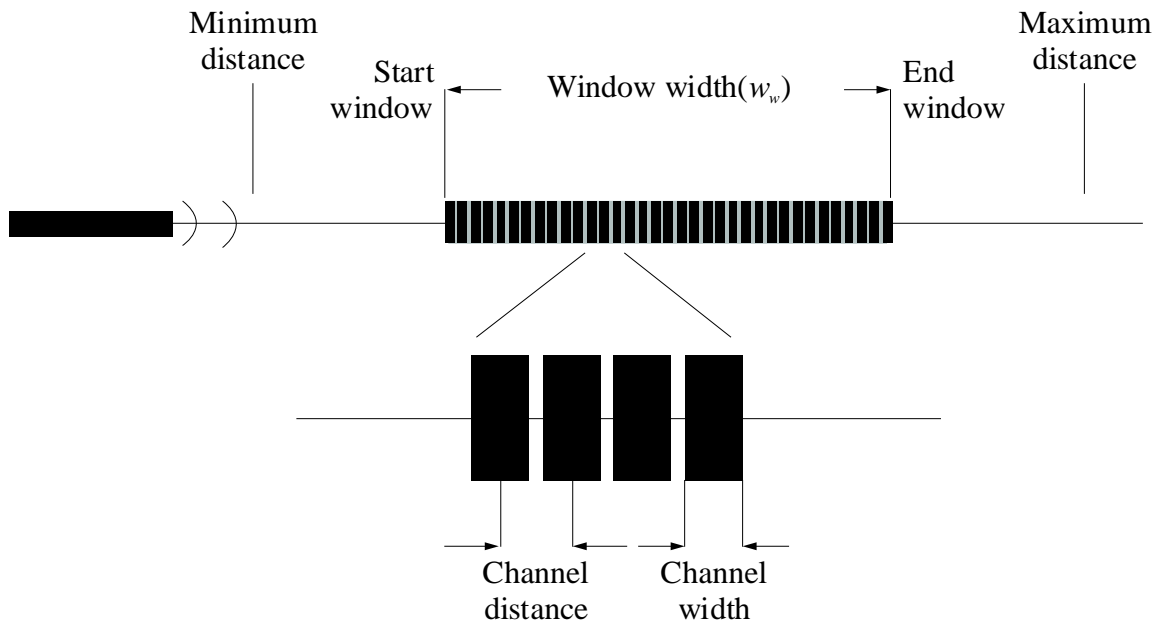


Figure 1A. Illustration of the terms connected with the UVP measurement window. A UVP probe is

shown top left emitting a beam of ultrasound to the right.

A1.2 UVP data processing

The UVP data were collected using Metflow UVP Monitor Version 3 software. After exporting, a Matlab GUI was used to separate the multiplexed data into individual transducer files, as well as saving a single multiplexed file. Instantaneous velocities were averaged over periods of 175-210 s, removing the instantaneous variation between each time-step and summarizing the fluid dynamics within the system, enabling comparison between different experimental runs. This averaging period was selected after analysis of the cumulative velocity variance associated with different sampling windows to ensure convergence of the mean velocity (e.g., Sukhodolov and Rhoads, 2001). To remove noise and spikes without smoothing the small-scale turbulence associated with eddies, a custom Matlab-scripted filter was applied to all the data. The instantaneous velocity data were filtered to replace any points in the time series more than two standard deviations from the mean. Each bin was filtered as a discrete time series and any edge effects were minimised by padding the start and end of each time series prior to the application of the filter. The mean was calculated using an 11-point moving average and the points were replaced with a 3-point moving mean (see Buckee et al., 2001; Keevil et al., 2006). The filter was commonly found to replace less than 5% of the data.

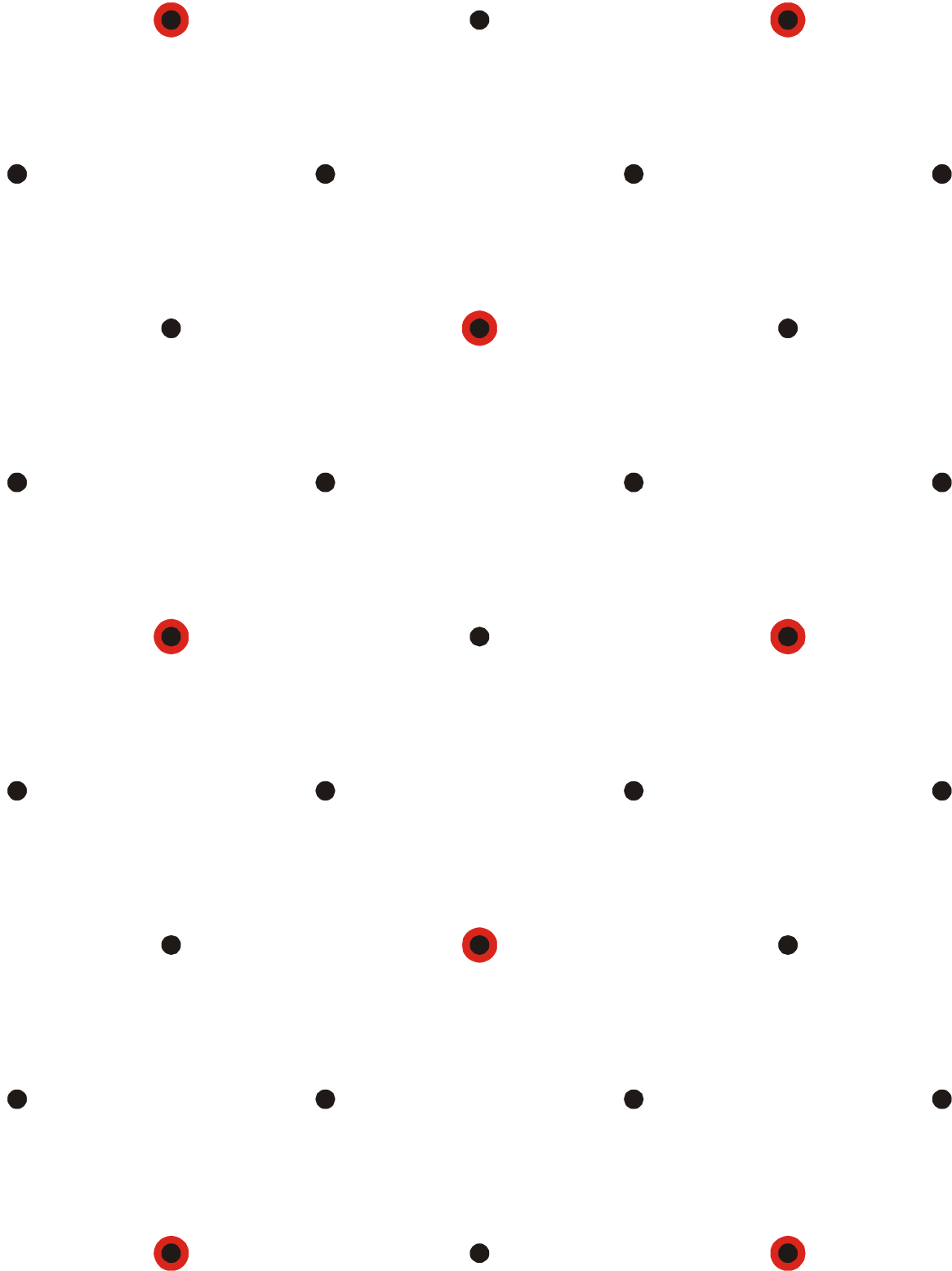


Figure A1. Staggered grid pattern used for reed canarygrass (black; 800 stems m⁻²) and *phragmites australis* (red; 200 stems m⁻²).

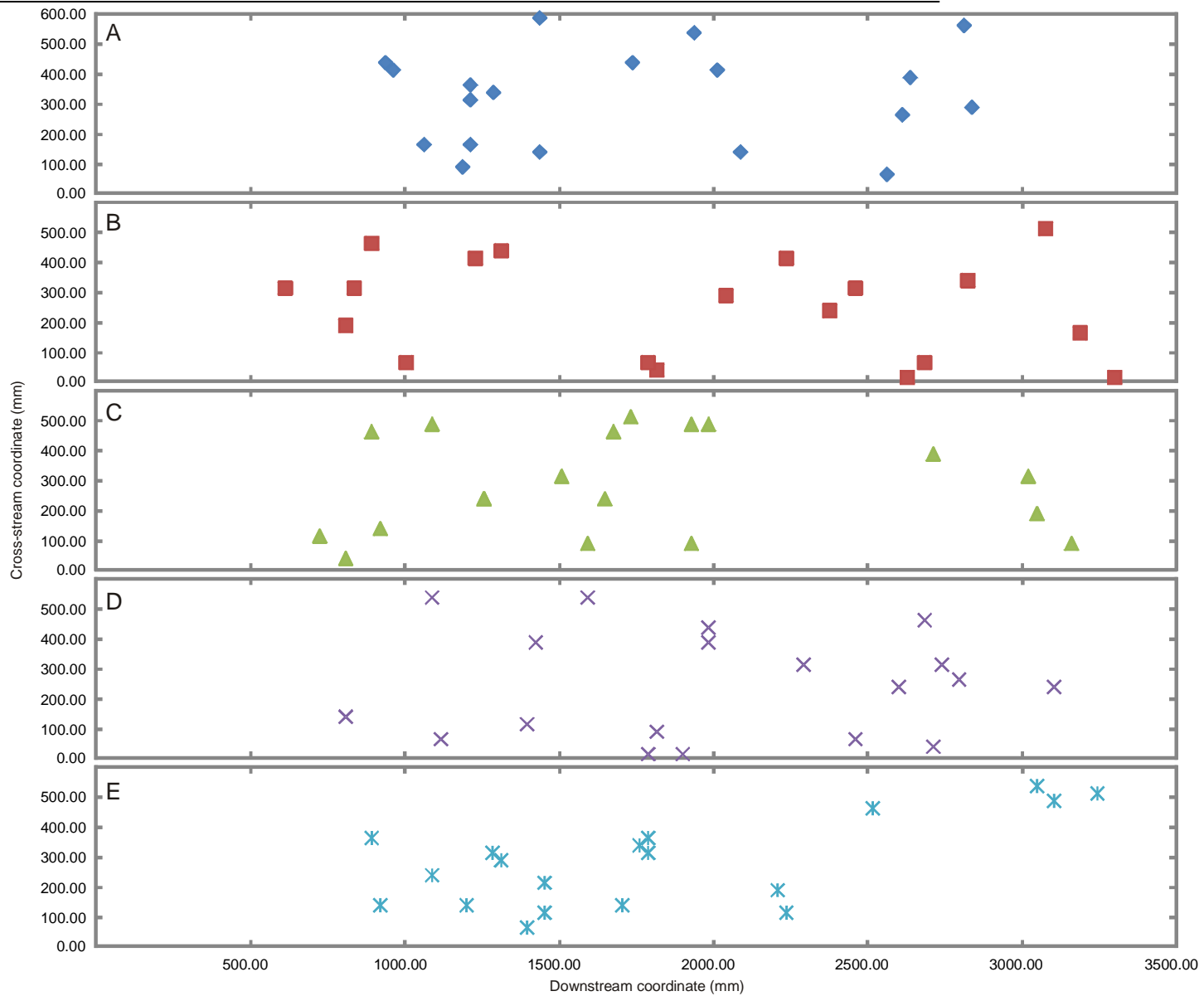


Figure A2. The five, alternative, randomly-generated arrangements of the cottonwood sapling mimics at an areal density of 13 stems m⁻². Double density runs employed the same arrangements but with an additional plant inserted in adjacent holes.

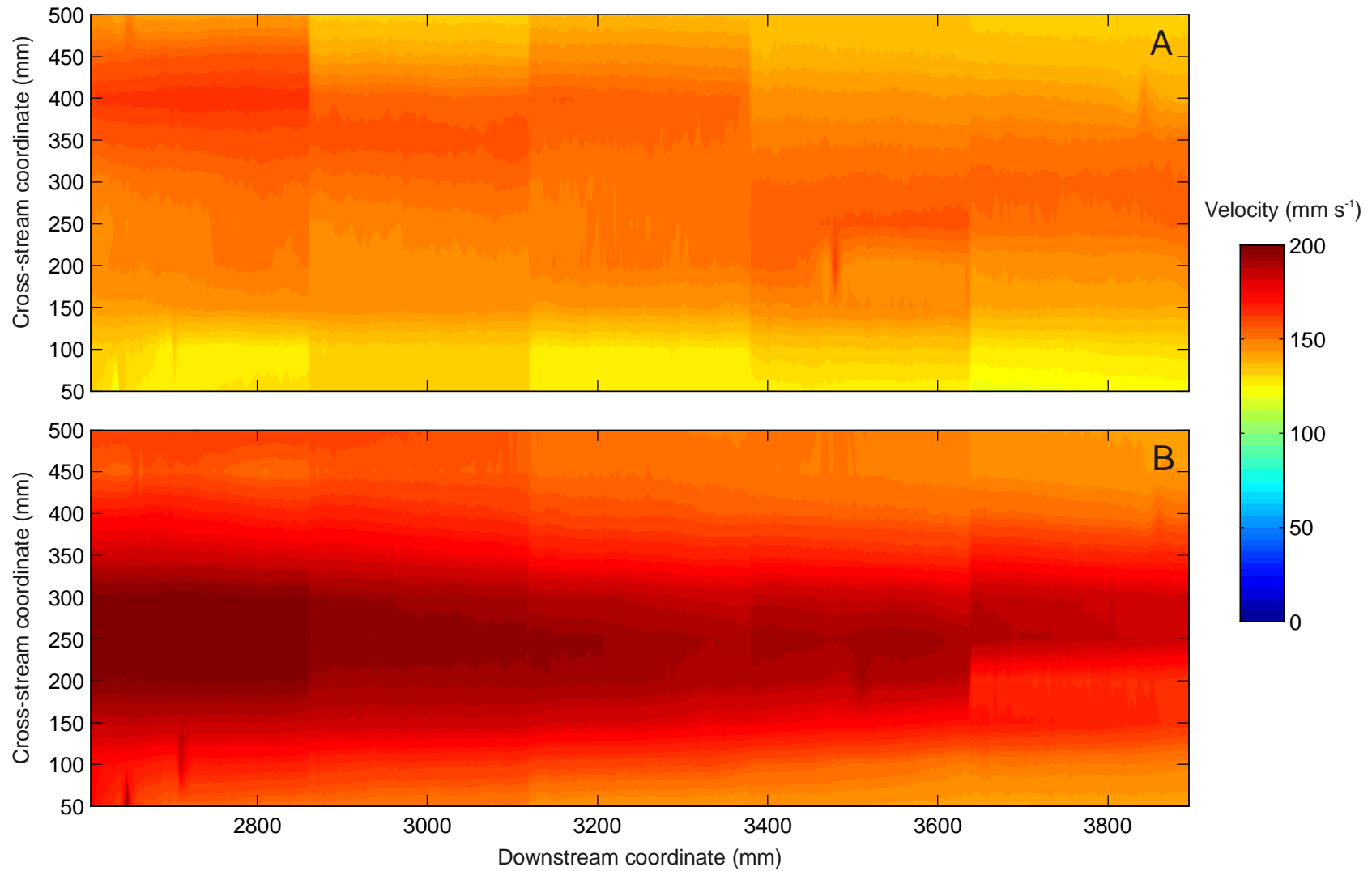


Figure A3. Example horizontal UVP profiles for the case cottonwoods, random arrangement 3, discharge = $0.028 \text{ m}^3\text{s}^{-1}$, weir height = 0.30 m. A. Measured 0.10 m above the bed, B. Measured 0.20 m above the bed. Note the imperfect but generally good match-up between profiles

Along-stream distance (m)	Flume bed elevation (m)	Water surface elevation (m)	Deviation of water surface from base case (m) with a 0.3 m weir height at low discharge (0.0285 cms)				
			Cottonwood double stem density	Cottonwood	Reed canarygrass 400 stem density	Reed canarygrass 800 stem density	Phragmites
Cross-stream distance is 0.1 m							
0.4	0.0527	0.3060	0.0006	-0.0006	0.0024	0.0064	0.0027
0.6	0.0539	0.3078	0.0009	0.0003	0.0030	0.0040	0.0037
0.8	0.0521	0.3103	0.0006	0.0000	0.0027	0.0064	0.0012
1	0.0524	0.3127	0.0003	-0.0006	0.0021	0.0061	0.0018
1.2	0.0527	0.3146	0.0006	0.0000	0.0027	0.0067	0.0018
1.4	0.0527	0.3167	0.0006	0.0000	0.0024	0.0064	0.0024
1.6	0.0518	0.3185	0.0006	0.0000	0.0027	0.0058	0.0015
1.8	0.0512	0.3210	0.0000	-0.0006	0.0018	0.0049	0.0012
2	0.0509	0.3231	0.0006	-0.0003	0.0018	0.0046	0.0009
2.2	0.0497	0.3255	0.0003	-0.0006	0.0012	0.0037	0.0003
2.4	0.0497	0.3274	0.0003	-0.0006	0.0012	0.0030	0.0000
2.6	0.0488	0.3298	0.0000	-0.0006	0.0006	0.0027	-0.0012
2.8	0.0500	0.3319	0.0009	-0.0003	0.0009	0.0027	0.0009
3	0.0491	0.3338	0.0006	0.0000	0.0009	0.0024	-0.0015
3.2	0.0475	0.3359	0.0009	0.0003	0.0006	0.0018	-0.0027
3.4	0.0482	0.3380	0.0009	0.0000	0.0006	0.0018	-0.0027
3.6	0.0494	0.3405	0.0006	0.0000	0.0006	0.0012	0.0000
3.8	0.0500	0.3429	0.0003	0.0000	0.0000	0.0009	0.0003
4	0.0500	0.3447	0.0006	0.0000	0.0003	0.0009	0.0003
4.2	0.0503	0.3472	-0.0003	0.0000	0.0003	0.0003	0.0006
4.334	0.0500	0.3487	0.0000	0.0000	0.0000	0.0000	0.0000
Cross-stream distance is 0.3 m							
0.4	0.0494	0.3057	0.0003	-0.0006	0.0021	0.0064	-0.0003
0.6	0.0530	0.3075	-0.0024	0.0003	0.0027	0.0067	0.0030
0.8	0.0512	0.3100	0.0006	-0.0003	0.0024	0.0061	0.0006
1	0.0509	0.3124	-0.0003	-0.0006	0.0015	0.0061	0.0009
1.2	0.0512	0.3142	0.0003	0.0000	0.0024	0.0067	0.0012
1.4	0.0506	0.3161	0.0006	0.0000	0.0024	0.0067	0.0006
1.6	0.0503	0.3182	0.0000	0.0000	0.0021	0.0058	0.0006
1.8	0.0494	0.3206	-0.0006	-0.0006	0.0015	0.0049	-0.0006
2	0.0503	0.3228	-0.0006	-0.0003	0.0012	0.0046	0.0000
2.2	0.0494	0.3252	0.0000	-0.0006	0.0009	0.0037	-0.0003

Along-stream distance (m)	Flume bed elevation (m)	Water surface elevation (m)	Deviation of water surface from base case (m) with a 0.3 m weir height at low discharge (0.0285 cms)				
			Cottonwood double stem density	Cottonwood	Reed canarygrass 400 stem density	Reed canarygrass 800 stem density	Phragmites
2.4	0.0494	0.3271	0.0000	-0.0003	0.0009	0.0030	-0.0009
2.6	0.0482	0.3295	0.0006	-0.0006	0.0003	0.0024	-0.0015
2.8	0.0482	0.3316	0.0006	-0.0003	0.0006	0.0027	0.0006
3	0.0472	0.3335	0.0003	0.0000	0.0003	0.0024	-0.0015
3.2	0.0469	0.3356	0.0009	0.0003	0.0003	0.0018	-0.0024
3.4	0.0475	0.3377	0.0006	0.0000	0.0003	0.0018	-0.0021
3.6	0.0479	0.3402	0.0003	0.0000	0.0003	0.0012	-0.0018
3.8	0.0488	0.3426	0.0003	0.0000	-0.0003	0.0009	-0.0003
4	0.0491	0.3444	0.0003	0.0000	0.0003	0.0009	0.0006
4.2	0.0488	0.3466	0.0003	0.0003	0.0003	0.0006	0.0006
4.334	0.0488	0.3484	0.0000	0.0000	0.0000	0.0000	0.0000
Cross-stream distance is 0.5 m							
0.4	0.0485	0.3054	-0.0006	-0.0006	0.0021	0.0064	0.0006
0.6	0.0500	0.3072	-0.0006	0.0003	0.0027	0.0067	0.0021
0.8	0.0500	0.3097	-0.0006	-0.0006	0.0021	0.0061	0.0024
1	0.0497	0.3121	-0.0018	-0.0009	0.0018	0.0061	0.0027
1.2	0.0500	0.3139	-0.0012	0.0000	0.0024	0.0067	0.0030
1.4	0.0491	0.3158	-0.0009	-0.0003	0.0024	0.0067	0.0030
1.6	0.0482	0.3179	-0.0009	0.0000	0.0021	0.0058	0.0018
1.8	0.0485	0.3203	-0.0009	-0.0006	0.0015	0.0049	0.0012
2	0.0482	0.3225	-0.0006	-0.0006	0.0012	0.0046	0.0003
2.2	0.0472	0.3246	-0.0009	-0.0003	0.0012	0.0040	0.0003
2.4	0.0488	0.3267	-0.0009	-0.0003	0.0009	0.0030	0.0009
2.6	0.0482	0.3292	-0.0009	-0.0009	0.0003	0.0024	0.0018
2.8	0.0469	0.3313	-0.0009	-0.0003	0.0006	0.0027	-0.0009
3	0.0475	0.3331	-0.0006	0.0000	0.0003	0.0024	-0.0012
3.2	0.0469	0.3353	-0.0003	0.0003	0.0003	0.0018	-0.0015
3.4	0.0482	0.3374	-0.0009	0.0000	0.0006	0.0018	-0.0012
3.6	0.0479	0.3399	-0.0003	0.0000	0.0003	0.0012	-0.0009
3.8	0.0488	0.3423	-0.0015	0.0000	0.0000	0.0009	0.0009
4	0.0485	0.3441	-0.0006	0.0000	0.0003	0.0009	0.0009
4.2	0.0482	0.3466	0.0000	0.0000	0.0000	0.0006	0.0009
4.334	0.0479	0.3481	0.0000	0.0000	0.0000	0.0000	0.0000

Along-stream distance (m)	Flume bed elevation (m)	Water surface elevation (m)	Deviation of water surface from base case (m) with a 0.35 m weir height at low discharge (0.0285 cms)				
			Cottonwood double stem density	Cottonwood	Reed canarygrass 400 stem density	Reed canarygrass 800 stem density	Phragmites
Cross-stream distance is 0.1 m							
0.4	0.0527	0.3536	0.0018	0.0006	0.0021	0.0046	0.0024
0.6	0.0539	0.3563	0.0015	-0.0003	0.0021	0.0043	0.0024
0.8	0.0521	0.3581	0.0015	0.0003	0.0024	0.0040	0.0006
1	0.0524	0.3603	0.0006	0.0003	0.0021	0.0043	0.0012
1.2	0.0527	0.3627	0.0009	0.0003	0.0021	0.0040	0.0009
1.4	0.0527	0.3645	0.0012	0.0003	0.0018	0.0037	0.0015
1.6	0.0518	0.3667	0.0009	0.0003	0.0015	0.0037	0.0006
1.8	0.0512	0.3685	0.0015	0.0006	0.0018	0.0037	0.0006
2	0.0509	0.3706	0.0012	0.0006	0.0018	0.0034	0.0006
2.2	0.0497	0.3728	0.0015	0.0006	0.0015	0.0027	0.0006
2.4	0.0497	0.3752	0.0006	-0.0003	0.0009	0.0015	0.0000
2.6	0.0488	0.3770	0.0018	0.0006	0.0015	0.0021	-0.0012
2.8	0.0500	0.3795	0.0015	0.0006	0.0015	0.0018	0.0006
3	0.0491	0.3819	0.0012	0.0003	0.0009	0.0009	-0.0021
3.2	0.0475	0.3844	0.0003	0.0000	0.0003	0.0006	-0.0034
3.4	0.0482	0.3865	0.0009	0.0003	0.0003	0.0006	-0.0037
3.6	0.0494	0.3886	0.0009	0.0000	0.0003	0.0000	-0.0006
3.8	0.0500	0.3908	0.0009	0.0003	0.0003	0.0003	0.0000
4	0.0500	0.3929	0.0006	0.0003	0.0003	0.0003	-0.0003
4.2	0.0503	0.3953	0.0009	-0.0003	0.0003	0.0000	0.0003
4.334	0.0500	0.3968	0.0000	0.0000	0.0000	0.0000	0.0000
Cross-stream distance is 0.3 m							
0.4	0.0494	0.3533	0.0012	0.0006	0.0018	0.0043	-0.0006
0.6	0.0530	0.3557	0.0012	-0.0003	0.0021	0.0043	0.0021
0.8	0.0512	0.3578	0.0012	0.0003	0.0018	0.0037	0.0000
1	0.0509	0.3600	0.0003	0.0000	0.0018	0.0040	0.0003
1.2	0.0512	0.3624	0.0006	0.0003	0.0018	0.0037	0.0006
1.4	0.0506	0.3642	0.0009	0.0003	0.0015	0.0034	-0.0003
1.6	0.0503	0.3664	0.0006	0.0003	0.0012	0.0034	-0.0003
1.8	0.0494	0.3682	0.0012	0.0006	0.0015	0.0034	-0.0012
2	0.0503	0.3703	0.0003	0.0006	0.0015	0.0030	-0.0003
2.2	0.0494	0.3725	0.0012	0.0006	0.0012	0.0024	0.0000

Along-stream distance (m)	Flume bed elevation (m)	Water surface elevation (m)	Deviation of water surface from base case (m) with a 0.3 m weir height at low discharge (0.0285 cms)				
			Cottonwood double stem density	Cottonwood	Reed canarygrass 400 stem density	Reed canarygrass 800 stem density	Phragmites
2.4	0.0494	0.3746	0.0012	0.0000	0.0009	0.0015	-0.0006
2.6	0.0482	0.3767	0.0015	0.0006	0.0012	0.0018	-0.0012
2.8	0.0482	0.3792	0.0012	0.0006	0.0012	0.0012	0.0006
3	0.0472	0.3816	0.0006	0.0003	0.0006	0.0006	-0.0018
3.2	0.0469	0.3840	0.0003	0.0000	0.0000	0.0003	-0.0030
3.4	0.0475	0.3862	0.0006	0.0003	0.0000	0.0003	-0.0030
3.6	0.0479	0.3883	0.0006	0.0000	0.0000	-0.0003	-0.0027
3.8	0.0488	0.3904	0.0009	0.0003	0.0000	0.0000	-0.0006
4	0.0491	0.3926	0.0006	0.0000	0.0000	0.0000	0.0000
4.2	0.0488	0.3950	-0.0003	-0.0006	0.0000	-0.0003	0.0000
4.334	0.0488	0.3962	0.0000	0.0000	0.0000	0.0000	0.0000
Cross-stream distance is 0.5 m							
0.4	0.0485	0.3527	0.0012	0.0009	0.0018	0.0046	0.0006
0.6	0.0500	0.3554	0.0006	-0.0003	0.0018	0.0043	0.0012
0.8	0.0500	0.3575	-0.0006	0.0000	0.0015	0.0037	0.0018
1	0.0497	0.3597	0.0000	0.0000	0.0015	0.0040	0.0021
1.2	0.0500	0.3618	0.0000	0.0006	0.0018	0.0040	0.0027
1.4	0.0491	0.3639	0.0000	0.0003	0.0012	0.0037	0.0018
1.6	0.0482	0.3661	-0.0006	0.0000	0.0009	0.0034	0.0009
1.8	0.0485	0.3679	0.0009	0.0009	0.0012	0.0030	0.0006
2	0.0482	0.3700	0.0000	0.0003	0.0012	0.0030	0.0000
2.2	0.0472	0.3722	0.0006	0.0003	0.0009	0.0024	0.0006
2.4	0.0488	0.3743	0.0006	0.0000	0.0006	0.0018	0.0012
2.6	0.0482	0.3764	0.0006	0.0006	0.0009	0.0018	0.0021
2.8	0.0469	0.3789	0.0006	0.0006	0.0009	0.0012	-0.0006
3	0.0475	0.3813	0.0003	0.0000	0.0003	0.0006	-0.0015
3.2	0.0469	0.3837	0.0000	0.0000	-0.0003	0.0003	-0.0024
3.4	0.0482	0.3859	0.0000	0.0003	-0.0006	0.0003	-0.0021
3.6	0.0479	0.3880	0.0000	0.0000	-0.0003	-0.0003	-0.0018
3.8	0.0488	0.3901	-0.0006	0.0003	-0.0003	0.0000	0.0006
4	0.0485	0.3923	-0.0006	0.0000	-0.0003	0.0000	0.0003
4.2	0.0482	0.3947	0.0000	-0.0006	-0.0003	-0.0003	0.0006
4.334	0.0479	0.3959	0.0000	0.0000	0.0000	0.0000	0.0000

Along-stream distance (m)	Flume bed elevation (m)	Water surface elevation (m)	Deviation of water surface from base case (m) with a 0.4 m weir height at low discharge (0.0285 cms)				
			Cottonwood double stem density	Cottonwood	Reed canarygrass 400 stem density	Reed canarygrass 800 stem density	Phragmites
Cross-stream distance is 0.1 m							
0.4	0.0527	0.4014	0.0003	0.0006	0.0012	0.0027	0.0015
0.6	0.0539	0.4036	0.0006	0.0000	0.0012	0.0027	0.0021
0.8	0.0521	0.4057	0.0003	0.0006	0.0012	0.0030	0.0000
1	0.0524	0.4078	0.0006	0.0003	0.0012	0.0027	0.0006
1.2	0.0527	0.4100	0.0006	0.0006	0.0015	0.0034	0.0000
1.4	0.0527	0.4118	0.0009	0.0006	0.0012	0.0030	0.0015
1.6	0.0518	0.4139	0.0003	0.0006	0.0012	0.0027	0.0006
1.8	0.0512	0.4164	0.0003	0.0003	0.0009	0.0021	0.0000
2	0.0509	0.4182	0.0006	0.0006	0.0012	0.0021	0.0000
2.2	0.0497	0.4203	0.0006	0.0006	0.0012	0.0018	0.0000
2.4	0.0497	0.4228	0.0000	0.0003	0.0003	0.0012	-0.0003
2.6	0.0488	0.4243	0.0012	0.0012	0.0012	0.0015	-0.0012
2.8	0.0500	0.4267	0.0012	0.0009	0.0009	0.0012	0.0003
3	0.0491	0.4295	0.0006	0.0003	0.0003	0.0003	-0.0024
3.2	0.0475	0.4319	0.0000	0.0003	0.0000	0.0000	-0.0034
3.4	0.0482	0.4337	-0.0003	0.0003	0.0000	0.0000	-0.0030
3.6	0.0494	0.4362	0.0000	0.0003	-0.0003	-0.0003	-0.0009
3.8	0.0500	0.4386	0.0003	0.0000	-0.0006	-0.0006	-0.0003
4	0.0500	0.4407	-0.0006	0.0000	-0.0003	-0.0006	-0.0006
4.2	0.0503	0.4429	-0.0003	0.0003	-0.0003	-0.0003	0.0000
4.334	0.0500	0.4441	0.0000	0.0000	0.0000	0.0000	0.0000
Cross-stream distance is 0.3 m							
0.4	0.0494	0.4011	-0.0003	0.0003	0.0009	0.0024	-0.0018
0.6	0.0530	0.4033	0.0003	-0.0003	0.0009	0.0024	0.0012
0.8	0.0512	0.4054	0.0000	0.0000	0.0009	0.0027	-0.0009
1	0.0509	0.4075	0.0003	-0.0003	0.0009	0.0024	-0.0006
1.2	0.0512	0.4093	0.0006	0.0006	0.0012	0.0034	-0.0003
1.4	0.0506	0.4115	0.0000	0.0003	0.0009	0.0027	-0.0009
1.6	0.0503	0.4133	0.0003	0.0006	0.0012	0.0027	-0.0006
1.8	0.0494	0.4157	0.0003	0.0000	0.0009	0.0021	-0.0018
2	0.0503	0.4179	0.0003	0.0003	0.0009	0.0018	-0.0012
2.2	0.0494	0.4197	0.0009	0.0006	0.0012	0.0018	-0.0006

Along-stream distance (m)	Flume bed elevation (m)	Water surface elevation (m)	Deviation of water surface from base case (m) with a 0.3 m weir height at low discharge (0.0285 cms)				
			Cottonwood double stem density	Cottonwood	Reed canarygrass 400 stem density	Reed canarygrass 800 stem density	Phragmites
2.4	0.0494	0.4225	-0.0003	-0.0003	0.0000	0.0009	-0.0015
2.6	0.0482	0.4240	0.0012	0.0009	0.0009	0.0012	-0.0021
2.8	0.0482	0.4264	0.0006	0.0006	0.0006	0.0009	0.0000
3	0.0472	0.4292	0.0003	0.0000	0.0000	0.0000	-0.0024
3.2	0.0469	0.4316	0.0000	0.0000	-0.0006	-0.0003	-0.0037
3.4	0.0475	0.4334	-0.0006	-0.0003	-0.0003	-0.0003	-0.0027
3.6	0.0479	0.4356	0.0003	0.0003	-0.0003	-0.0003	-0.0027
3.8	0.0488	0.4383	-0.0003	-0.0006	-0.0009	-0.0009	-0.0012
4	0.0491	0.4401	-0.0006	0.0000	-0.0003	-0.0006	-0.0003
4.2	0.0488	0.4426	-0.0006	0.0000	-0.0006	-0.0006	-0.0006
4.334	0.0488	0.4435	0.0000	0.0000	0.0000	0.0000	0.0000
Cross-stream distance is 0.5 m							
0.4	0.0485	0.4008	-0.0009	0.0003	0.0009	0.0027	-0.0009
0.6	0.0500	0.4029	-0.0003	-0.0006	0.0009	0.0024	0.0003
0.8	0.0500	0.4051	-0.0003	0.0000	0.0009	0.0027	0.0009
1	0.0497	0.4072	0.0000	-0.0003	0.0009	0.0024	0.0012
1.2	0.0500	0.4090	-0.0003	0.0006	0.0012	0.0030	0.0018
1.4	0.0491	0.4112	0.0000	0.0003	0.0009	0.0024	0.0015
1.6	0.0482	0.4130	0.0000	0.0006	0.0012	0.0027	0.0006
1.8	0.0485	0.4154	-0.0006	0.0000	0.0009	0.0021	0.0000
2	0.0482	0.4176	0.0000	0.0003	0.0009	0.0018	-0.0009
2.2	0.0472	0.4194	0.0000	0.0006	0.0012	0.0018	0.0000
2.4	0.0488	0.4221	-0.0006	-0.0003	0.0003	0.0009	0.0003
2.6	0.0482	0.4240	0.0000	0.0006	0.0006	0.0012	0.0009
2.8	0.0469	0.4261	0.0003	0.0006	0.0006	0.0009	-0.0012
3	0.0475	0.4289	-0.0003	0.0000	0.0000	0.0000	-0.0021
3.2	0.0469	0.4313	-0.0003	-0.0003	-0.0006	-0.0003	-0.0027
3.4	0.0482	0.4331	-0.0003	-0.0003	-0.0003	-0.0003	-0.0018
3.6	0.0479	0.4353	-0.0006	0.0003	-0.0003	-0.0003	-0.0015
3.8	0.0488	0.4380	-0.0006	-0.0006	-0.0009	-0.0009	0.0000
4	0.0485	0.4398	-0.0006	0.0000	-0.0003	-0.0003	0.0000
4.2	0.0482	0.4423	-0.0009	0.0000	-0.0006	-0.0006	0.0000
4.334	0.0479	0.4432	0.0000	0.0000	0.0000	0.0000	0.0000

Along-stream distance (m)	Flume bed elevation (m)	Water surface elevation (m)	Deviation of water surface from base case (m) with a 0.3 m weir height at high discharge (0.0478 cms)				
			Cottonwood double stem density	Cottonwood	Reed canarygrass 400 stem density	Reed canarygrass 800 stem density	Phragmites
Cross-stream distance is 0.1 m							
0.4	0.0527	0.3377	0.0012	0.0006	0.0067	0.0131	0.0070
0.6	0.0539	0.3405	0.0009	0.0000	0.0061	0.0128	0.0073
0.8	0.0521	0.3426	0.0009	0.0000	0.0064	0.0128	0.0055
1	0.0524	0.3450	0.0003	0.0000	0.0061	0.0128	0.0058
1.2	0.0527	0.3472	0.0006	0.0000	0.0067	0.0134	0.0055
1.4	0.0527	0.3490	0.0009	0.0006	0.0064	0.0128	0.0061
1.6	0.0518	0.3511	0.0003	0.0006	0.0058	0.0113	0.0049
1.8	0.0512	0.3536	0.0000	0.0003	0.0052	0.0094	0.0037
2	0.0509	0.3557	0.0003	0.0003	0.0049	0.0085	0.0030
2.2	0.0497	0.3575	0.0006	0.0003	0.0043	0.0079	0.0030
2.4	0.0497	0.3597	0.0006	0.0006	0.0037	0.0064	0.0021
2.6	0.0488	0.3624	0.0003	0.0003	0.0024	0.0052	0.0003
2.8	0.0500	0.3648	0.0000	0.0000	0.0018	0.0037	0.0012
3	0.0491	0.3667	0.0006	0.0006	0.0018	0.0034	-0.0009
3.2	0.0475	0.3685	0.0006	0.0006	0.0018	0.0024	-0.0018
3.4	0.0482	0.3712	0.0003	0.0000	0.0006	0.0012	-0.0034
3.6	0.0494	0.3737	0.0000	-0.0003	0.0000	0.0000	-0.0009
3.8	0.0500	0.3758	-0.0003	0.0000	0.0000	0.0000	-0.0003
4	0.0500	0.3780	-0.0006	0.0000	0.0000	-0.0003	-0.0006
4.2	0.0503	0.3801	0.0000	0.0000	0.0000	0.0000	0.0000
4.334	0.0500	0.3816	0.0000	0.0000	0.0000	0.0000	0.0000
Cross-stream distance is 0.3 m							
0.4	0.0494	0.3374	0.0012	0.0003	0.0061	0.0128	0.0037
0.6	0.0530	0.3402	0.0003	-0.0003	0.0058	0.0125	0.0064
0.8	0.0512	0.3423	0.0006	-0.0003	0.0061	0.0125	0.0046
1	0.0509	0.3444	0.0006	-0.0003	0.0061	0.0128	0.0049
1.2	0.0512	0.3469	0.0006	-0.0003	0.0064	0.0131	0.0046
1.4	0.0506	0.3487	0.0012	0.0003	0.0064	0.0125	0.0040
1.6	0.0503	0.3508	0.0003	0.0003	0.0055	0.0082	0.0034
1.8	0.0494	0.3530	0.0003	0.0003	0.0052	0.0091	0.0021
2	0.0503	0.3554	0.0003	0.0000	0.0046	0.0082	0.0018
2.2	0.0494	0.3572	0.0006	0.0000	0.0043	0.0076	0.0021

Along-stream distance (m)	Flume bed elevation (m)	Water surface elevation (m)	Deviation of water surface from base case (m) with a 0.3 m weir height at low discharge (0.0285 cms)				
			Cottonwood double stem density	Cottonwood	Reed canarygrass 400 stem density	Reed canarygrass 800 stem density	Phragmites
2.4	0.0494	0.3594	0.0009	0.0000	0.0034	0.0061	0.0009
2.6	0.0482	0.3621	0.0003	-0.0003	0.0024	0.0049	-0.0003
2.8	0.0482	0.3642	0.0003	-0.0003	0.0018	0.0037	0.0012
3	0.0472	0.3664	0.0003	0.0003	0.0018	0.0030	-0.0009
3.2	0.0469	0.3682	0.0009	0.0003	0.0015	0.0021	-0.0018
3.4	0.0475	0.3709	0.0000	-0.0003	0.0003	0.0009	-0.0027
3.6	0.0479	0.3734	-0.0003	-0.0006	-0.0003	-0.0003	-0.0030
3.8	0.0488	0.3755	-0.0006	-0.0003	-0.0003	-0.0003	-0.0012
4	0.0491	0.3776	-0.0003	-0.0006	-0.0003	-0.0003	-0.0006
4.2	0.0488	0.3798	0.0000	-0.0003	-0.0003	-0.0003	-0.0006
4.334	0.0488	0.3810	0.0000	0.0000	0.0000	0.0000	0.0000
Cross-stream distance is 0.5 m							
0.4	0.0485	0.3368	0.0012	0.0009	0.0064	0.0131	0.0049
0.6	0.0500	0.3399	0.0009	0.0000	0.0058	0.0125	0.0055
0.8	0.0500	0.3420	0.0003	0.0000	0.0058	0.0125	0.0064
1	0.0497	0.3441	0.0003	0.0000	0.0061	0.0128	0.0067
1.2	0.0500	0.3463	0.0009	0.0003	0.0070	0.0134	0.0070
1.4	0.0491	0.3484	0.0009	0.0006	0.0055	0.0125	0.0061
1.6	0.0482	0.3502	0.0009	0.0009	0.0055	0.0113	0.0049
1.8	0.0485	0.3523	0.0006	0.0009	0.0055	0.0098	0.0040
2	0.0482	0.3548	0.0006	0.0006	0.0049	0.0085	0.0030
2.2	0.0472	0.3569	0.0003	0.0003	0.0043	0.0076	0.0027
2.4	0.0488	0.3594	0.0006	0.0000	0.0030	0.0058	0.0024
2.6	0.0482	0.3618	0.0003	0.0000	0.0024	0.0049	0.0030
2.8	0.0469	0.3639	0.0003	0.0000	0.0018	0.0040	-0.0003
3	0.0475	0.3661	0.0003	0.0006	0.0018	0.0030	-0.0006
3.2	0.0469	0.3682	0.0006	0.0003	0.0012	0.0018	-0.0015
3.4	0.0482	0.3706	0.0000	0.0000	0.0003	0.0009	-0.0021
3.6	0.0479	0.3731	-0.0003	-0.0003	-0.0003	-0.0003	-0.0021
3.8	0.0488	0.3749	0.0000	0.0003	0.0000	0.0000	0.0003
4	0.0485	0.3773	0.0000	-0.0003	-0.0003	-0.0003	-0.0003
4.2	0.0482	0.3795	-0.0003	0.0000	-0.0003	-0.0003	0.0000
4.334	0.0479	0.3807	0.0000	0.0000	0.0000	0.0000	0.0000

Along-stream distance (m)	Flume bed elevation (m)	Water surface elevation (m)	Deviation of water surface from base case (m) with a 0.35 m weir height at high discharge (0.0478 cms)				
			Cottonwood double stem density	Cottonwood	Reed canarygrass 400 stem density	Reed canarygrass 800 stem density	Phragmites
Cross-stream distance is 0.1 m							
0.4	0.0527	0.3862	0.0009	-0.0003	0.0055	0.0098	0.0058
0.6	0.0539	0.3877	0.0012	0.0006	0.0064	0.0110	0.0070
0.8	0.0521	0.3908	0.0003	-0.0006	0.0049	0.0101	0.0040
1	0.0524	0.3926	0.0006	0.0003	0.0052	0.0107	0.0052
1.2	0.0527	0.3950	0.0003	0.0000	0.0055	0.0107	0.0040
1.4	0.0527	0.3972	0.0006	0.0003	0.0049	0.0094	0.0049
1.6	0.0518	0.3990	0.0003	0.0006	0.0043	0.0088	0.0037
1.8	0.0512	0.4011	0.0006	0.0006	0.0043	0.0073	0.0034
2	0.0509	0.4036	0.0006	0.0003	0.0030	0.0064	0.0021
2.2	0.0497	0.4057	0.0006	0.0003	0.0027	0.0055	0.0015
2.4	0.0497	0.4075	0.0006	0.0003	0.0021	0.0049	0.0015
2.6	0.0488	0.4103	0.0003	0.0000	0.0015	0.0037	-0.0006
2.8	0.0500	0.4124	0.0003	0.0003	0.0012	0.0034	0.0012
3	0.0491	0.4145	0.0003	0.0003	0.0009	0.0024	-0.0015
3.2	0.0475	0.4167	0.0000	0.0000	0.0009	0.0015	-0.0024
3.4	0.0482	0.4191	0.0000	0.0000	0.0003	0.0006	-0.0030
3.6	0.0494	0.4212	0.0000	0.0000	0.0000	-0.0003	-0.0006
3.8	0.0500	0.4237	-0.0003	-0.0003	0.0000	-0.0003	-0.0003
4	0.0500	0.4255	0.0000	0.0000	0.0000	0.0000	-0.0003
4.2	0.0503	0.4276	0.0000	0.0000	0.0003	0.0000	0.0006
4.334	0.0500	0.4292	0.0000	0.0000	0.0000	0.0000	0.0000
Cross-stream distance is 0.3 m							
0.4	0.0494	0.3859	0.0009	-0.0003	0.0055	0.0098	0.0027
0.6	0.0530	0.3874	0.0012	0.0006	0.0064	0.0110	0.0067
0.8	0.0512	0.3901	0.0006	-0.0003	0.0052	0.0104	0.0037
1	0.0509	0.3923	0.0006	0.0003	0.0052	0.0107	0.0043
1.2	0.0512	0.3944	0.0003	0.0003	0.0058	0.0110	0.0040
1.4	0.0506	0.3968	0.0006	0.0003	0.0052	0.0094	0.0027
1.6	0.0503	0.3987	0.0003	0.0006	0.0043	0.0088	0.0024
1.8	0.0494	0.4008	0.0003	0.0006	0.0043	0.0073	0.0015
2	0.0503	0.4033	0.0000	0.0003	0.0030	0.0064	0.0015
2.2	0.0494	0.4054	0.0003	0.0003	0.0027	0.0055	0.0009

Along-stream distance (m)	Flume bed elevation (m)	Water surface elevation (m)	Deviation of water surface from base case (m) with a 0.3 m weir height at low discharge (0.0285 cms)				
			Cottonwood double stem density	Cottonwood	Reed canarygrass 400 stem density	Reed canarygrass 800 stem density	Phragmites
2.4	0.0494	0.4072	0.0006	0.0000	0.0021	0.0049	0.0006
2.6	0.0482	0.4100	0.0003	0.0000	0.0015	0.0037	-0.0009
2.8	0.0482	0.4121	0.0000	0.0003	0.0012	0.0034	0.0012
3	0.0472	0.4142	0.0003	0.0000	0.0009	0.0024	-0.0012
3.2	0.0469	0.4164	0.0000	-0.0003	0.0009	0.0015	-0.0021
3.4	0.0475	0.4188	0.0000	0.0000	0.0003	0.0006	-0.0024
3.6	0.0479	0.4209	0.0000	0.0000	0.0000	-0.0003	-0.0024
3.8	0.0488	0.4231	-0.0003	0.0000	0.0003	0.0000	-0.0006
4	0.0491	0.4252	-0.0003	0.0000	0.0000	0.0000	0.0000
4.2	0.0488	0.4273	0.0000	0.0000	0.0003	0.0000	0.0003
4.334	0.0488	0.4289	0.0000	0.0000	0.0000	0.0000	0.0000
Cross-stream distance is 0.5 m							
0.4	0.0485	0.3856	0.0006	0.0000	0.0052	0.0098	0.0037
0.6	0.0500	0.3874	0.0009	0.0003	0.0058	0.0107	0.0055
0.8	0.0500	0.3898	0.0003	0.0000	0.0052	0.0104	0.0058
1	0.0497	0.3920	0.0003	0.0003	0.0052	0.0107	0.0061
1.2	0.0500	0.3941	0.0006	0.0003	0.0058	0.0110	0.0061
1.4	0.0491	0.3965	0.0003	0.0003	0.0052	0.0094	0.0049
1.6	0.0482	0.3984	0.0003	0.0006	0.0043	0.0085	0.0040
1.8	0.0485	0.4005	0.0003	0.0003	0.0043	0.0073	0.0034
2	0.0482	0.4029	0.0003	0.0003	0.0030	0.0064	0.0018
2.2	0.0472	0.4051	0.0000	0.0000	0.0027	0.0055	0.0018
2.4	0.0488	0.4069	0.0006	0.0000	0.0024	0.0049	0.0024
2.6	0.0482	0.4093	0.0006	0.0003	0.0018	0.0043	0.0027
2.8	0.0469	0.4118	-0.0003	0.0003	0.0012	0.0034	-0.0003
3	0.0475	0.4136	0.0003	0.0003	0.0012	0.0027	-0.0006
3.2	0.0469	0.4164	-0.0003	-0.0006	0.0006	0.0012	-0.0018
3.4	0.0482	0.4185	0.0000	0.0000	0.0003	0.0006	-0.0015
3.6	0.0479	0.4206	0.0000	0.0000	0.0000	-0.0003	-0.0015
3.8	0.0488	0.4228	-0.0003	0.0000	0.0003	0.0000	0.0006
4	0.0485	0.4249	0.0000	0.0000	0.0000	0.0000	0.0003
4.2	0.0482	0.4270	0.0000	0.0000	0.0006	0.0000	0.0009
4.334	0.0479	0.4285	0.0000	0.0000	0.0000	0.0000	0.0000

Along-stream distance (m)	Flume bed elevation (m)	Water surface elevation (m)	Deviation of water surface from base case (m) with a 0.4 m weir height at high discharge (0.0478 cms)					
			Cottonwood double stem density	Cottonwood	Cottonwood re-do	Reed canarygrass 400 stem density	Reed canarygrass 800 stem density	Phragmites
Cross-stream distance is 0.1 m								
0.4	0.0527	0.4340	0.0006	0.0006	0.0006	0.0046	0.0094	0.0034
0.6	0.0539	0.4362	0.0006	0.0000	0.0006	0.0049	0.0091	0.0043
0.8	0.0521	0.4383	0.0006	0.0006	0.0009	0.0046	0.0098	0.0024
1	0.0524	0.4407	0.0003	0.0003	0.0006	0.0043	0.0091	0.0027
1.2	0.0527	0.4429	0.0006	0.0006	0.0009	0.0046	0.0094	0.0021
1.4	0.0527	0.4453	0.0003	0.0006	0.0006	0.0040	0.0082	0.0021
1.6	0.0518	0.4471	0.0003	0.0006	0.0006	0.0040	0.0073	0.0012
1.8	0.0512	0.4490	0.0000	0.0009	0.0009	0.0037	0.0070	0.0012
2	0.0509	0.4511	0.0003	0.0009	0.0012	0.0034	0.0061	0.0012
2.2	0.0497	0.4535	0.0000	0.0003	0.0006	0.0027	0.0052	0.0006
2.4	0.0497	0.4560	-0.0009	0.0003	0.0003	0.0018	0.0040	0.0000
2.6	0.0488	0.4581	0.0000	0.0006	0.0006	0.0018	0.0034	-0.0012
2.8	0.0500	0.4602	0.0003	0.0006	0.0009	0.0018	0.0030	0.0006
3	0.0491	0.4627	-0.0003	0.0006	0.0006	0.0012	0.0021	-0.0021
3.2	0.0475	0.4648	-0.0006	0.0006	0.0006	0.0009	0.0012	-0.0030
3.4	0.0482	0.4670	0.0000	0.0009	0.0006	0.0006	0.0009	-0.0030
3.6	0.0494	0.4694	0.0000	0.0003	0.0003	0.0000	0.0000	-0.0009
3.8	0.0500	0.4715	0.0000	0.0006	0.0003	0.0000	0.0000	0.0000
4	0.0500	0.4737	0.0000	0.0006	0.0006	0.0000	0.0000	-0.0006
4.2	0.0503	0.4758	0.0000	0.0006	0.0006	0.0000	0.0003	0.0003
4.334	0.0500	0.4773	0.0000	0.0000	0.0000	0.0000	0.0000	0.0000
Cross-stream distance is 0.3 m								
0.4	0.0494	0.4337	0.0006	0.0006	0.0006	0.0043	0.0094	0.0003
0.6	0.0530	0.4359	0.0003	0.0000	0.0006	0.0046	0.0091	0.0037
0.8	0.0512	0.4380	0.0009	0.0006	0.0009	0.0043	0.0098	0.0015
1	0.0509	0.4401	0.0006	0.0006	0.0009	0.0043	0.0094	0.0021
1.2	0.0512	0.4426	0.0006	0.0006	0.0009	0.0043	0.0094	0.0018
1.4	0.0506	0.4450	0.0003	0.0006	0.0003	0.0034	0.0082	0.0003
1.6	0.0503	0.4468	0.0003	0.0003	0.0006	0.0037	0.0073	0.0003
1.8	0.0494	0.4487	0.0003	0.0009	0.0009	0.0034	0.0070	-0.0006
2	0.0503	0.4508	0.0003	0.0006	0.0012	0.0030	0.0061	0.0003
2.2	0.0494	0.4532	0.0003	0.0003	0.0006	0.0024	0.0052	0.0000

Along-stream distance (m)	Flume bed elevation (m)	Water surface elevation (m)	Deviation of water surface from base case (m) with a 0.4 m weir height at high discharge (0.0478 cms)					
			Cottonwood double stem density	Cottonwood	Cottonwood re-do	Reed canarygrass 400 stem density	Reed canarygrass 800 stem density	Phragmites
2.4	0.0494	0.4554	0.0003	0.0006	0.0006	0.0018	0.0043	-0.0006
2.6	0.0482	0.4581	-0.0006	0.0003	0.0003	0.0012	0.0030	-0.0018
2.8	0.0482	0.4599	0.0000	0.0006	0.0009	0.0015	0.0030	0.0006
3	0.0472	0.4624	-0.0003	0.0006	0.0006	0.0006	0.0021	-0.0018
3.2	0.0469	0.4645	-0.0003	0.0006	0.0006	0.0006	0.0012	-0.0027
3.4	0.0475	0.4666	0.0000	0.0009	0.0006	0.0003	0.0009	-0.0024
3.6	0.0479	0.4691	0.0000	0.0003	0.0003	-0.0003	0.0000	-0.0027
3.8	0.0488	0.4712	0.0000	0.0003	0.0003	-0.0003	0.0000	-0.0006
4	0.0491	0.4734	0.0000	0.0003	0.0003	-0.0003	0.0000	-0.0003
4.2	0.0488	0.4755	0.0000	0.0006	0.0006	-0.0003	0.0003	0.0000
4.334	0.0488	0.4770	0.0000	0.0000	0.0000	0.0000	0.0000	0.0000
Cross-stream distance is 0.5 m								
0.4	0.0485	0.4334	0.0006	0.0003	0.0006	0.0043	0.0094	0.0012
0.6	0.0500	0.4356	0.0006	0.0000	0.0006	0.0046	0.0091	0.0027
0.8	0.0500	0.4377	0.0009	0.0006	0.0009	0.0043	0.0098	0.0034
1	0.0497	0.4398	0.0006	0.0006	0.0009	0.0043	0.0094	0.0040
1.2	0.0500	0.4423	0.0006	0.0006	0.0009	0.0043	0.0094	0.0037
1.4	0.0491	0.4447	0.0006	0.0003	0.0003	0.0034	0.0082	0.0027
1.6	0.0482	0.4465	0.0003	0.0003	0.0006	0.0037	0.0073	0.0015
1.8	0.0485	0.4484	0.0003	0.0009	0.0009	0.0034	0.0070	0.0012
2	0.0482	0.4508	0.0003	0.0003	0.0009	0.0027	0.0058	0.0003
2.2	0.0472	0.4529	0.0003	0.0003	0.0006	0.0024	0.0052	0.0006
2.4	0.0488	0.4551	0.0000	0.0006	0.0006	0.0018	0.0043	0.0012
2.6	0.0482	0.4578	-0.0003	0.0003	0.0003	0.0012	0.0030	0.0015
2.8	0.0469	0.4596	0.0000	0.0006	0.0009	0.0015	0.0030	-0.0009
3	0.0475	0.4621	0.0000	0.0003	0.0006	0.0006	0.0021	-0.0015
3.2	0.0469	0.4642	-0.0003	0.0006	0.0003	0.0006	0.0012	-0.0021
3.4	0.0482	0.4663	0.0000	0.0009	0.0006	0.0003	0.0009	-0.0015
3.6	0.0479	0.4688	0.0000	0.0003	0.0003	-0.0003	0.0000	-0.0018
3.8	0.0488	0.4709	-0.0003	0.0000	0.0003	-0.0012	0.0000	0.0006
4	0.0485	0.4730	0.0000	0.0003	0.0003	-0.0003	0.0000	0.0000
4.2	0.0482	0.4752	0.0003	0.0006	0.0006	-0.0003	0.0003	0.0006
4.334	0.0479	0.4767	0.0000	0.0000	0.0000	0.0000	0.0000	0.0000

APPENDIX B

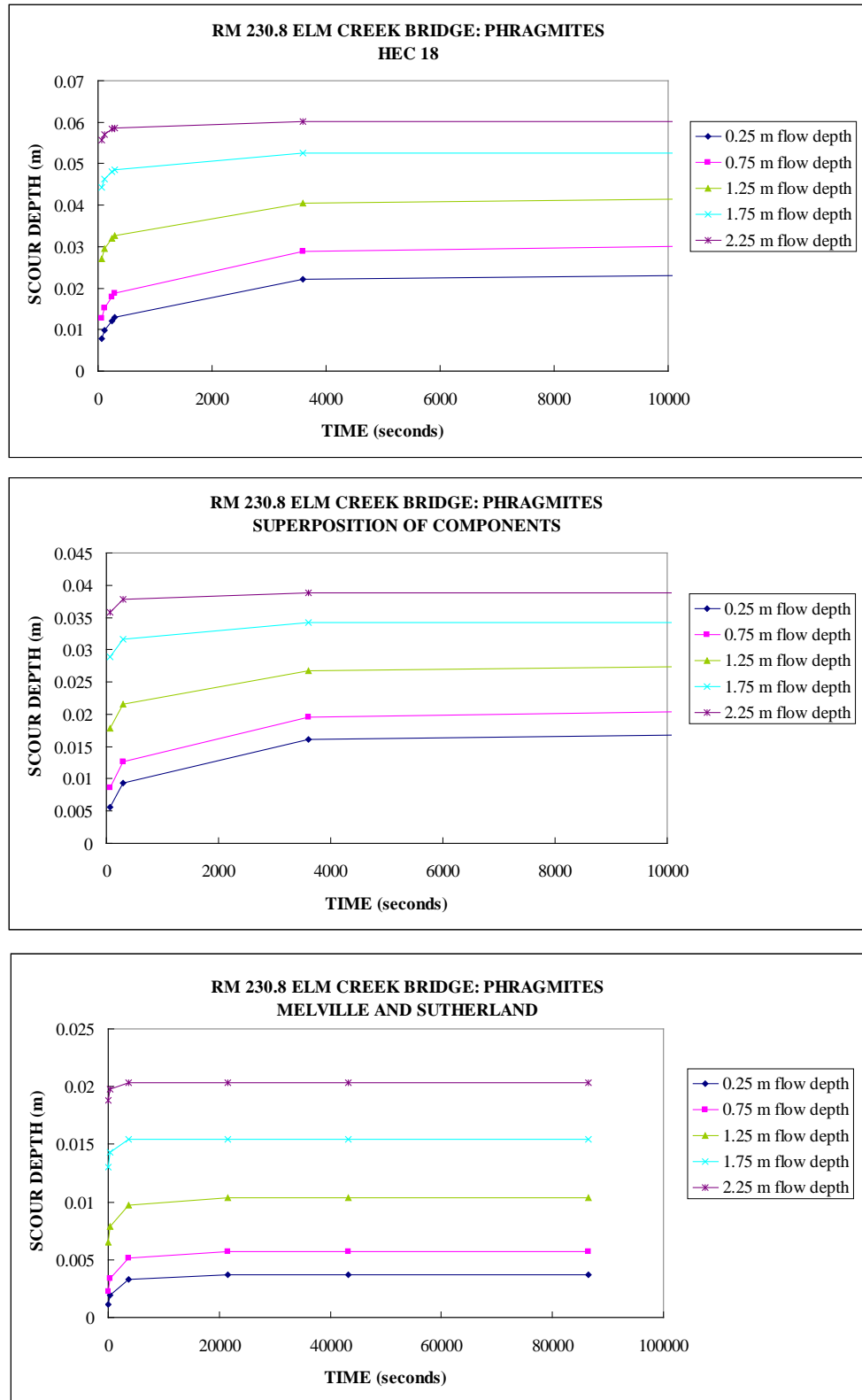


Figure B1. Time to reach equilibrium scour depth for *Phragmites* stems at RM 230.8.

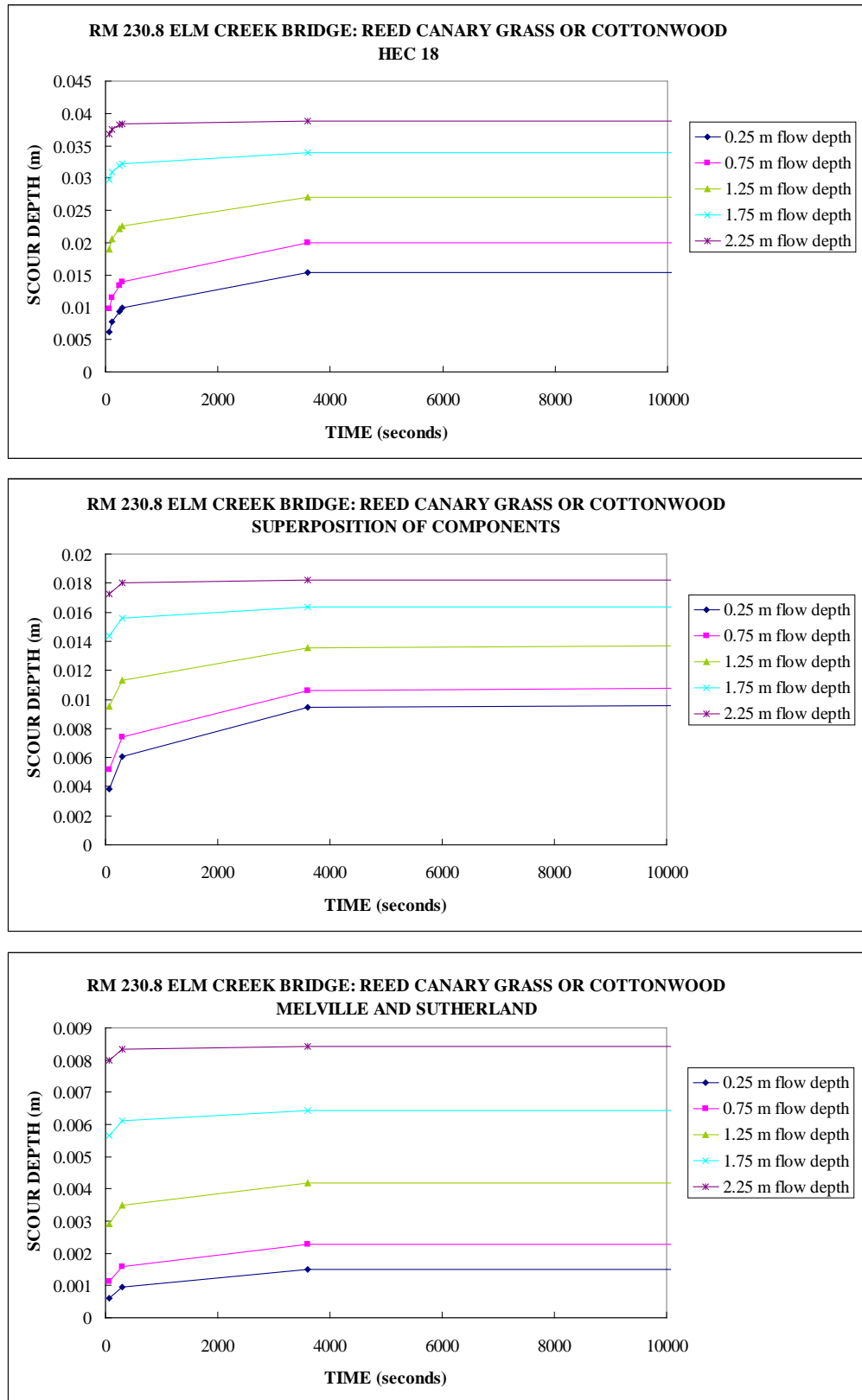


Figure B2. Time to reach equilibrium scour depth for Reed canarygrass and cottonwoods at RM 230.8.

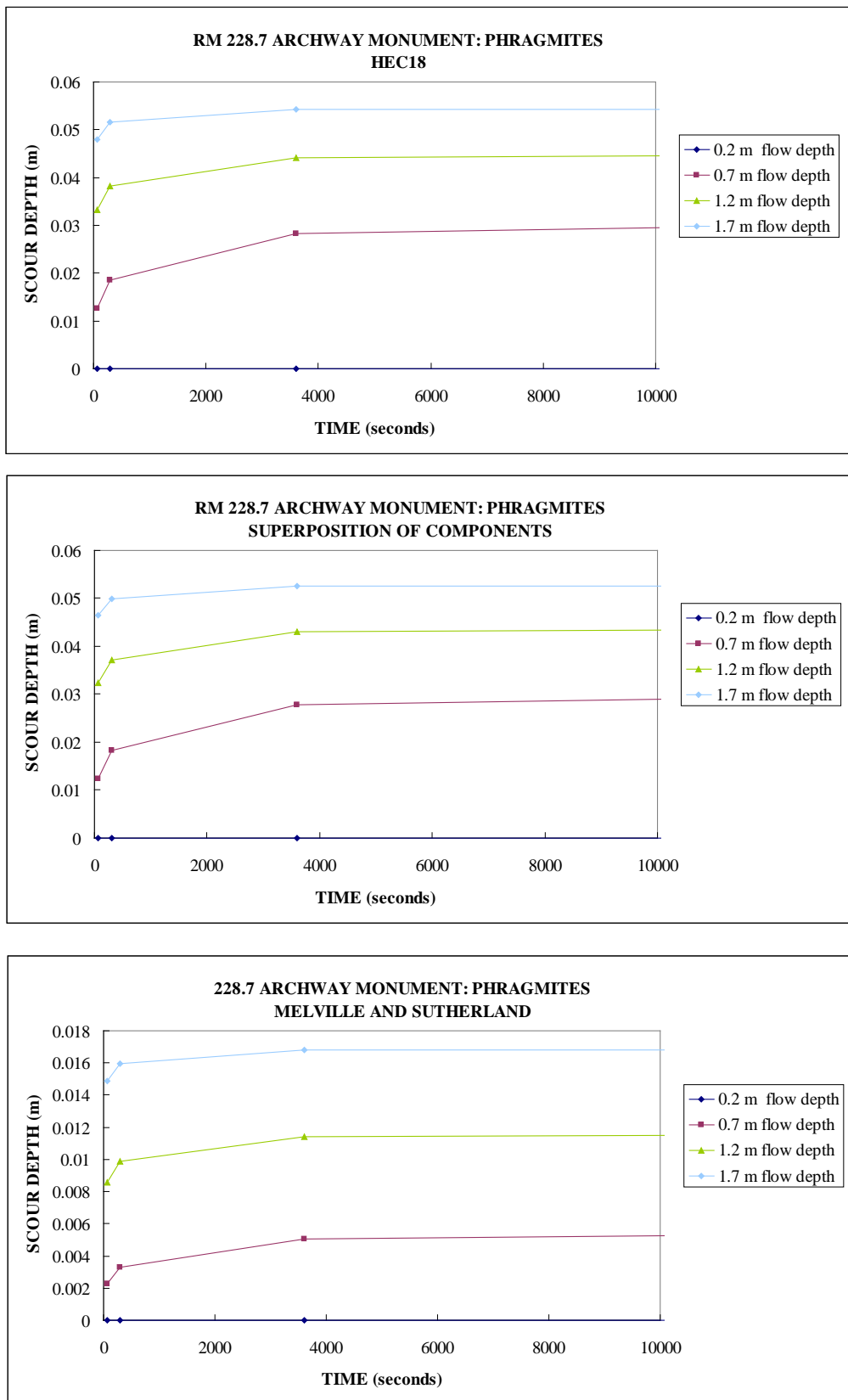


Figure 52. Time to reach equilibrium scour depth for *Phragmites* stems at RM 228.7

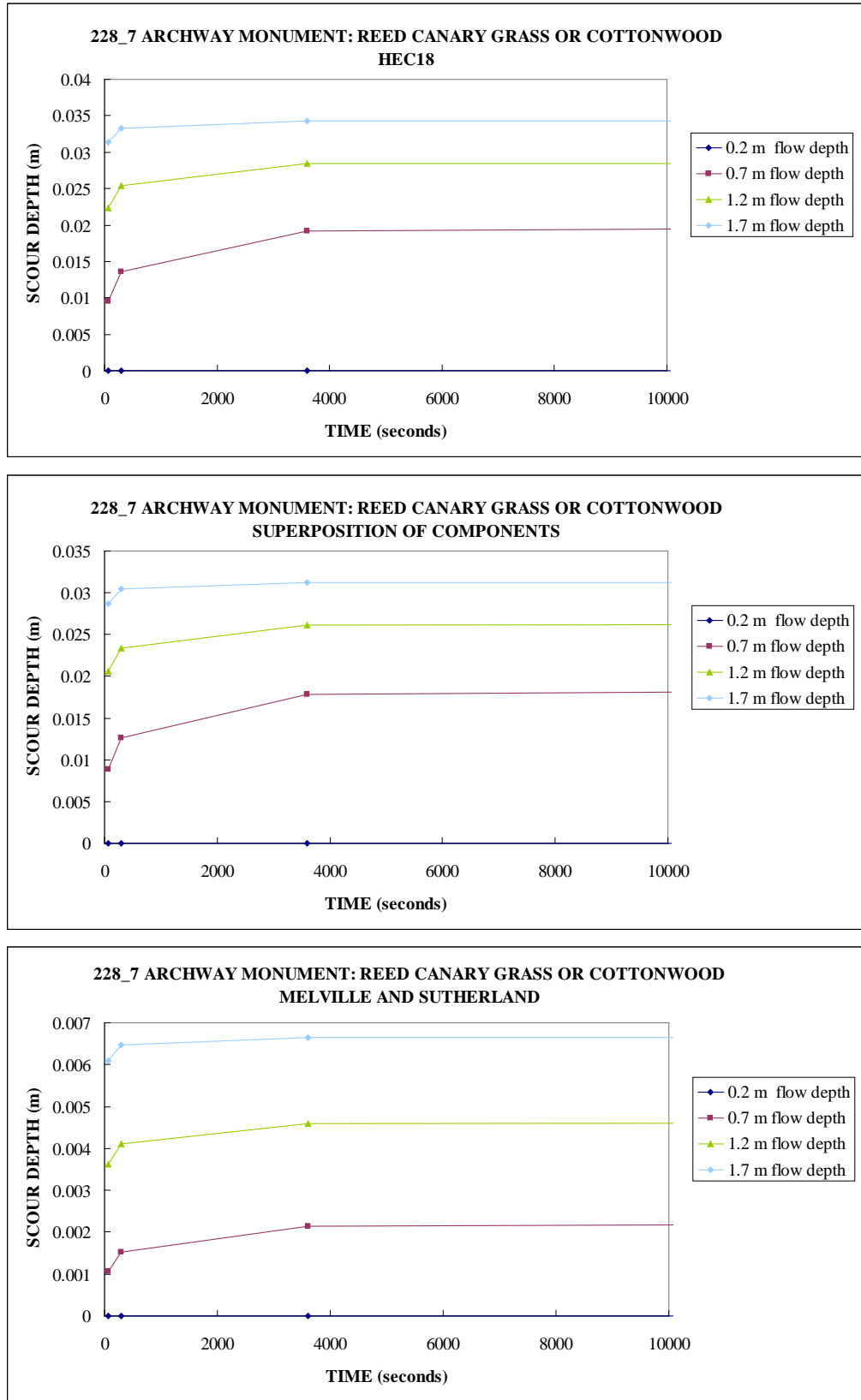


Figure B4. Time to reach equilibrium scour depth for Reed canarygrass and cottonwood at RM 228.7

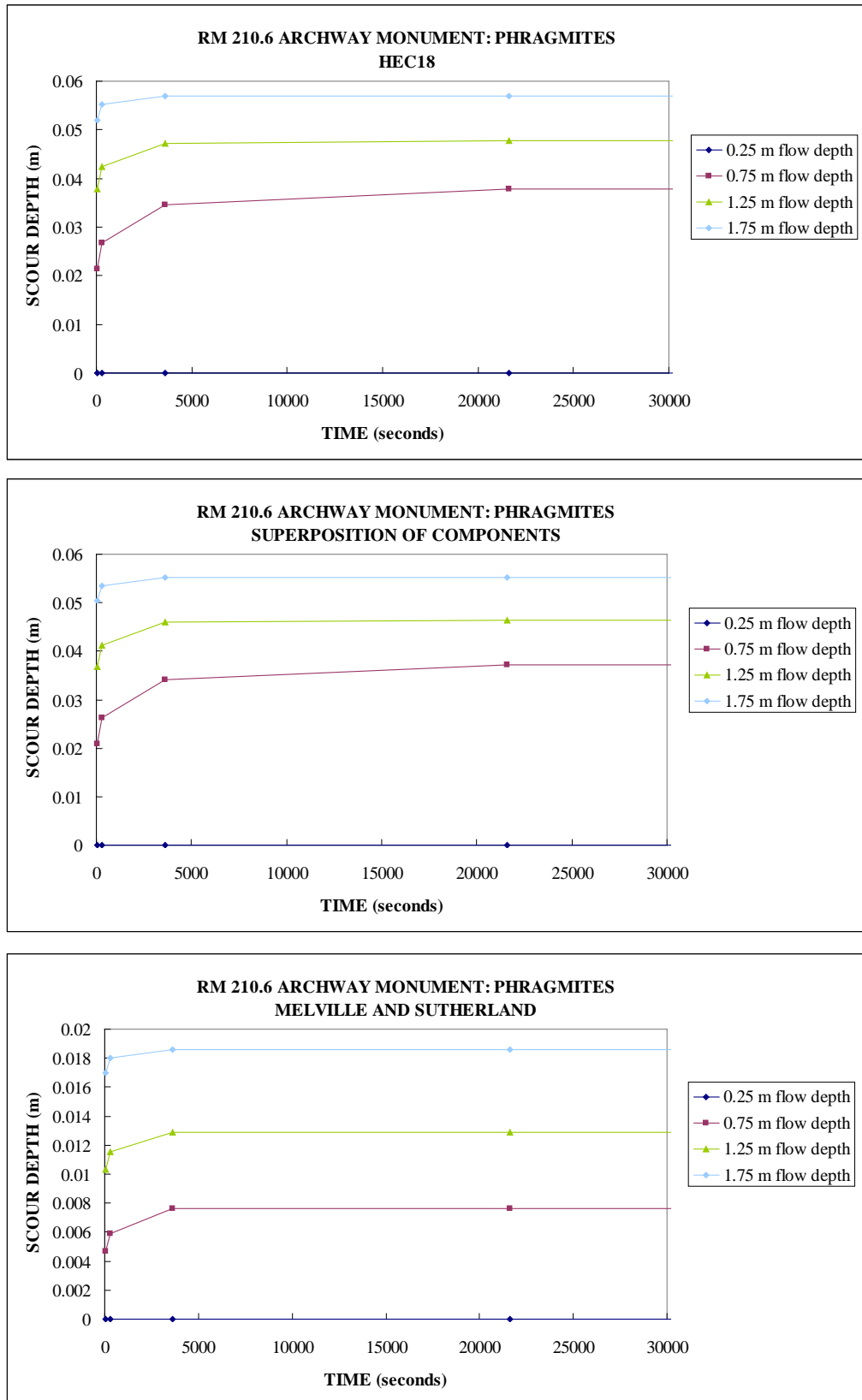


Figure B5. Time to reach equilibrium scour depths for *Phragmites* stems at RM 210.6

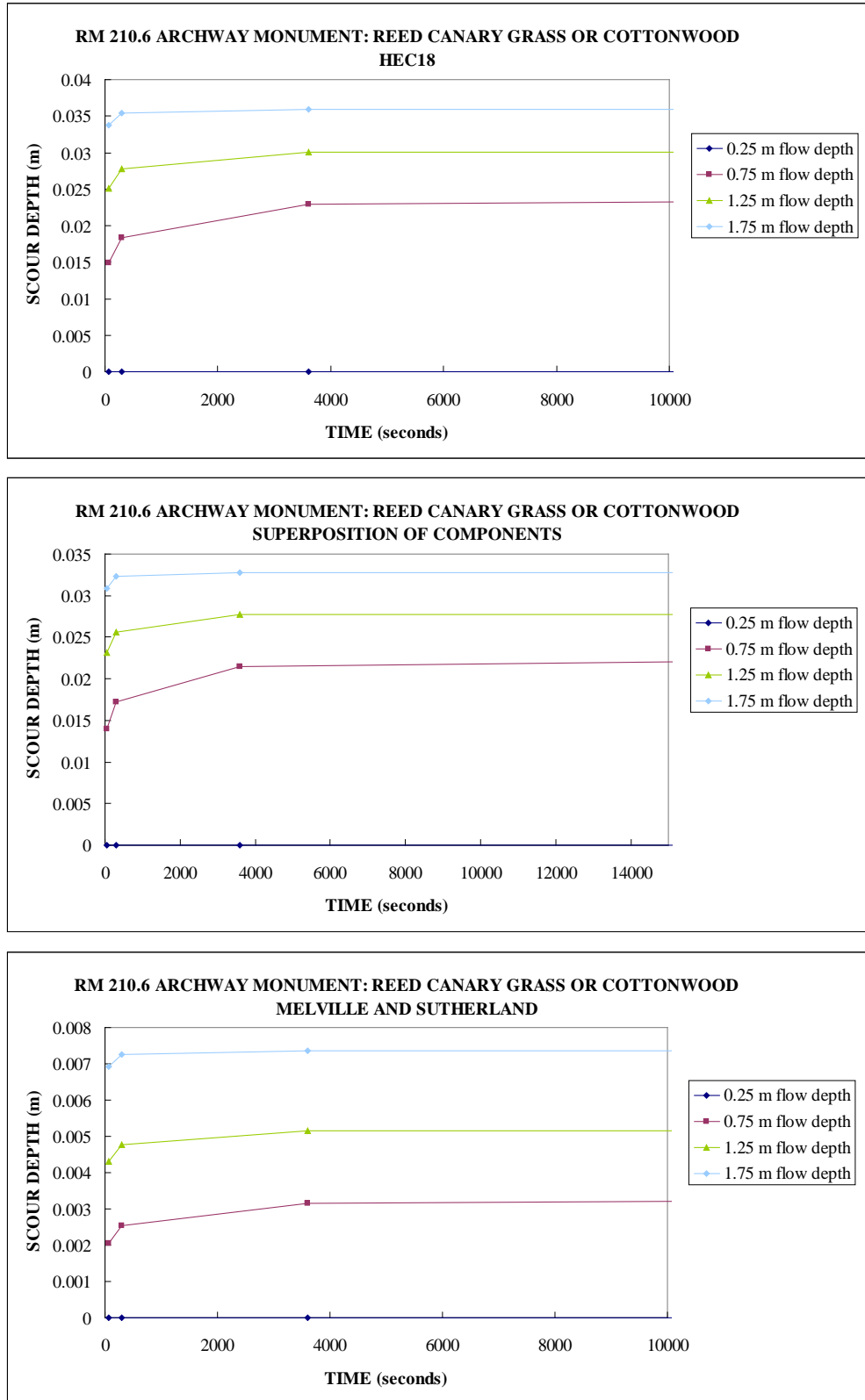


Figure B6. Time to reach equilibrium scour depths for Reed canarygrass and cottonwood at RM 210.6

